Bypassing of path-blocking proteins on microtubules in kinesin-mediated cargo transport

Dissertation

zur Erlangung des akademischen Grades doctor rerum naturalium

(Dr. rer. nat.)

vorgelegt dem Rat der Chemisch-Geowissenschaflichen Fakultät

der Friedrich-Schiller-Universität Jena

von Diplom-Chemikerin (Umweltchemie) Kerstin Dreblow,

geboren am 08.08.1981 in Meiningen

Die vorliegende Arbeit wurde durchgeführt am:

Leibniz-Institut für Altersforschung
Fritz-Lipmann-Institut e.V. (FLI)

1. Gutachter: Prof. Dr. Wolfgang Weigand
                       Friedrich-Schiller-Universität Jena

2. Gutachter: Prof. Dr. Karl Otto Greulich
                       Friedrich-Schiller-Universität Jena

Tag der öffentlichen Verteidigung: 15.07.2009

Durch Stolpern kommt man bisweilen weiter;
man muss nur nicht fallen und liegenbleiben.

Johann Wolfgang von Goethe

Table of Contents

The work contains: 126 pages

                      72 figures

                      2 tables

List of Figures and Tables

Figures

Tables

Abbreviations

ADP	Adenosine-5`-diphosphate
AMP-PNP	Adenosine-5`-(β,γ-imido)triphosphate tetralithium salt
ATP	Adenosine-5`-triphosphate
AVEC-DIC	Allen video-enhanced differential interference contrast microscopy
BSA	Bovine serum albumin
DNA	Deoxyribonucleic acid
DTT	Dithiothreitol
EDTA	Ethylenediaminetetraacetic acid
EGTA	Glycol ether diamine tetraacetic acid
GDP	Guanosine-5`-diphosphate
GTP	Guanosine-5`-triphosphate
IPTG	Isopropyl-β-thiogalactopyranoside
LB	Lysogeny Broth
k_{cat}	Turnover number
K_D	Dissociation constant
MAP	Microtubule-associated proteins
MTOC	Microtubule-organizing centre
PAGE	Polyacrylamide gel electrophoresis
PBS	Phosphate-buffered saline
PDDA	Poly(diallyldimethylammonium chloride)
PIPES	Piperazine-N,N`-bis(2-ethanesulfonic acid)
RNA	Ribonucleic acid
SD	Standard deviation
SDS	Sodium dodecyl sulfate
TRIS	Tris(hydroxymethyl)-aminomethan
TPP	Tripolyphosphate

1 INTRODUCTION

Living cells can be regarded as miniaturized factories performing a tremendous amount of complicated tasks, *e.g.*, the internal energy supply or the production of proteins and other bio macromolecules and their directed, coordinated delivery to highly specialized compartments. Moreover, cells are able to sense their environment and respond to it by generating motility or adaptation of their shape and morphology.

Motility is a decisive feature of life. Nature has evolved a large number of sophisticated protein machines to maintain the diverse motility and transport functions within cells. Such machines can be classified into rotary motors including flagellar motors of bacteria (Berg, 1995; Berg, 2000) and the ATP-synthase (Engelbrecht and Junge, 1997; Montemagno and Bachand, 1999; Cross, 2000) or linear motors including RNA-polymerases and the cytoskeleton-associated motors (Gelles and Landick, 1998; Wang 1999). The high specificity of the particular motor proteins involved in motility generation, especially their high potency to bind distinct ligands makes them superior to be employed as archetypes for constructing molecular machines with a highly specialized functionality.

Specialized cytoskeleton-associated motors are amazing biological machines responsible for different forms of movement like cell locomotion, muscle contraction, and the active intracellular transport of cell organelles and macromolecules. A property that no man-made machine possesses is the ability to convert the chemical energy of ATP directly into mechanical energy without the usage of an intermediate like heat or electrical energy. Motor proteins are able to move micrometer-sized objects at relatively high velocities along proteinaceous filamentous rails, constituting the cytoskeleton network. In eukaryotic cells different types of cytoskeletal motor proteins (myosins, dyneins, kinesins) are ubiquitously expressed.

The present work is focused on kinesin-1, which is fundamentally involved in, *e.g.*, the realization of diverse functions within neuronal cells, including the maintenance of a distinct morphology and the signal transfer. Unlike other cell types, where cargoes have to be transported a short distance only, the axons of neuronal cells lack an own protein

synthesis machinery and have developed an advanced transport system being able to transport biomolecules in the axon over wide distances.

Kinesin is a linear motor that binds to and moves along microtubules, which represent proteinaceous filaments forming together with microfilaments and intermediate filament the cytoskeleton. The microtubules have a pronounced chemical polarity, essentially in determining the direction into which a given kinesin moves. Opposite to the microtubule binding site, kinesins possess a structural domain for coupling diverse cellular cargoes, such as neuronal vesicles and other cell organelles or macromolecules. This structural organization enables moving kinesins to realize transport functions.

Especially the members of the kinesin-1 family are characterized by their ability to walk along the microtubule up to some micrometers without being released (Vale et al., 1985; Hancock and Howard, 1998), what makes them superior above other motor proteins regarding their potential to be used for the development of artificial nanomachines. It is well documented that kinesin-mediated force generation can be realized in cell-free environment (Vale et al., 1985; Block et al., 1990; Cross, 1995; Mazumdar and Cross, 1998). In addition, the kinesin was found to be potent to transport cargoes, made of technologically relevant materials like silicon, quartz, polystyrene or gold (Limberis and Stewart, 2000; Böhm et al., 2001; Hiratsuka et al., 2001; Doot et al., 2007; Yokokawa et al., 2008). These results have awaken great interest to integrate this biological machinery in the development of novel nanoscaled actuators, *e.g.*, to transport chemical components into or out of microreactors to support chemical reactions, or to deliver diverse micro- and nanoparticles or single molecules (*e.g.* delivery system to convey therapeutic drugs) to predefined destinations (Yokokawa et al., 2004; Bachand et al., 2006; Dinu et al., 2006; Ramachandran et al., 2006; van den Heuvel and Dekker, 2007).

However, to approach the ambitious aim of nanotechnological exploitation of kinesins, methodological and technical problems have still to be solved. Such problems concern not only the thermal and temporal stability of the kinesin machinery and its directional control, but also the track fidelity of kinesin movement. Additionally, a detailed understanding of the molecular mechanisms of motility generation is still lacking.

In the viscous, dense intracellular matrix of living cells the kinesin-mediated transport represents a highly complex mechanism exposed to a great number of associated cell constituents which might interact with the motor itself or with the microtubule rail. There seems to be a high probability that a kinesin molecule moving along its track encounters other proteins, which might compete for the same binding site on the microtubule. Such

interactions could sterically hinder the kinesin-mediated transport and finally cause cargo stalling, comparable with a traffic jam (Martin et al., 1999; Seitz et al., 2002). In the artificial environment of cell-free systems, irregularities in the microtubule structure, *e.g.*, defects in tubulin-tubulin binding or tubulin dimer failure might additionally impair the kinesin-mediated transport.

Kinesin functions and interactions are also related to severe neurodegenerative diseases (Alzheimer's disease, amyotrophic lateral sclerosis) where in most cases the long-distance transport of physiological cargoes is constrained. Aggregations of proteins or macromolecular crowding lead to steric blocking and finally to cargo stalling. Understanding the molecular mechanisms and events underlying the inhibition of the cellular activity of motor proteins are believed to provide the basis to design strategies to treat diseases.

In this context, one main question is what happens when a kinesin molecule encounters defective sites of kinesin binding during movement along the microtubule. The present work contributes to deeper understanding of the molecular mechanisms of cytoplasmic transport processes over long distances. Despite the progress that has been made in explaining the maintenance of kinesin motility along microtubules covered by blocking molecules, the detailed mechanism of passing blockages is controversially discussed. It has been reported that moving kinesin competing with a motility-deficient kinesin construct for binding sites on the microtubule surface stops at the site where this construct is located. Movement is suggested to continue only after freeing the blocked site (Seitz and Surrey, 2006). In another approach where the surface of biotinylated microtubules was decorated by streptavidin (Korten and Diez, 2008), kinesin molecules were found to stop frequently upon encounters with the blockages. The authors considered that passing would be possible only in cases when the streptavidin does not block the kinesin binding site. In cases when the kinesin binding site is not accessible the motor was suggested to temporarily detach from the microtubule, diffuse along the microtubule lattice, and rebind. Both mechanisms are based on the principle of contingency. Therefore, they seem to be insufficient to realize a reliable transport of cell organelles or macromolecules. The existence of a more efficient mechanism, enabling to overcome permanent obstacles or, additionally, defects in the microtubule lattice (Chretien et al., 1992) along the protofilament track, has to be expected.

The main goal of this work was to elucidate how kinesin can overcome irreversibly bound blockages on the microtubule. Using an *in vitro* single-molecule approach the

effects of microtubule crowding by different protein constructs (kinesin-1, Eg5, microtubule-associated proteins) on main parameters of kinesin motility (transport velocity, dwell time, transport distance) were studied. Kinesin binding sites on the microtubule were artificially occupied by the block proteins and chemically cross-linked to avoid their exchange. Thereafter, native kinesin, coupled to nanometer-sized gold beads, was allowed to move along the partially blocked microtubules. To reveal basic insights in the binding frequency of block proteins on the microtubule surface electron microscopic studies were additionally performed.

The present work provides evidence that kinesin is able to overcome even irreversibly bound blockages along the microtubule. To explain the result, a bypassing mechanism is proposed. Bypassing blockages can be regarded as a fundamental mechanism by which the track fidelity of a molecular motor, transporting a nanoscaled cargo, along filamentous rails can be improved. Elucidation of this mechanism is of great relevance not only for understanding the biomolecular mechanisms of organelle and macromolecule transport within living organisms, but also for engineering motor protein-based nanotransport and sorting machines delivering various kinds of biological and inorganic cargoes to predetermined destinations.

2 FUNDAMENTALS

2.1 The cytoskeleton

A cell undergoes permanent changes to react on environmental alterations. Eukaryotic cells have developed an efficient dynamic network that enables the fast rearrangement and adaption of its compartments to respond to signals. This network, called the cytoskeleton (Figure 1) supports both, the cellular architecture and motility. The diverse functions, including the maintenance of the cell shape, movement and positioning of organelles, segregation of genetic material during cell division, intracellular transport, reinforcement of the plasma membrane, and regulation of tension are performed by three types of filamentous structures: actin microfilaments, intermediate filaments, and microtubules. Intermediate filaments are responsible for mechanical strength and drags against shear forces whereas actin microfilaments enable movement of whole cells and maintaining the cell shape. Microtubules arrange the position of membranous organelles and chromosomes during mitosis, and guide the intracellular transport (Alberts et al., 2002).

The dynamic and adaptable design of the cytoskeleton enables rapid structural changes without large energy input due to low covalent bonds between the subunits. But, to maintain intracellular functions, additional proteins are necessary. Such proteins (motor proteins) are adsorbed to the cytoskeletal structures for controlling the dynamic behaviour and the spatial distribution.
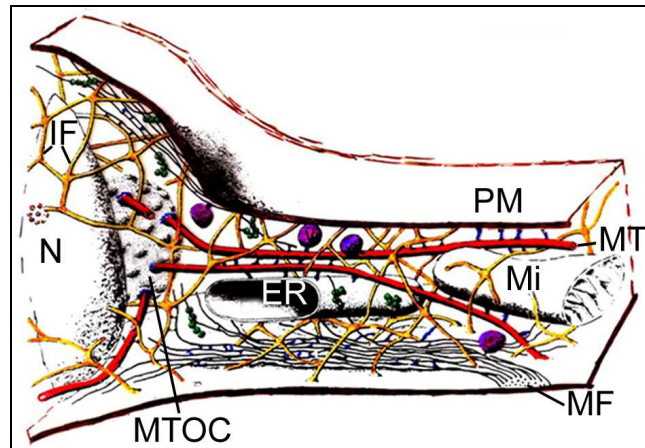
Figure 1: *The cytoskeleton.*
The cytoskeleton is a filamentous cytoplasmic network of eukaryotic cells. ER: endoplasmatic reticulum, Mi: mitochondria, MTOC: microtubule-organizing center, N: nucleus, PM: plasma membrane. Figure designed by M. Girbardt, H. Hädrich (ZIMET Jena).

2.1.1 Microtubules

Microtubules are ubiquitious and obligate proteinaceous structures that can be found in almost all eukaryotic cells (Figure 2). The main component is a 50-kD globular protein called tubulin. There are two closely related basic forms, α- and β-tubulin, forming heterodimers of 8-nm length (Figure 3a).
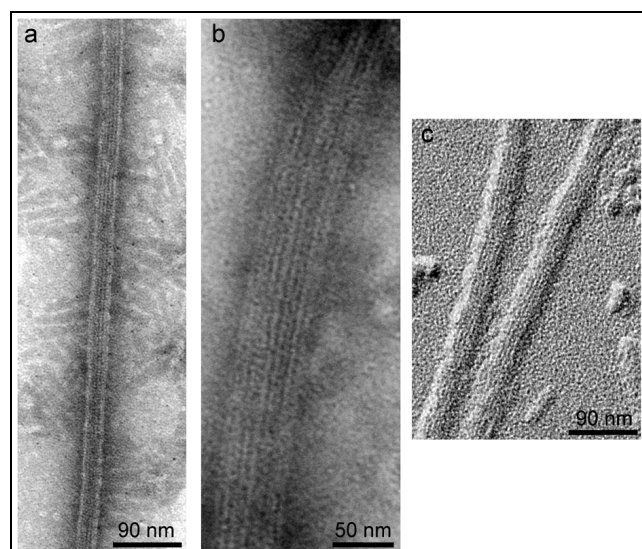
Figure 2: *Electron microscopy images of microtubules.*
a,b) Uranylacetate-stained microtubules.
c) Pt/W-shadowed microtubules.
The longitudinal striations represents the protofilaments constituting the microtubule wall.

Microtubules are rigid hollow-cylindrical structures (25 nm - 30 nm outer diameter) buildup by linear polymers, the protofilaments (Figure 3b). Protofilaments are formed by longitudinal association of αβ-tubulin heterodimers. The cylindrical structure (Figure 3c) of the microtubule is based on lateral association of parallel protofilaments axially staggered by 0.94 nm in a left-handed direction (Chretien and Fuller, 2000; Neek-Amal et al., 2008). *In vivo*, the microtubule wall normally consists of 13 protofilaments, even though the number can change under particular conditions (Böhm et al., 1984). The longitudinal association (head to tail) of alternating tubulin monomers results in a structural polarity whereby α- and β-tubulin define the minus- and plus end, respectively.

The total length of microtubules varies widely and can reach up to 100 µm (Kristofferson and Purich, 1981).

Each of the monomers binds GTP, but only β-tubulin is able to hydrolyze it what has a high impact on microtubule dynamics. When the heterodimers are associated to form protofilaments, GTP in β-tubulin is hydrolyzed to GDP as a consequence of the interaction with α-tubulin at the adjacent dimer (Amos, 2004). A special feature of tubulin dimers is their ability to form microtubules by self-assembly *in vitro* at physiological temperatures in the presence of Mg^{2+} and GTP. But, in the cold microtubules easily disassemble into dimers. Based on this, microtubules can be purified by repeated cycles of assembly/dissasembly, especially from mammalian brain tissue which is the main source for isolation. At steady state the association of tubulin dimers from the pool of unpolymerized protein dominates at the plus end, whereas dissociation preferentially occurs at the minus end. When growing and shrinking are in equilibrium state, the whole length of the microtubule remains constant (treadmilling effect). In addition, it has been reported that phases of elongation and rapid shrinking (Kristofferson et al., 1986) can occur within microtubule populations (dynamic instability). Microtubules depolymerize on GDP-containing ends 100-fold faster than on a GTP-containing end. Therefore, a GTP-cap conveys growing, but its disappearance leads to shrinking.
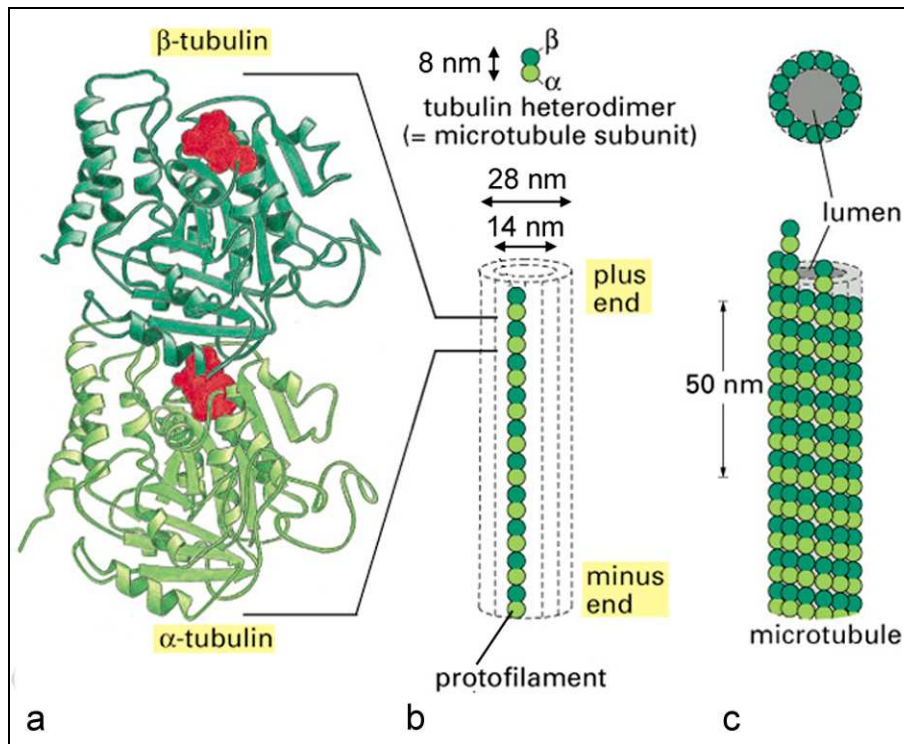
Figure 3*: Microtubule structure and its subunits.*
a) Ribbon model of an αβ-tubulin dimer, which is the basic building unit of the microtubule. Both, α- and β-tubulin contain one GTP (red) bound.
b) Single protofilaments formed by longitudinal association of αβ-tubulin dimers.
c) The lateral association of protofilaments form the hollow cylinder of the microtubule. The figure is adapted from Alberts (2002).

2.1.2 Microtubule-associated proteins

Microtubules in different tissues were found to be accompanied by a set of additional proteins, the so-called microtubule-associated proteins (MAP). These non-motile proteins bind to the surface of microtubules (Figure 4) without the requirement of nucleotides. MAPs are playing an essential role in stabilizing microtubules against disassembly by changing their dynamic behaviour. Moreover, they are involved in inter-bridging cytoplasmic microtubules with each other and also with microfilaments or intermediate filaments.

MAPs consist of a conserved carboxyl-terminal domain containing the microtubule binding site and an amino terminal projection domain of varying size (Dehmelt and Halpain, 2004).

The most prominent associated proteins MAP1, MAP2 and tau were preferentially found in mammalian brain. The high molecular weight MAP1 and MAP2 consist of various subspecies of 270 kD - 350 kD. Tau exists in several isoforms with a molecular mass ranging between 53 kD – 70 kD (Cleveland et al., 1977 (a,b); Drubin and Kirschner, 1986).
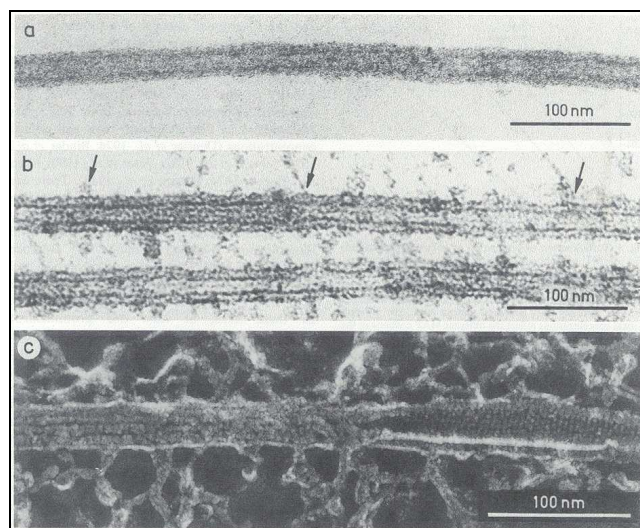
Figure 4: *Electron microscopy images showing MAPs.*
a) Microtubule in the absence of associated proteins shows a smooth surface.
b) Microtubules in the presence of associated proteins, which are visible as filamentous projections along the surface (arrows).
c) Quick-freeze, deep-etched image of a microtubule containing associated proteins.
The pictures were taken from Unger et al. (1990).

2.1.2.1 Tau

Tau was the first associated-protein identified that consists of a complex of polypeptides. The number of polypeptides varies from species to species, ranging between three and six (Olmsted, 1986).

Important functions of tau are the stabilization of microtubules, determination of neuronal polarity, and promoting microtubule nucleation and growth as well as the outgrowth of axons.

Tau mostly occurs as a mammalian neuronal protein most abundant in axons. But, it has been also found in other cells and tissues like heart, skeletal muscle, lung, kidney, testis, stomach, and liver (Friedhoff and Mandelkow, 1999).

The protein appears as a rod-like structure with around 35-nm length (Wille et al., 1992 a) behaving like a natively unfolded protein (Schweers et al., 1994). Special features of tau are the hydrophilic character and the resistance against diluted acids and heat (Weingarten et al., 1975; Lindwall and Cole, 1984) what seems to be consistent with the unfolded structure.

Tau is thought to bind stochastically to multiple sites on the microtubule. Evidence, that tau binds to the outer surface by forming extensions has been found, likewise the binding in the inner lattice of microtubules (Amos, 2004).

Recently, researchers are interested in understanding the relevance of tau, since in the neurons of Alzheimer´s disease patients tau was found in abnormal phosphorylated form. As a consequence, hyperphosphorylated tau might contribute in the destabilization of the microtubule network, impaired axonal transport and neurofibrillary tangle formation. The collapse of the microtubule network leads to obstructed nerve cells. The intracellular transport processes are stalled resulting in neuronal cell death (Mandelkow and Mandelkow, 1998).

2.1.2.2 MAP2

Like tau, MAP2 is found in neuronal cells, but specifically segregates to the dendrites. It appears as an elongated protein with an estimated size of 185-nm length (Kim et al., 1979). The domain organization comprises a microtubule binding site (35 kD - 40 kD), occupying much as one third of the total length, and a projection domain (240 kD) (Vallee, 1980;

Gottlieb and Murphy, 1985). The large projection domain can serve as a spacer between microtubules and as an anchoring point for organelles and proteins, including enzymes (Chen et al., 1992).

On the microtubule surface MAP2 forms lateral filamentous projections (Kim et al., 1979). The projections were found to extend out of the outer microtubule surface. These long sidearms are suggested to represent obstacles for motor proteins (Lopez and Sheetz, 1993). Inhibition of motor protein movement is suggested to be due to steric competition of MAP2 with motor proteins for binding to the microtubule surface (Lopez and Sheetz, 1993; Hagiwara et al., 1994; Seitz et al., 2002)

2.2 Molecular Motors

Motility is an essential feature of life. During evolution nature has evolved a great number of highly specialized protein machines, the so-called molecular motors that realize biological movement. Motility generation is realized by energy-dependent conformational changes resulting in unidirectional movement along the cytoskeleton. Among them, three classes of cytoskeletal motors are known: myosins, which move along actin filaments, and the microtubule-associated motors (Figure 5). Kinesin and dynein constitute the class of microtubule motors which generate motility along microtubules. Motor proteins perform specific cargo transport functions within the cell. The general constitution of these motors is quite similar. All of them comprise a globular motor domain (head domain) with an ATP-binding site and a binding site for the filament. Additional domains outside the head unit are responsible for dimerization, regulation, and the interaction with the cargo to be transported, *e.g.*, organelles or biomacromolecules.

Motors proteins constitute superfamilies with dozens of members. The single members of these superfamilies show a variety of optimized structures due to the highly specialized functions they have to perform inside the cell. Additionally, they differ in basic properties like working as monomers, dimers, trimers, tetramers, moving to the plus or minus end of their track, or taking one or multiple steps before dissociation. Taking the modular design into consideration 18 different classes of myosins, 10 different kinesin families, and two groups of dyneins, each with some dozen members can be distinguished (Schliwa and Woehlke, 2003).

The number of motors varies not only between the organisms but also between the different cell types an organism is built of. In yeast, for example, genes for 6 kinesins, 5 myosins, and 1 dynein cover all the motility functions. In contrast, mammals have genes for 40 kinesins, 40 myosins and more than a dozen dyneins (Schliwa and Woehlke, 2003).

Though, notable insights into mechanochemistry and function have been gained in the past years, there are numerous unsolved questions concerning the understanding of motor protein function on molecular level.
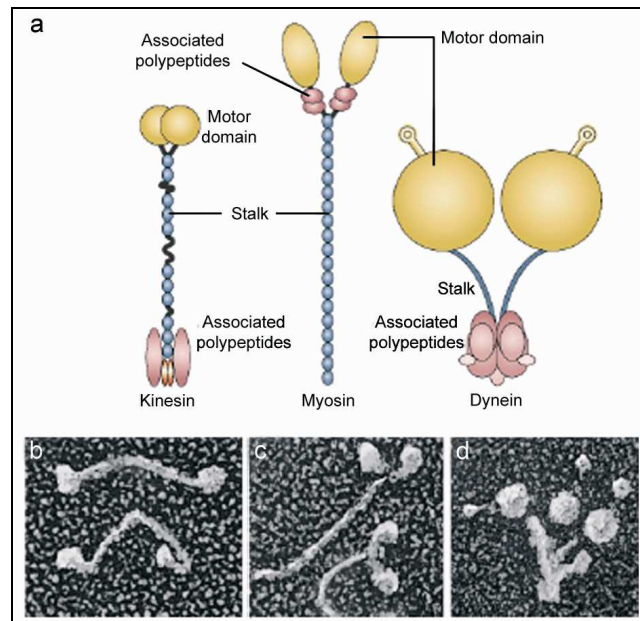
Figure 5: *Cytoskeleton-associated motors.*
a) The microtubule motors kinesin (left), dynein (right), and the microfilament-associated myosin (middle) are dimers with globular motor domains (yellow). The stalk region, forming extended coiled-coils is shown in blue. Additional associated polypeptides, or light chains (2 in conventional kinesin, 4 in muscle myosin, and a set of intermediates, light-intermediates and light chains in dynein) are displayed in purple. The dynein motor domain exhibits antennae-like extensions containing the microtubule binding site. In contrast, the microtubule binding site of kinesin and myosin is incorporated within the complex head domain. The picture was adapted from Schliwa and Woehlke (2003).
b-d) High-resolution electron micrographs of quick-frozen, rotary-shadowed kinesin, myosin, and dynein molecules, respectively. The picture was adapted from Woehlke and Schliwa (2000).

2.2.1 Kinesin superfamily

The kinesin superfamily contains various microtubule-based motor proteins performing diverse functions, including the transport of vesicles, organelles, chromosomes, protein complexes, or the regulation of microtubule dynamics (Lawrence et al., 2004). The first member of the kinesin family was discovered in 1985 in the axoplasm of the squid giant axon and mammalian brain (Brady, 1985; Vale et al., 1985). Vale et al. (1985) described a protein being able to move microtubules on glass. Moreover, it was shown to move latex beads and axoplasmic organelles along microtubules. The name given based on the greek word "kinein" what means "to move". Subsequently, numerous kinesins have been discovered by molecular biological and genetic screens and named by diverse criteria. To prevent confusion a standard kinesin nomenclature was established (Miki et al., 2001; Lawrence et al., 2004).

The kinesin family members (KIFs) can be grouped into three types corresponding to the location of their motor domain. The so-called N-kinesins have the motor domain at the NH$_2$-terminus, M-kinesins in the central part of the protein sequence, and the C-kinesins at the COOH-terminus, respectively. The intramolecular position of the motor domain is crucial for the directionality of the motor. While N-kinesins drive a plus-end directed movement, C-kinesins are characterized by a minus-end directed motility.

The KIF genes in human and mouse have been systematically identified and are described in a phylogenic tree along with the KIFs from *D. melanogaster*, *C. elegans*, and *S. cerevisiae* (Miki et al., 2001). Presently, it can be distinguished between 14 families including one M-kinesin family, 1 C-kinesin family, and 12 N-kinesin families (Figure 6).
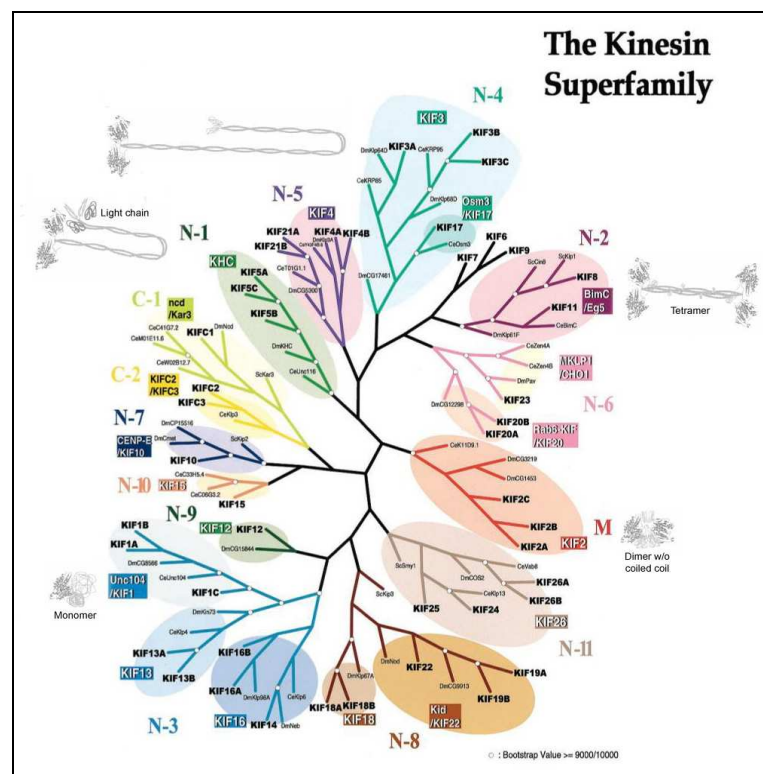
Figure 6: *Kinesin superfamily.*
Phylogenic analysis of all kinesin family members expressed in mouse/human, *D. melanogaster, C. elegans, and S. cerevisiae*. The picture was adapted from Miki et al. (2001); Kim et al. (2000).

To describe the different domains of kinesin motors a special terminology is used. Kinesin molecules commonly reveal a distinct a globular motor domain, the coiled-coil stalk region and the globular tail domain (Figure 7). The motor domain represents the force-producing element and is divided into two major parts: the globular catalytic core

and the neck region. The catalytic core comprises the ATP-binding site and the microtubule binding site. The neck region consists of about 40 amino acids and works in concert with the catalytic core to generate movement. Additionally, the neck region plays a major role in dimerization. Beyond the motor domain, most of the kinesins contain a flexible stalk region built up by a long coiled-coil. At the end of the stalk an additional globular domain follows (Vale and Fletterick, 1997). The so-called tail region is thought to target the motor to a particular cargo. Throughout the family members the motor domain shows 30% - 60% sequence homologies whereas the other regions are quite variable (Hirokawa and Noda, 2008).

Kinesins occur in different oligomerization states. The kinesin-1 is a homodimer consisting of two identical protein chains (Figure 7b). The kinesin-5 family members are composed of a bipolar tetrameric motor being self-associated through the tail domain (Figure 7c).
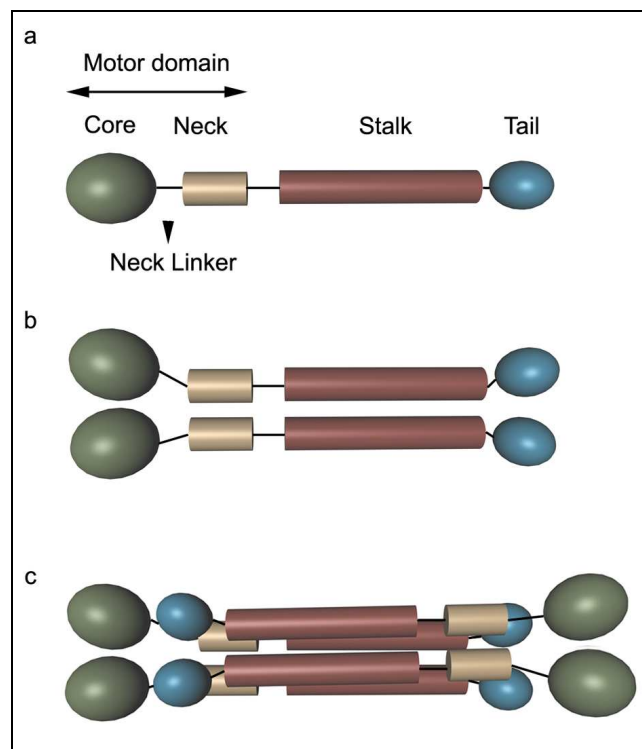
Figure 7: *Domain organization of kinesins.*
a) A single kinesin chain.
b) A homodimeric kinesin molecule, like observed for kinesin-1.
c) A bipolar homotetrameric molecule, like observed for kinesin-5.

2.2.2 Conventional kinesin

2.2.2.1 Structure

Conventional kinesin (kinesin-1) is the first discovered kinesin superfamily member and the best studied one (Vale, 1985; Hirokawa et al., 1989). There are three closely related subtypes of kinesin-1: KIF5A, KIF5B, and KIF5C (Aizawa et al., 1992; Kanai et al., 2000). While KIF5B is ubiquitiously expressed in different tissues, KIF5A and KIF5C are specifically expressed in the nervous system. KIF5 proteins form homodimers through the coiled-coil region located in their stalk region (Kanai et al., 2000).

Functionally active kinesin-1 consists of two 120-kD chains, each of which possessing a globular head with ~10 nm in diameter, a long stalk (60 nm - 80 nm) with alternating flexible and coiled-coil segments, and a fan-like globular tail domain (Figure 8). On cellular level, the kinesin-1 dimers are found to be associated with two 64-kD light chains, tightly binding at the C-terminus (Brady, 1985; Vale et al., 1985; Bloom et al., 1988). These light chains most probably have cargo-binding and regulatory functions (Stenoien and Brady, 1997; Vale and Fletterick, 1997; Gindhart et al., 1998; Verhey et al., 1998) and are not essential for motility generation (Yang et al., 1990).
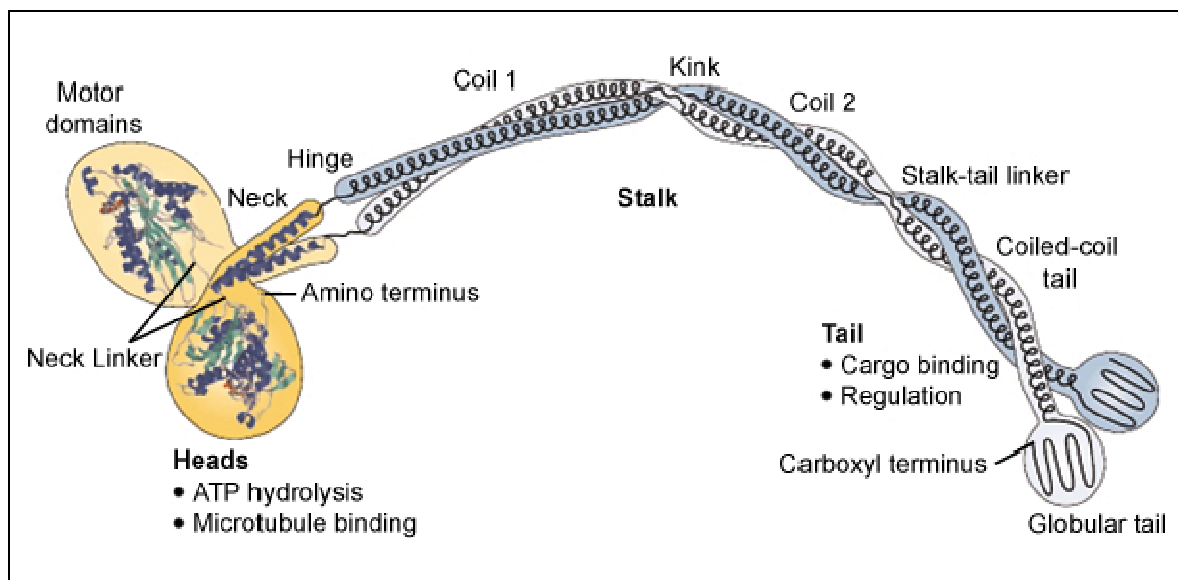
Figure 8: *Domain organization of conventional kinesin.*
The figure is adapted from Woehlke and Schliwa (2000).

Like other kinesin family members, the motor domain of conventional kinesin consists of the catalytic core and the neck region. The catalytic core comprises the microtubule-binding site and a nucleotide-binding pocket crucial for ATP-hydrolyis. The two heads of dimeric kinesin bind along one microtubule protofilament, rather than bridging two protofilaments (Hoenger et al., 2000). The contact between kinesin and the microtubule is mediated through electrostatic interactions of positively charged amino acids from kinesin interacting with the highly negatively charged surface on the β-tubulin (Hoenger et al., 2000). The neck region connects the two 120-kD chains by forming stable dimers essential for processive movement. Processivity is an important property of conventional kinesin that maintains the long-distance intracellular transport by taking hundreds of steps without being released from the microtubule track. Another feature essential for kinesin motility is the directionality of movement. Conventional kinesin moves towards the plus end of the microtubule which is thought to be a property determined by the neck (Endow and Barker, 2003).

The catalytic core and the neck region are connected via the flexible neck linker. During kinesin motility generation the neck linker undergoes large conformational changes depending on the nucleotide-bound state. The conformational changes are accompanied by alternating phases of weak and strong binding of the motor domain on the microtubule which guarantees that during the catalytic cycle at least on head remains bound (Hackney, 1995).

Distal to the neck region, the stalk contains two coiled-coil regions whose function is still unknown. Torsional flexibility of the stalk is gained by two hinge regions (Vale and Fletterick, 1997). It is suggested that they serve as a swivel point for the motor domain, allowing them to rotate and position themselves independently of the geometry of the stalk/tail domain (Vale and Fletterick, 1997).

Conventional kinesin binds their intracellular cargoes through the tail region at the carboxyl terminal end either directly or via light chains (Stenoien and Brady, 1997; Gindhart et al., 1998; Verhey et al., 1998; Hirokawa and Noda, 2008).

2.2.2.2   Functions

KIF5 proteins play an essential role in the axonal transport of neurons. Neurons are highly specialized cells consisting of a central soma containing the nucleus and other typical cell organelles. In this part of the neuron, most protein synthesis occur. Around the soma numerous widely branched dendrites are arranged. A striking cable-like projection, the so-called axon extends from the soma. The axon, which lacks an own protein synthesis machinery is extremely thin and might be up to 1 m long. It transfers signals away from and back to the soma. Therefore, unlike other cell types, where cargoes have to be transported over short distances only, the neuron has developed an advanced transport system being able to transport biomolecules in the axon over wide ranges. Considering the fact that diffusion of membranous organelles to their place of destination is a time consuming process, it becomes clear that the cell needs a reliable transport mechanism.

In axons, the microtubule plus end points towards the cell periphery. Therefore, anterograde motors drive the cargo delivery from the neuronal cell body to the pre-synaptic region of the axon (Figure 9). Proximal dendrites have a mixed polarity of microtubules, in which anterograde and retrograde motors, *e.g.*, kinesin and dynein, respectively, can work (Baas et al., 1988; Burton, 1988).

In *Drosophila,* where only one KIF5 gene exists, mutants show severe motor neuronal disease phenotypes and lethality (Saxton et al., 1991; Hurd et al., 1996). In cells, kinesin and dynein functions are interdependently realized. Beside the so-called fast axonal transport, where cargoes are transported at velocities of about 0.5 μm s^{-1} - 10 μm s^{-1} (Duncan and Goldstein, 2006), KIF5 proteins are suggested to play a role also in the slow axonal transport (0.01 μm s^{-1} - 0.001 μm s^{-1}; Duncan and Goldstein, 2006). By the slow axonal transport cytoskeletal proteins like tubulin and neurofilament proteins are transported. But, the detailed transport mechanism is still unknown (Hirokawa and Noda, 2008).
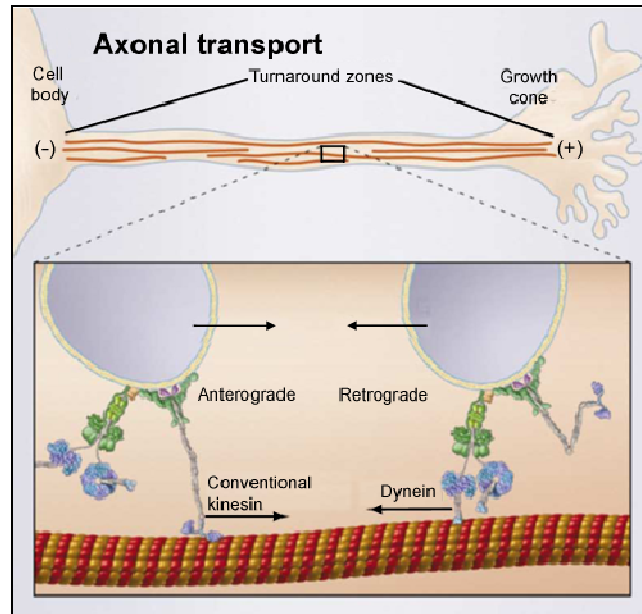
Figure 9: *Coordination of motors with opposite polarity in axonal transport.*
Kinesin motors carry the cargo in anterograde direction towards the microtubule plus end
(cell periphery). Dynein is carried along with the anterograde cargo in a repressed form. At
the turnaround zone dynein is activated and kinesin is repressed. The retrograde transport
is now performed carrying the cargo back to the cell body. The figure is adapted from Vale
(2003).

Within the cell body microtubule-associated motor proteins support the recruitment
and integration of membrane organelles (Figure 10). Vesicular structures and organelles
are transported from the endoplasmatic reticulum towards the Golgi apparatus, and *vice
versa*. The concerted transport is performed bidirectionally, whereas KIF5 proteins moving
the vesicles back to the endoplasmatic reticulum directed toward the microtubule plus end.
In the course of intracellular transport, kinesin moves anterogradely various
macromolecular complexes, mitochondria, lysosomes or tubulin oligomers.

Additionally, KIF5 proteins are involved in the processes of endosomal recycling
by supporting the transport of recycled vesicular structures between the subcellular
compartments and the plasma membrane (Hirokawa and Noda, 2008).
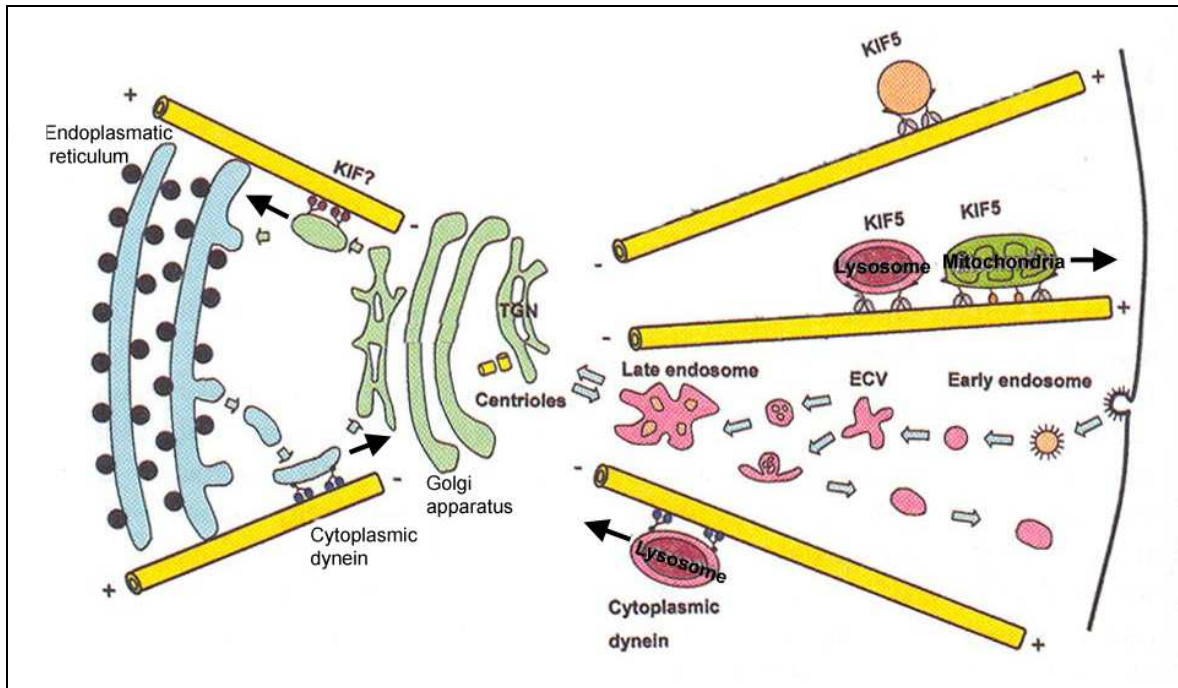
Figure 10: *Motor protein-mediated transport in the cell.*
The picture was adapted from Hirokawa N., Takemura R.: in Molecular Motors (2003).

Taken the amount of essential cellular functions into consideration one can easily imagine that the inhibition or interruption of the long-distance transport leads to a catastrophe for the cell. Many neurodegenerative diseases (amyotrophic lateral sclerosis, Alzheimer`s disease, Parkinson`s disease) can be ascribed to an impaired transport system whereby the molecular mechanisms are still a matter of debate.

2.2.2.3 Hand-over-hand model for kinesin motility

Kinesin uses the energy derived from ATP-hydrolysis to generate mechanical energy for its transport along microtubules. In the past, great efforts have been made to gain insights in the transduction of chemical energy into mechanical work at single molecule level.

The most widely accepted model is the hand-over-hand model in which, the rear head takes a step while the front head remains stationary bound on the track (Rice et al., 1999; Yildiz et al., 2004). During movement each step comprises a 16-nm displacement of the moving head and an 8-nm displacement of the stalk (Mandelkow and Johnson, 1998) what is consistent with the longitudinal distance between adjacent tubulins (Yildiz and Selvin, 2005). Per step, kinesin hydrolyzes a single ATP molecule (Hua et al., 1997; Schnitzer and Block, 1997). The energy release per hydrolysis cycle is relatively high (50 kJ mol^{-1}) enabling the powerful movement of kinesin (Berg et al., 2003). The motor protein can complete about ~100 ATP turnovers on average and move at a velocity of ~800 nm s^{-1} along a single microtubule protofilament (Kamimura and Mandelkow, 1992; Ray et al., 1993). A single powerstroke of the motor generates a force of ~6 pN (Svoboda et al., 1993). On the basis of the step size and the maximum force the maximum work done per step is 48 pN·nm. Kinesin is doing this work at each single step. Under cellular conditions, the free energy derived from ATP hydrolysis is about 100 pN·nm, *i.e.* the kinesin motor works with a 50% efficiency (Howard, 2001).

Within cells, kinesin pulls the cargo over long distances to a predefined destination. The highly processive movement requires a tight coordination of both motor domains during the catalytic cycle to prevent a simultaneous dissociation.

The unidirectional movement of kinesin is accompanied by a large conformational change within the neck linker. A crucial step to coordinate the teamwork between both heads is the affinity of kinesin to the microtubule what depends on the type of nucleotide bound. Free in solution, the molecule rests in an inactive ADP-bound form where the neck linker is in equilibrium between a disordered and a docked conformation (Sindelair et al., 2002). The catalytic cycle is initiated upon microtubule binding (Figure 11). During hydrolysis chemical and mechanical cycles are coupled. A chemical step (nucleotide binding/release) catalyzes a mechanical step (head attachment/detachment) and *vice versa*. Microtubule binding leads to a rapid release of ADP and its replacement by ATP. During this step only 50% of the ADP is released immediately (100 s^{-1}). The other half comes off with a low rate (0.01 s^{-1}) indicating that when one kinesin head is attached in the absence

of a bound nucleotide, the other head cannot attach in a conformation that promotes ADP release (Howard, 2001). The binding of ATP causes a large conformational change within the catalytic core pulling the trailing head (B) 16 nm forward to the next tubulin dimer. Within this conformational change, the C-terminus of the neck linker, formerly pointed rearward to the microtubule minus end (Figure 11, frame 1, red linker), points now towards the microtubule plus end, what is accompanied by neck-linker docking (Figure 11, frame 2, yellow linker). The immobilized, docked neck linker causes to the detachment of the trailing head (B). After a diffusional search, the now becoming leading head (B) binds tightly to the tubulin. In this intermediate state, both heads are temporarily bound to adjacent tubulins. Upon binding of the new leading head (B), the release of ADP is accelerated. At the same time, ATP hydrolyzes to ADP-Pi in the trailing head (A). After Pi release conformational changes cause neck-linker undocking (Figure 11, frame 4, red linker). ATP binding in the leading head (B) causes a docked neck-linker conformation (Figure 11, frame 4, orange linker). The trailing head (A), which has released its Pi, is now in the state of being pulled forward starting the next cycle (Schief and Howard, 2001; Kasprzak and Hajdo, 2002; Asbury et al., 2003; Shao et al., 2006; Skowronek et al., 2007).

The conformational changes within the kinesin molecule are nucleotide dependent and arise from an intrinsic communication of the microtubule-binding site with the nucleotide site and the neck linker. The presence or absence of phosphate groups are sensed by a so-called nucleotide-state sensor (Kull et al., 1996; Sack et al., 1997; Kikkawa et al., 2001). Depending on the nucleotide state, this sensor performs a small move, resulting in the transmission to the catalytic core.

In the past, researchers focused on the question what kind of walking machine kinesin represents. Recently, Kaseda et al. (2003) and Asbury et al. (2003) found evidence that kinesin exhibits alternating fast and slow molecular steps. This kind of limping suggests that kinesin moving underlies a left-right walking action, called asymmetric hand-over-hand motion.

Alternatively to the hand-over-hand model, a so-called inchworm model is proposed. Similar to the movement of a caterpillar, it was thought that kinesin extends the leading head and drags the other one to meet it. In this model, always the same head is leading and the other one drags behind (Hua et al., 2002). But, this model has not found general approval due to experimental results which favour the hand-over-hand model.
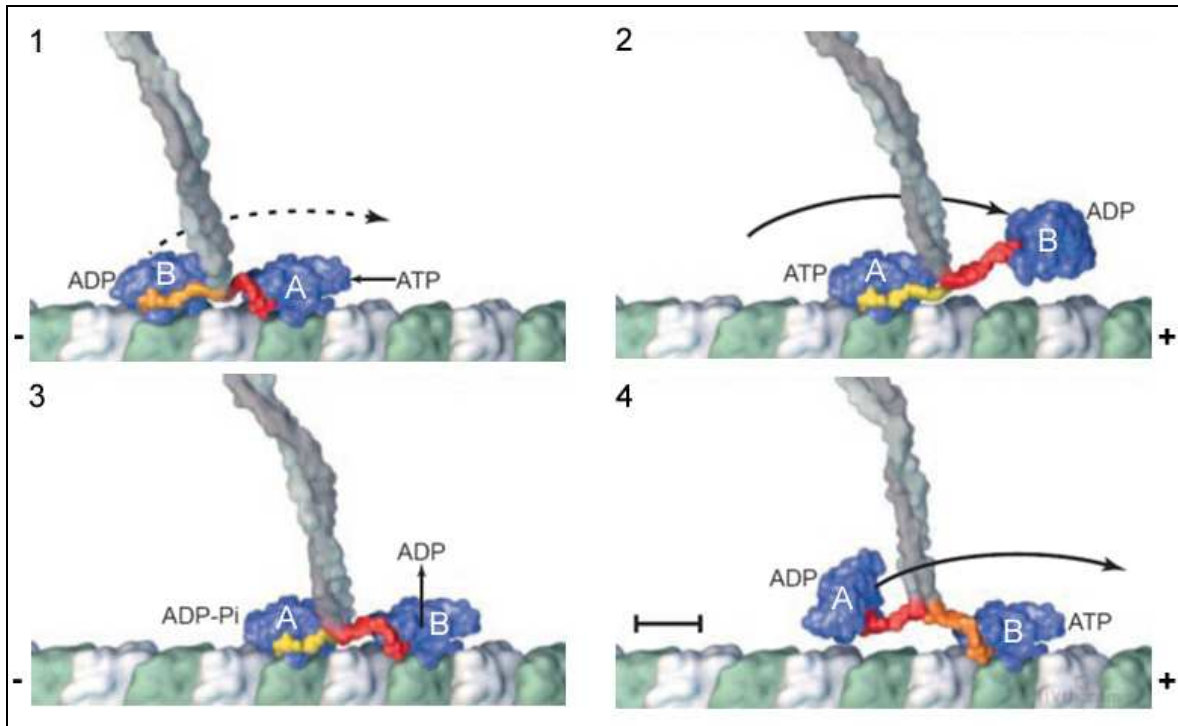
Figure 11: *Hand-over-hand model for kinesin motility.*
The two heads of the kinesin dimer work in coordinated manner to move processively along the microtubule protofilament (green: β-tubulin, light grey: α-tubulin). The kinesin molecule is depicted up to its coiled-coil region (dark grey). During the catalytic cycle the neck linker undergoes a series of conformational changes (partly docked: orange, docked: yellow, undocked: red). The picture is adapted from Vale (2000).

2.2.3 Eg5 kinesin

The Eg5, which belongs to the kinesin-5 family, is also a plus-end directed molecular motor. The protein is crucial for the assembly and organization of the mitotic spindle, representing a dynamic microtubule-based structure that orchestrates chromosome segregation in dividing cells.

In contrast to kinesin-1, Eg5 is a homotetrameric protein of two dimers forming an antiparallel coiled-coil tetramer containing four motor domains (Figure 7). The tetrameric structure of Eg5 makes it superior for cross-linking two adjacent microtubules (Figure 12) and sliding them apart (Kapitein et al., 2005; Krzysiak et al. 2006). It has been shown that Eg5 deletion leads to abnormal spindle formation.

To gain insights into the mechanochemical cycle of Eg5, recombinant truncated monomeric and dimeric constructs were expressed (Cochran et al., 2004; Krzysiak et al., 2006). Like kinesin-1, the dimeric Eg5 is a processive motor protein, albeit it moves at

very low velocities of around 40 nm s^{-1} (Kalchishkova and Böhm, 2008) along the microtubule. Both kinesin family members share a similar mechanochemical cycle. But, unlike kinesin-1 taking hundreds of steps before dissociating, Eg5 was found to take 8-10 steps. The limited processivity is suggested to be required for the cooperative work of multiple motors within the spindle to realize efficient sliding (Valentine et al., 2006).
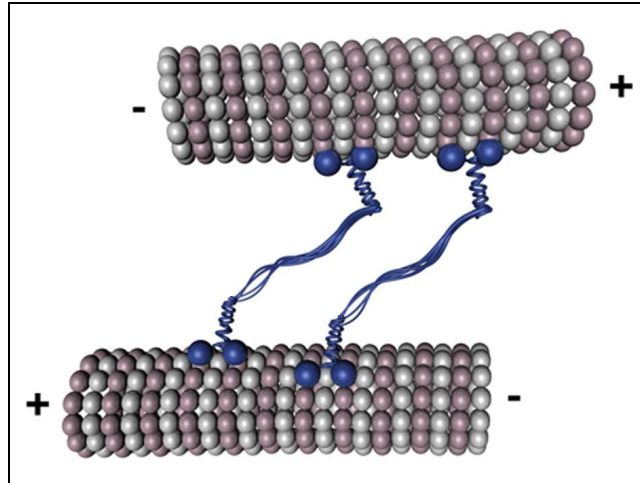
Figure 12: *Eg5 cross-linking anti-parallel microtubules.*
Eg5 can slide microtubules apart by walking to the plus end of each microtubule.

The interaction of different kinesin family members inside the cell is complex. Recently, it was found that Eg5 plays a key role in the development of the nervous system (Myers and Baas, 2007). Therefore, it can be assumed that KIF5A encounters the slowly moving Eg5 during its long-distance transport. The question what happens if both motor proteins converge is still unanswered.

3 MATERIALS AND METHODS

3.1 Protein preparation

3.1.1 Expression and purification of motor protein constructs

The kinesin constructs (KIF5A$_{fl}$, KIF5A$_{560}$, KIF5A$_{330}$, Eg5$_{513}$; Table 1) were expressed in *E. coli* as recombinant proteins after the protocol recently described (Kalchishkova and Böhm, 2008; Kalchishkova, 2008).

Construct	Molecular mass (kD)
KIF5A$_{fl}$	120
KIF5A$_{560}$	63.5
KIF5A$_{330}$	36.9
KIF5A$_{330}$S	38
Eg5$_{513}$	57.6

Table 1: *Theoretically calculated molecular masses of the constructs used.*
The molecular masses were calculated on the basis of their amino acid sequence.

The corresponding pTYB vectors encoding the C-terminally truncated kinesin constructs or chimeric proteins were transformed in *E. coli* strain ER 2566 (New England Biolabs) and expressed as fusion proteins with a C-terminal chitin-binding intein tag. *E. coli* cells were grown first in LB-medium with 50 µg ml^{-1} carbenicillin at 37°C overnight and sedimented (5000 rpm, 5 min, 4°C in a Sorvall centrifuge, using an angle-fixed rotor SLA-1000). The pellet was resuspended in culture medium, containing 0.1% N-Z-amine, 94.2 mM NaCl, 72 mM Na$_2$HPO$_4$, 2.2 mM KH$_2$PO$_4$, 18.6 mM NH$_4$Cl, 1 mM MgSO$_4$, 0.4% glucose, and 50 µg ml^{-1} carbenicillin, and grown at 37°C until reaching an optical density of ~0.8 at 600 nm. Protein expression was induced by adding 0.1 mM IPTG.

After growing for 16 h at 16°C, the cells were harvested (5000 rpm, 5 min, 4°C in a Sorvall centrifuge, using an angle-fixed rotor SLA-3000) and resuspended in lysis buffer (PBS, with additional 360 mM NaCl, 0.1 mM EDTA, 0.1% TritonX-100, pH 7.4), supplemented with 1 mM Pefabloc (Roche, Germany), 1 mM sodium ATP, and 40 ng ml^{-1} DNase I. A crude extract was obtained by a triple passage of the cells through a French Press. After obtaining a clear extract by a high speed centrifugation (35000 rpm, 45 min, 4°C, using a Beckman Optima ultracentrifuge and an angle-fixed Ti 50.2 rotor), the fusion protein was bound to chitin beads (New England Biolabs) by 1 h incubation at 4°C. After washing with lysis buffer, the beads were incubated in elution buffer (20 mM NaH$_2$PO$_4$, 500 mM NaCl, 1 mM EDTA, 0.1% Triton X-100, pH 7.4) containing 1 mM Pefabloc and 50 mM DTT for 40 h at 4°C under rotation. At this step, the DTT induces the release of the intein tag from the motor protein construct, which thereafter can be easily separated from the chitin beads by high speed centrifugation (25 000 rpm, 45 min, 4°C in a Beckman Optima ultracentrifuge, using an angle-fixed Ti 50.2 rotor). The proteins were concentrated by centrifugation (6000 rpm, 45 min, 4°C in an angle-fixed rotor 8 x 50 ml, Sigma 3K30 centrifuge; Sigma Laborzentrifugen GmbH, Germany) in Amicon ultra filter units (Millipore) with different pore diameters according to their molecular weight and stored in motility buffer (50 mM imidazole, 0.5 mM MgCl$_2$, 0.5 mM EGTA, and 0.5 mM DTT, pH 6.8) supplemented with 150 mM NaCl and 1 M glycerol at -80°C (Kalchishkova, 2008). The resulting protein samples lack any artificial tags or sequences. The protein concentration was determined by the Lowry method (Lowry et al., 1951) using BSA as standard.

Analogously, the fusion protein (KIF5A$_{330}$S) consisting of the KIF5A motor domain and a streptavidin-binding tag was expressed and purified (Table 1). The KIF5A$_{330}$S was cloned into the pTYB2 vector (New England Biolabs) after amplification using 5`- ttt aag *cta gca* tgg cgg aga cca aca acg -3` as N-terminal primer (with NheI cloning site in italics) and 5`- ttt aaa *ctc gag* ttt ttc gaa ctg cgg gtg gct cca agt gtt ctt aat ggt ctt tgc ccg c – 3` as C-terminal primer (with XhoI site in italics) and the parental vector encoding for the KIF5A$_{330}$. The sequences underlined encode for the tag (WSHPQFEK) which had been added to the C-terminal end of the KIF5A$_{330}$. Concerning its mechanochemical properties, the KIF5A$_{330}$S was undistinguishable from the KIF5A$_{330}$ lacking the streptavidin-binding tag.

3.1.2 Electrophoretic characterization of motor protein constructs

The expressed and purified motor proteins were characterized by electrophoresis using 7.5% SDS-polyacrylamide (Carl Roth, Germany) gels (Figure 13, Figure 14, Figure 15, Figure 16). The samples were incubated at 95°C for 5 min in Laemmli sample buffer (50 mM TRIS-HCl, pH 6.8, 2.5 mM EDTA, 2% SDS, 5% glycerol, 2.5% β-mercaptoethanol, 0.01% bromphenol blue; Laemmli, 1970). The proteins were loaded onto the gel (6 μg per lane) and separated in running buffer (2.5 mM TRIS-HCl, 0.01% SDS, 19.2 mM glycine) at 25 mA for at least 1 h. A broad range protein standard (covering the range between 6.5 kD and 205 kD) was used (SIGMA-ALDRICH, Germany). Gels were stained for 30 min in 0.2% Coomassie Blue R solution (Carl Roth, Germany). Thereafter, the gels were rinsed with distilled water, destained with a solution of 10% acetic acid and 20% ethanol, and treated for 20 min in a mixture of 10% glycerine and 20% methanol. Before drying, the gels were documented by a Duoscan T1200 scanner (AGFA).
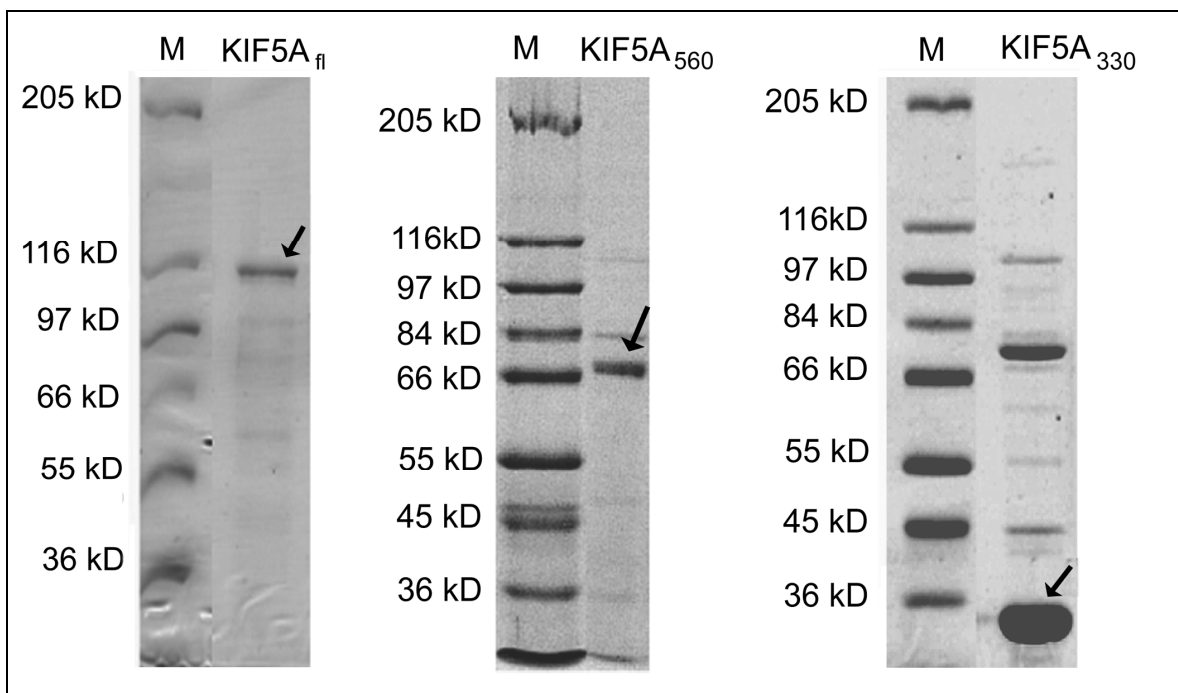
Figure 13: *SDS gels of the purified KIF5A constructs.*
M: molecular mass standard.
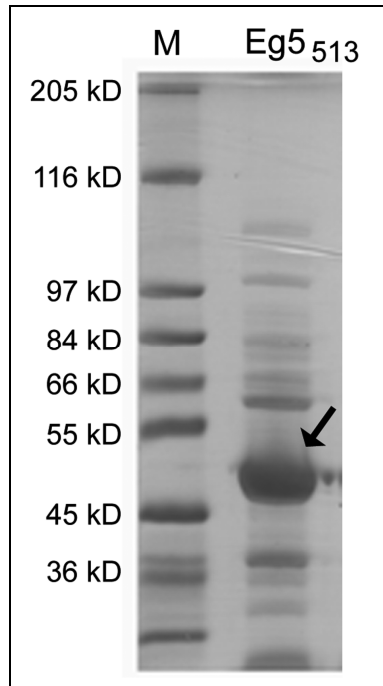
Figure 14: *SDS gel of the purified Eg5$_{513}$.*
M: molecular mass standard.
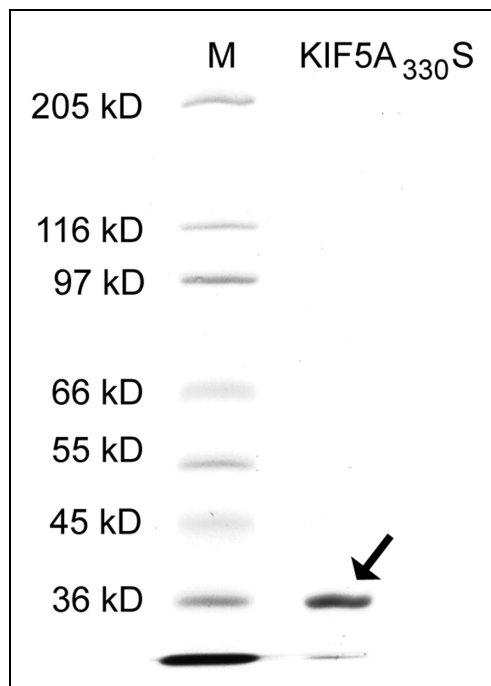
Figure 15: *SDS gel of the purified KIF5A$_{330}$S.*
M: molecular mass standard.
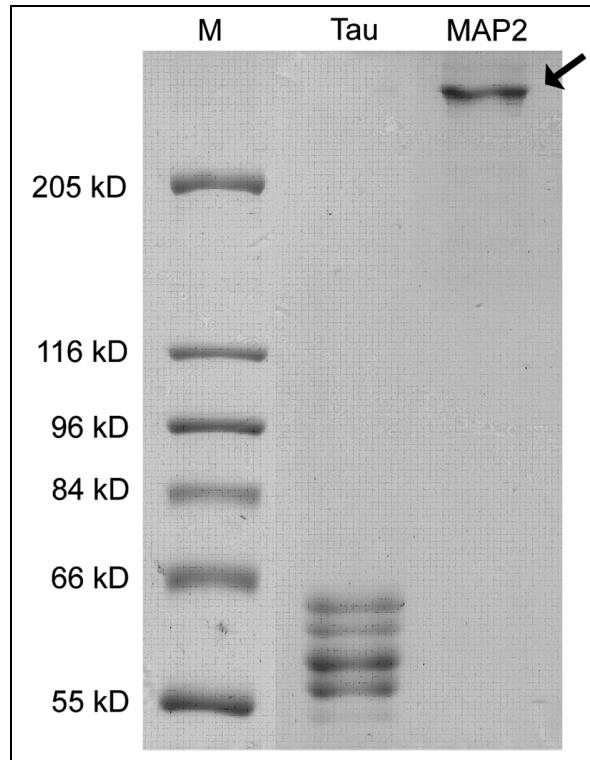
Figure 16: *SDS gels of the purified MAPs.*
Electrophoresis revealed four subspecies of tau with molecular masses between ~56 kD - 64 kD and a MAP2 fraction with a molecular mass of ~280 kD. M: molecular mass standard.

3.1.3   Preparation of tubulin and microtubules

The tubulin was purified from porcine brain homogenates by two cycles of temperature-dependent disassembly/reassembly (Shelanski et al., 1973) followed by phosphocellulose column chromatography (Weingarten et al., 1979). Microtubules were formed by taxol-promoted self-assembly at 37°C from tubulin (20 µM) in assembly buffer (20 mM PIPES, 80 mM NaCl, 1 mM EGTA, 0.5 mM $MgCl_2$ at pH 6.8). The microtubules prepared were free of associated proteins and typically consisted of 12 protofilaments (Böhm et al., 1984).

3.1.4   Preparation of MAPs

3.1.4.1   MAP2 and tau purification

The tubulin was purified from porcine brain homogenates by two cycles of temperature-dependent disassembly/reassembly (Shelanski et al., 1973) followed by phosphocellulose

column chromatography (Weingarten et al., 1979). The MAP fraction, eluted from the cellulose by 0.6 M KCl in assembly buffer containing 1 mM DTT was concentrated by centrifugation (10 kD filter, Millipore) for 3 hours. The retentate was dialyzed for 15 hours against 2 l cold assembly buffer. The dialysat was hold for 5 minutes at 95°C. After centrifugation (40000 rpm, 45 min, 2°C, using the rotor 50.2Ti, Beckman Optima ultracentrifuge) the extract was sieved by using a 100 kD filter (Millipore). The tau proteins which passed the the filter were concentrated by ultrafiltration using a 10-kD filter (Millipore) and stored in assembly buffer at -80°C. The retentate, containing MAP2 (molecular mass ~280 kD), was stored in assembly buffer at -80°C.

3.1.4.2 Determination of assembly promoting activity

The activity of MAP2 and tau to promote microtubule formation was proved by recording tubulin assembly at different MAP-to-tubulin ratios. For this, purified tubulin (20 µM) was allowed to form microtubules by self-assembly at 37°C in the presence of varying amounts of tau (Figure 17a) or MAP2 (Figure 17b) and 0.5 mM GTP. Microtubule formation was recorded by measuring the turbidity at 360 nm (UV/VIS Spectrophotometer Cary 4E, Varian). After 45 minutes, 20 µM taxol was added.
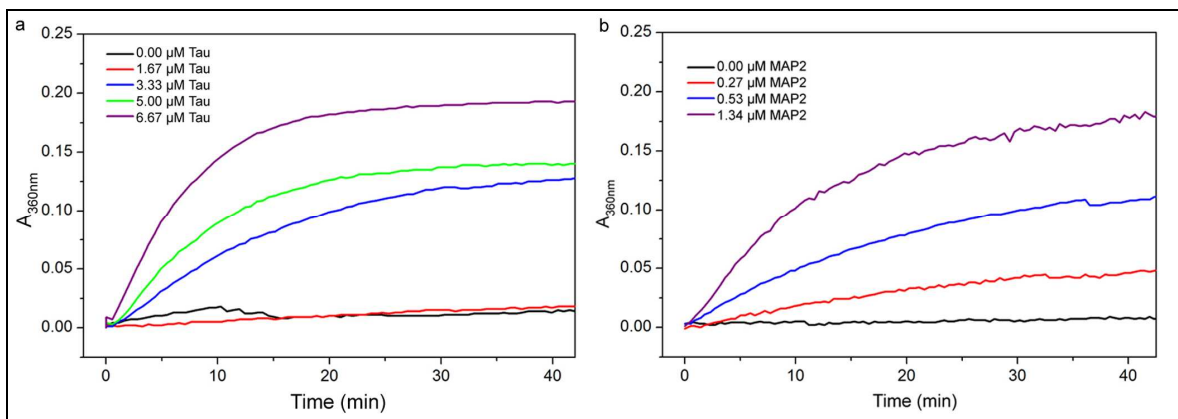
Figure 17: *Promotion of tubulin assembly by purified MAPs.*
a) Tubulin assembly in the presence of tau.
b) Tubulin assembly in the presence of MAP2.

3.1.4.3   Demonstration of tau binding to microtubules

Microtubules were formed by tubulin (20 µM) self-assembly at 37°C in the presence of 5.7 µM tau and 0.5 µM GTP corresponding to a tau-to-tubulin ratio of ~0.3. After 45 min assembly, taxol (final concentration of 20 µM) was added. The tau-complexed microtubules were allowed to sediment by centrifugation (45 min, 40000 rpm, TLA45 rotor, Beckman Optima TLX). The sediment was separated from the supernatant and resuspended in assembly buffer. SDS-gel electrophoresis was performed for each fraction (Figure 18). Control experiments were performed according to the same protocol ommitting the addition of tau (Figure 18, supernatant 1 and sediment 1). Around 60% of the whole amount of tau added, sedimented with the micotubules.
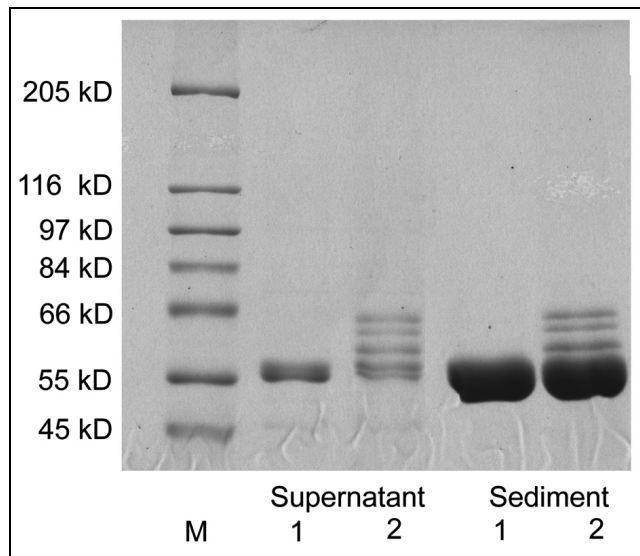
Figure 18: *SDS gel documenting tau binding to microtubules.*
Supernatant 1: Control-microtubules obtained from pure tubulin in the absence of tau; supernatant 2: microtubules obtained from pure tubulin in the presence of 5.7 µM tau; sediment 1: sedimented microtubules in the absence of tau; sediment 2: tau-complexed microtubules; M: molecular mass standard.

3.2 Motility measurements and ATPase activity determination

3.2.1 Motility measurements

3.2.1.1 Gliding assay

Kinesin (40 nM; final concentration), taxol (10 µM), NaCl (1 mM; final concentration), and MgATP (5 mM, final concentration) in motility buffer were mixed with microtubules (final concentration of 8 µM tubulin). The mixture was transferred onto the glass slide pretreated with casein (5 mg ml^{-1}, SIGMA-ALDRICH) and covered by a coverslip. Microtubule gliding was monitored by AVEC-DIC microscopy (see 3.3.1). Gliding velocities of individual microtubules were determined from video records by measuring the distance the microtubules were moved within a defined time or, alternatively by using Argus-20 software during observation.

3.2.1.2 Bead assay

The bead assay was performed in a flow chamber formed between a glass slide (76 mm x 26 mm) and a coverslip (18 mm x 18 mm) (Figure 19). The kinesin-bead suspension was applied to the one end and excess of liquid sucked off with filter paper from the other end. The 20-nm gold beads were needed to visualize the movement of kinesin along the microtubules.
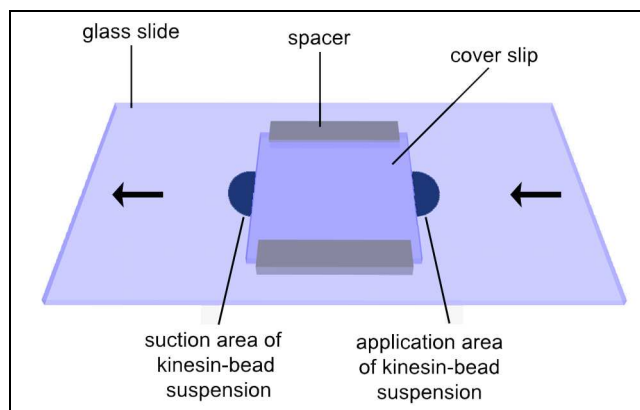
Figure 19: **Illustration of the flow chamber used for bead assay.**
The bead assay was performed in a narrow flow chamber between a glass slide and a coverslip spaced by rubber cement.

Preparation of block protein-complexed microtubules

For irreversible block protein binding on the microtubule surface taxol-stabilized microtubules (20 μM tubulin) were mixed with different amounts of blocking proteins in the presence of the non-hydrolyzable ATP analogue AMP-PNP (2 mM) or tripolyphosphate (pentasodium salt, SIGMA-ALDRICH, Germany). Under these conditions both motor domains (heads) of a kinesin dimer are believed to bind to the microtubule. For blocking, beside the dimeric $KIF5A_{fl}$ and $KIF5A_{560}$ also the monomeric $KIF5A_{330}$ was applied. Correspondingly, the head-to-tubulin ratio was used to compare the effects of block proteins with different dimensions. After binding to the glass surface (pretreated with PDDA, SIGMA-ALDRICH) and casein (5 mg ml^{-1})), the microtubules were chemically fixed for 15 min by fresh glutaraldehyde (0.1%, grade I, SIGMA-ALDRICH), which guarantees an irreversible binding of block proteins to the microtubule surface. Residual active aldehyde groups were neutralized by 15-min treatment with glycine (0.1 mM, SIGMA-ALDRICH; Böhm et al., 2001). As a result, microtubules were obtained with a reproducible density of blocking molecules, which occupy kinesin binding sites on the microtubule surface. For control experiments, microtubules without block proteins were bound to pretreated glass slides and chemically fixed. Chemical fixation of microtubules by low-concentrated glutaraldehyde does not impair the kinesin-driven transport of gold beads (Böhm et al., 2001; Boal et al., 2006; Dreblow et al., 2009).

In the case of reversible binding, glutaraldehyde fixation and glycine treatment were omitted to keep the block proteins in native state. The other preparation steps coincide with those described for irreversible binding.

Kinesin binding and gold bead transport

As transporter protein, $KIF5A_{fl}$ was used throughout this study. Kinesin (90 ng in motility buffer) was 100-fold diluted in distilled water and allowed to bind to $9.1 \cdot 10^9$ beads (20-nm gold colloid, SIGMA-ALDRICH). After adding 10-fold concentrated motility buffer to restore normal motility buffer conditions, 10 μl of this bead suspension were mixed with 9 μl casein (10 mg ml^{-1}; SIGMA-ALDRICH) and 1 μl MgATP (10 mM; SIGMA-ALDRICH) and allowed to bind to the blocked microtubules, immobilized onto the glass slides (Figure 20). The transport of the gold beads was monitored by AVEC-DIC microscopy (see 3.3.1).
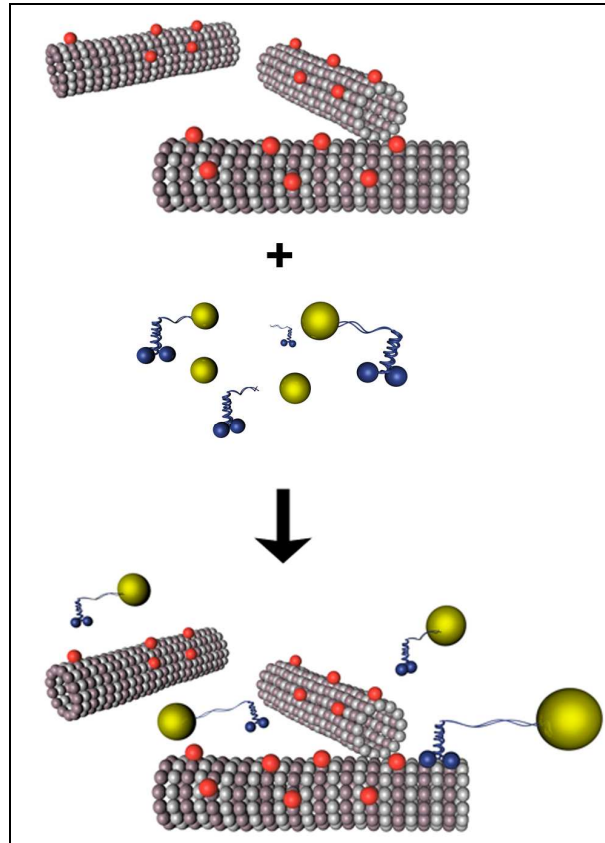
Figure 20: *Illustration of bead assay preparation.*
Microtubules were decorated with block proteins and immobilized on a glass surface. Afterwards, kinesin-complexed 20-nm gold beads were allowed to bind and move along the microtubules in the presence of ATP.

3.2.2 ATPase activity determination

The catalytic activities of the recombinant kinesins in the presence of MAPs were determined by measuring the free inorganic phosphate released during ATP hydrolysis, using a Malachite green staining technique (Biomol, Germany; Martin et al., 1985).

Taxol-stabilized microtubules complexed with MAPs at varying MAP-to-tubulin concentrations (MAP2 0.13 µM - 1.32 µM, tau 0.12 µM - 1.19 µM) were mixed with 35 nM KIF5A$_{560}$. ATP hydrolysis was initiated by adding MgATP (SIGMA-ALDRICH) at final concentrations of 2 mM. After 25 min incubation at 37°C the reaction was stopped by addition of HCl (0.1 N final concentration). The phosphate content was assayed after addition of the Malachite-green stain and 25-min incubation in the dark by reading extinctions at 650 nm in triple aliquots. The values obtained were plotted against the microtubule (tubulin) concentration. Exponential fitting of the plot, using Microcal Origin 7.5 software (Additive GmbH, Germany) provided the k_{cat} value.

3.3 Microscopy

3.3.1 Light microscopy

Movement of the gold beads along the microtubules was visualized by Allen video-enhanced differential interference contrast microscopy (AVEC-DIC) using an Axiophot microscope (ZEISS, Germany) with an oil immersion objective (100x/1.30), equipped with a Chalnicon video camera (HAMAMATSU PHOTONICS GmbH, Germany) and the image processing system Argus 20 (HAMAMATSU), which enables background subtraction and electronic contrast enhancement.

The differential interference contrast microscopy is based on the visualization of structures by contrast. Hereby, light first passes a polarizer and becomes laterally split-up by a Normaski prism into two coherent wave fronts with equal amplitude, but perpendicular oriented oscillations plane. At the same time, the Normaski prism induces an optical retardation between both wave fronts. The condenser parallelizes the wave fronts which have to pass the object level at a certain distance to each other. This distance is in real below the resolution limit. The wave fronts pass a second Normaki prism where they get merged. The second polarizer, called analyzer, results in interferences between the merged wave fronts (Figure 21). The relief-like image contrast obtained, reflects the optical retardation of both wave fronts. Steep reliefs are preferentially detected at edges of the sample due to the greatest density differences. The steepness of the reliefs depends on the difference in the refractive indices of a detail and its surround shape of details and the optical retardation (Allen et al., 1981). Finally, the video image processing system removes background noise and electronically amplifies the contrast.

The application of AVEC-DIC microscopy enables the examination of natural occurring proteins lacking any tags or fluorochromes, required by alternative methods like fluorescence microscopy. Moreover, an excessive heating of the sample at high light intensities can be excluded.

Movement was documented on a digital hard-disk recorder. The video sequences, were digitized resulting in single images of 30 frames per second which were analyzed using a Plug-In (Beeg et al., 2008) for ImageJ (public domain software, http://rsbweb.nih.gov/ij/). The mean transport velocity, transport distance, and dwell time were calculated from trajectories the single beads moved. The motility parameters were

analyzed from the moment of bead binding to a microtubule up to final stopping or its detachment.
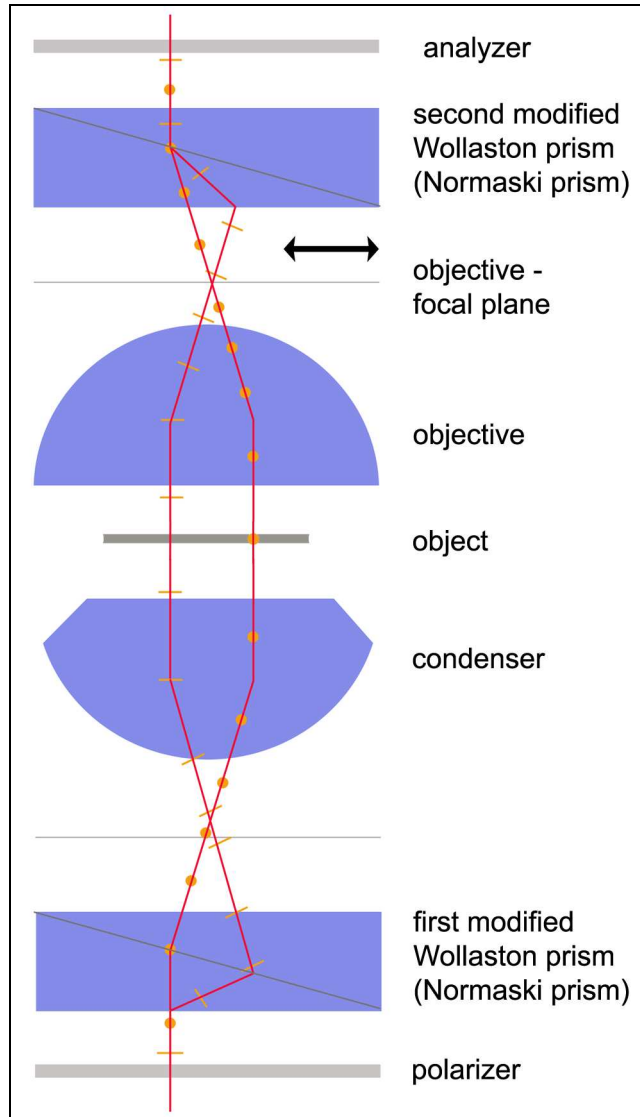
Figure 21: *Principle of the differential interference contrast (DIC).*
Images obtained by differential interference constrast exhibit shadowcast details due to gradients of the optical path introduced by interfaces (microtubules).

3.3.2 Transmission electron microscopy

To determine the number of block proteins bound to the microtubule transmission electron microscopy was used.

3.3.2.1 Visualization of KIF5A$_{330}$S on the microtubule surface

KIF5A$_{330}$S was bound to the taxol-stabilized microtubules under conditions described for KIF5A$_{330}$ blockages and labeled by a total amount of $2.8 \cdot 10^{10}$ 10-nm streptavidin-colloidal gold (SIGMA-ALDRICH, Germany). Afterwards, the gold-KIF5A$_{330}$S-microtubule complexes were fixed with glutaraldehyde (0.1%, SIGMA-ALDRICH), transferred to the Formvar/carbon-coated 400-mesh copper grids, and examined in a ZEISS CEM 902 transmission electron microscope (ZEISS, Germany). For control preparations, in the absence of blockages, taxol-stabilized microtubules were transferred to Formvar/carbon-coated 400-mesh copper grids and negatively stained with 1% uranyl acetate.

3.3.2.2 Immunogoldlabeling

MAP2 (1.7 mg ml^{-1} – 3.7 mg ml^{-1}) and tau (0.4 mg ml^{-1} – 0.7 mg ml^{-1}), respectively, were bound to taxol-stabilized microtubules (120 µM) and transferred to Formvar/carbon-coated 400 mesh gold grids. Afterwards, block protein-complexed microtubules were fixed for 15 min with glutaraldehyde (0.5%, SIGMA-ALDRICH) and subsequently washed with PBS (5 min; 137 mM NaCl, 2.7 mM KCl, 8.1 mM Na$_2$HPO$_4$, and 1.5 mM KH$_2$PO$_4$ at pH 7.2). Free aldehyde groups were blocked by 15-min incubation with freshly prepared NaBH$_4$ (26 mM) in PBS. Grids were washed once with PBS (5 min) and twice with PBS/0.5% Tween20 (15 min) to prevent unspecific antibody binding. The diluted primary antibody (anti-MAP2 (V:V 1:125) or anti-tau (V:V 1:1000), respectively, SIGMA-ALDRICH) was allowed to bind to the microtubules by 1 h incubation in a wet chamber. After triple washing with PBS/Tween20 (5 min) the grids were incubated for 1 h with the secondary antibody (anti-mouse IgG 10-nm gold conjugate, SIGMA-ALDRICH; V:V 1:2). Subsequently, before drying on air, the grids were washed twice with PBS/Tween20 (5 min) and double distilled water (5 min), respectively.

4 RESULTS AND DISCUSSION

4.1 Kinesin motility assay

A special feature of the motor protein kinesin is its relative robustness enabling force generation in cell-free environment. This, together with the possibility to be expressed in recombinant bacterial systems in large quantities, makes kinesin superior for exploitation in artificial force-generating devices.

To study the molecular mechanisms of kinesin-mediated force generation *in vitro*, two approaches, which mimic the intracellular transport, can be applied.

A simplified approach, the so-called gliding assay (Figure 22, Figure 23), can be used where the microtubules are propelled by surface-bound motor proteins. The high flexibility of the kinesin hinge (Figure 8) enables the motor domain to turn into one and the same orientation allowing microtubule binding and movement with their minus end leading.
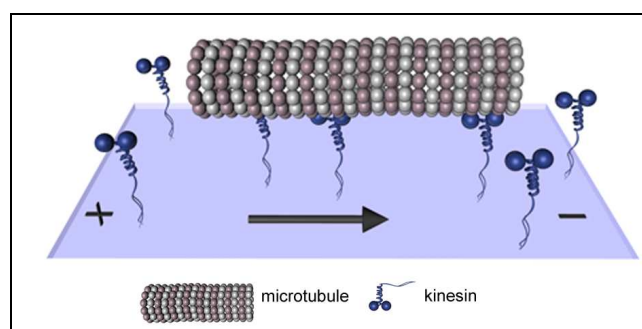
Figure 22: *Gliding assay.*
The plus-end directed motor kinesin, adsorbed to a surface, propels a microtubule with their minus end leading.
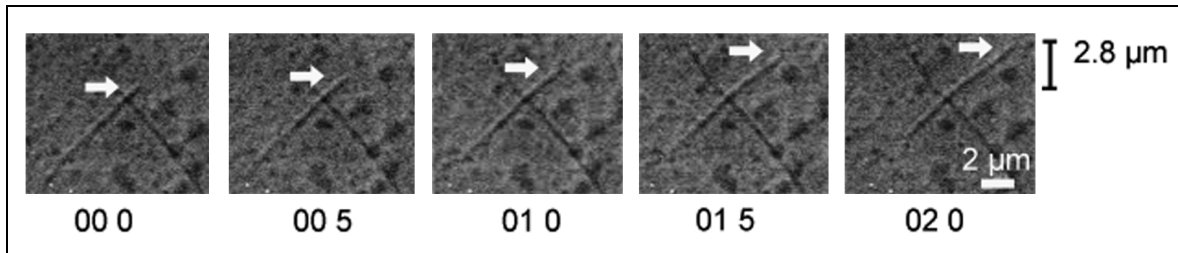
Figure 23: *Gliding assay image sequence.*
Microtubule gliding across a kinesin-coated glass surface. The moving microtubule is marked by an arrow. The time scale indicates seconds and tenth of a second. AVEC-DIC microscopy.

An alternative method to study kinesin-mediated motility is the so-called bead assay (Figure 24, Figure 25). Here, the microtubules are immobilized on a substratum and kinesin acting as a locomotive that is able to pull a cargo towards the microtubule plus end. Such cargo might be not only cell organelles or bio macromolecules, but also subjects made of technologically relevant materials like silicon, quartz, polystyrene or gold.

Throughout the present work, the bead assay was used due to its better control of single molecule behaviour, assembly, actuation, and functionalization.
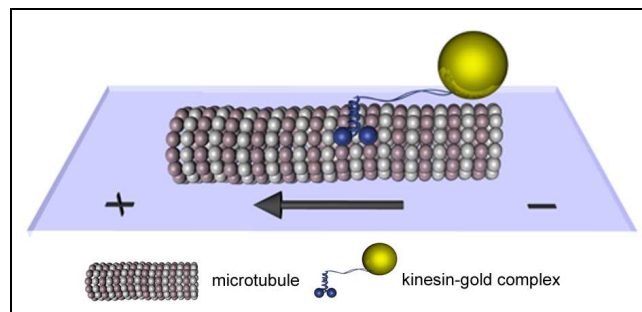
Figure 24: *Bead assay.*
The kinesin pulls its cargo like a locomotive from the minus to the plus end of the microtubule, immobilized on a substratum.
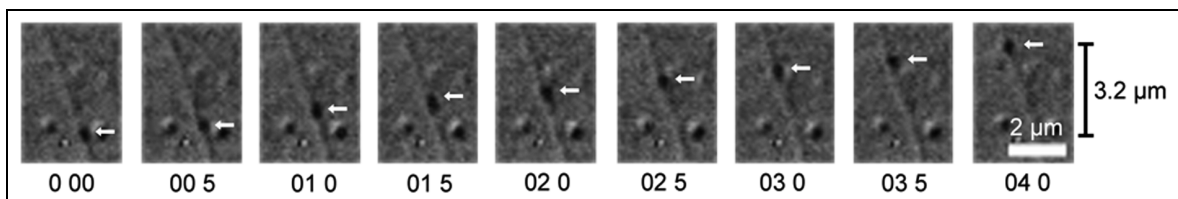
Figure 25: *Bead assay image sequence.*
Movement of a kinesin-complexed 20-nm gold bead along a microtubule. The moving bead is marked by an arrow. The time scale indicates seconds and tenth of a second. AVEC-DIC microscopy.

In the gliding assay, microtubules were found to be moved by kinesin at a mean velocity of 927 nm s^{-1} ± 104 nm s^{-1} (arithmetic mean ± SD). Kinesin-complexed gold beads were transported at a mean velocity of 784 nm s^{-1} ± 265 nm s^{-1} along the microtubule. Main differences become evident when the velocity frequency histograms are compared (Figure 26). For the bead assay the width of the frequency histogram was found to be strikingly greater. This discrepancy can be explained by the number of involved motor molecules. In the bead assay, 20-nm gold beads were used as artificial cargo. Due to the small surface area of a 20-nm bead, it is unlikely that multiple motors bind (see also 4.3.7). In this assay, single kinesin molecules, transporting the cargo along the rail, can easily be disturbed by irregularities in the microtubule lattice or by blocked binding sites resulting in a lowered mean velocity and a broader frequency. In the gliding assay, the microtubule is moved by the concerted work of multiple motors resulting in a uniformly velocity distribution.
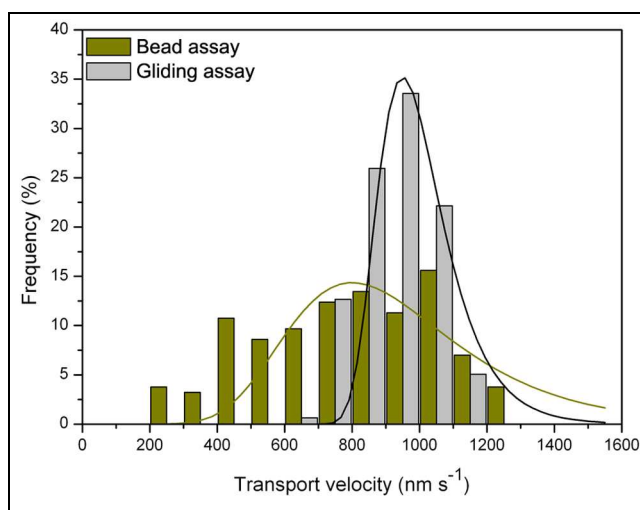
Figure 26: *Velocity histogram of kinesin motility assays.*
Velocity frequency histograms for the bead and the gliding assay, respectively. The x-values indicate velocity intervals ± 50 nm s^{-1}. 158 microtubules and 186 beads were measured for the gliding assay and bead assay, respectively.

4.2 Immobilization of microtubules by chemical fixation

By chemical fixation, proteins become cross-linked and fine structural details are stabilized without destruction. With cross-linking, two or more molecules are chemically joined by covalent bonds.

Due to its small size, glutaraldehyde rapidly penetrates into cells and insolubilizes proteins. Glutaraldehyde possesses two reactive CHO-groups which react with the amino groups of proteins to cross-link them (Figure 27). Hereby, both inter- and intramolecular protein bridges can be formed. Under neutral conditions, glutaraldehyde exists as a monomer whereby both aldehyde groups are fully reactive. Upon nucleophilic attack by the lysine residues in the protein, aldehydes are believed to form Schiff bases. Schiff bases are unstable and break down to regenerate the aldehyde and amine. Therefore, reducing agents convert the Schiff base into a stable secondary amine (Walt and Agayn, 1994). Nonetheless, cross-linking by glutaraldehyde (0.01 % - 0.1 %) was shown to effectively stabilize microtubules and extend their lifetime up to several days without affecting the ability of kinesin to bind to and move along microtubules (Boal et al., 2006).
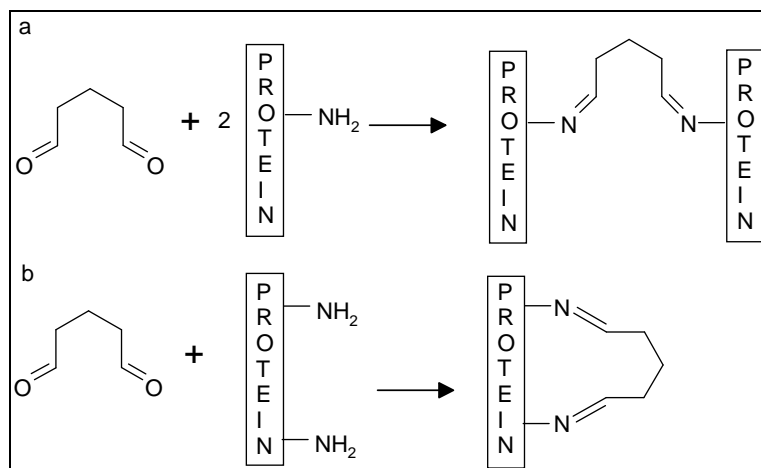
Figure 27: *Principle of glutaraldehyde fixation.*
Schiff base formation by glutaraldehyde.
a) Intermolecular cross-linking between proteins.
b) Intramolecular cross-linking.

Beside stabilization of proteins, glutaraldehyde can also be used to immobilize proteins onto solid matrices, functionalized by, *e.g.*, substances with free amino groups. In

the experimental approach used in this study, the block proteins were bound to the kinesin binding sites along the microtubule and chemically cross-linked by glutaraldehyde. Under these conditions, the microtubule looses its dynamic behaviour, becomes stabilized, and the kinesin blockages were irreversibly bound to the microtubule. To stabilize the cross-linked complex and to prevent unspecific protein binding, residual aldehyde groups were blocked by glycine.

To test whether under the conditions used in this study glutaraldehyde treatment impairs the kinesin-mediated movement, control experiments were performed with kinesin-complexed 20-nm beads moving along either, fixed or native microtubules in the absence of block proteins.

After fixation, the beads were observed to be transported continuously at a mean velocity of 789 nm s^{-1} ± 233 nm s^{-1}. Resting events were observed rarely. Experiments with native microtubules, not treated with glutaraldehyde, proved that chemical fixation does not affect the transport velocity (Figure 28). In this case, an average velocity of 784 nm s^{-1} ± 265 nm s^{-1} was measured. These results confirm the statement of Turner et al. (1996) that microtubule cross-linking by glutaraldehyde does not impair kinesin-mediated movement. Glutaraldehyde represents a small molecule not changing the charge of tubulin. Consequently, it is assumed not to hinder kinesin binding to the microtubule sterically or electrostatically.
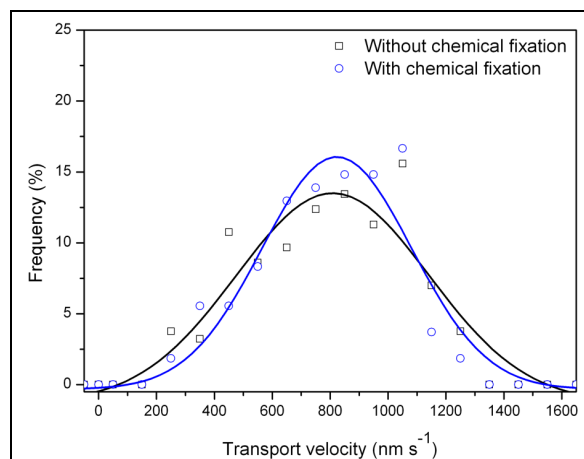
Figure 28: *Frequency diagram of velocity distribution of control experiments.*
Gaussian-like fitted velocity distribution measured for kinesin-coated beads moving along either glutaraldehyde fixed or non-fixed microtubules without block proteins. The x-values of the data points reflect the velocities of individual beads ± 50 nm s^{-1}. For statistics, individual beads were followed from the moment of binding to a microtubule up to their detachment. 185 and 163 beads were analyzed in the case of native and of chemically fixed microtubules, respectively.

4.3 Kinesin-mediated cargo transport in the presence of KIF5A

4.3.1 Strategy

In the crowded environment of a living cell, various motor proteins coexist while performing different motility functions. In addition to diverse kinesins and dynein, non-motile microtubule-associated proteins compete for microtubule binding with transporter proteins which might result in blocking motility. Little is known how kinesin maintains the long-distance transport when its path is blocked. Concerning this subject, Seitz and Surrey (2006) reported that the presence of a mutant kinesin not being able to step efficiently reduces the average speed without significant change of processivity. The authors concluded that kinesin waits in a strongly bound state till the blockage detaches and frees the binding site enabling kinesin to continue movement. In another approach where biotinylated microtubules were decorated with streptavidin (Korten and Diez, 2008) kinesin molecules were found to rest upon encountering blockages. The authors assume that passing is possible if the streptavidin blockage and kinesin do not occupy the same site on the microtubule. Alternatively, they suggested that kinesin temporarily detaches, diffuses along the microtubule lattice, and rebinds.

Intracellular transport processes might be impaired not only by reversibly bound blockages, but also by rigid blockages which might arise from stalled cargoes or by irregularities in the microtubule structure. So far, it has been not clear what happens when kinesin stalls or continues movement.

To contribute to understanding the molecular mechanisms in the case when transporting kinesin encounters blocked or defective binding sites, an experimental approach was worked out, were KIF5A was employed for both blocking and transporting. This approach guarantees that exactly the kinesin-binding sites along microtubules were occupied. In addition, the block proteins were chemically fixed by glutaraldehyde to prevent exchange.

4.3.2 Construct design

Usually, microtubules reconstituted from pure tubulin without additional proteins were used to investigate kinesin-dependent motility. To study the kinesin-dependent transport in the case of crowded microtubule rails, 20-nm gold beads were driven by kinesin along immobilized microtubules whose surface was covered by different block proteins. The block proteins were chosen due to their ability to compete with the transporter kinesin for the same microtubule binding site. Therefore, human full-length KIF5A with 1032 amino acids was used both as block protein and as transporter.

Additionally, truncated constructs were expressed to study how the length of a blockage affects motility. Experiments with a truncated KIF5A and the KIF5A motor domain, including amino acids 1-560 and 1-330, respectively, were performed (Figure 29).

The KIF5A constructs were produced in *E. coli* without an artificial tag. KIF5A$_{fl}$ and KIF5A$_{560}$ are dimeric proteins being able to move microtubules across glass surfaces at velocities between 800 nm s^{-1} - 1000 nm s^{-1}, which is in the same range as determined for kinesins purified from brain tissue (von Massow et al., 1989; Böhm et al., 2000) or from *Drosophila* embryos (Saxton et al., 1988). The KIF5A motor domain is a monomeric immotile protein lacking parts of the neck-linker and the complete neck, stalk, and tail region.
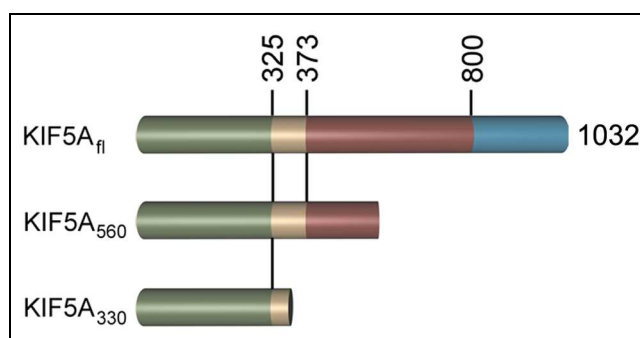
Figure 29: *Bar diagrams depicting the domain structures of KIF5A constructs.*
Full-length KIF5A served as both transporter protein and blockage. Additionally, the truncated construct KIF5A$_{560}$ and the motor domain KIF5A$_{330}$ were adopted to block kinesin binding sites. The motor domain is displayed in green, neck linker/neck region in ochre, stalk in red, and the tail domain in blue.

4.3.3 Effect of block protein size on kinesin motility parameters

4.3.3.1 Comparison of KIF5A$_{fl}$ and KIF5A$_{560}$ as block proteins

In the presence of a non-hydrolyzable ATP analogue, KIF5A$_{fl}$ or KIF5A$_{560}$ was tightly bound to microtubules and additionally cross-linked by glutaraldehyde. As a result, this KIF5A, irreversibly occupies kinesin-binding sites on the microtubule surface. Following, kinesin motility parameters were analyzed in dependence on the kinesin head-to-tubulin ratio, which determines the density of blockages bound to the microtubule surface.

In control preparations without block proteins, the beads were found to be moved by kinesin continuously at a mean transport velocity of 783 nm s^{-1} ± 194 nm s^{-1}.

When block proteins were irreversibly attached to the microtubules, bead movement was characterized by phases of transport alternating with resting ones (Figure 30, Figure 31). Accordingly, the mean transport velocity decreased. Between resting phases, the velocity was found to be nearly the same as in control experiments (compare the ascent of Figure 31b with that of the control experiment in Figure 31a).
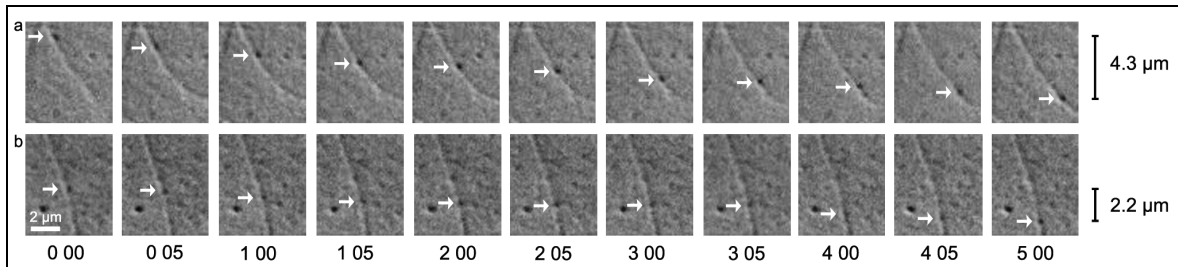
Figure 30: *Image sequences of kinesin-mediated bead transport along microtubules.*
a) Continuous transport in the absence of block proteins.
b) Discontinuous transport in the presence of KIF5A$_{fl}$ blockages at a head-to-tubulin ratio of 0.2.
The moving beads are marked by arrows. The time scale indicates seconds and tenth of a second. AVEC-DIC microscopy.

Figure 31: *Distance-time diagram in the presence of KIF5A$_{fl}$.*
a) Continuous transport in the absence of block proteins. Within the time interval of this sequence the mean transport velocity was 1061 nm s^{-1}.
b) Discontinuous transport with alternating phases of movement and resting observed in the presence of KIF5A$_{fl}$ blockages (mean velocity including resting phases 651 nm s^{-1}). KIF5A$_{fl}$ head-to-tubulin ratio 0.1. This value, which determines the density of block proteins bound along the microtubule, was calculated on the basis of the number of motor domains (heads) the blockages comprises. The data were obtained by measuring the X-Y-shift of single beads on digitized video sequences (30 frames per second).

Compared with the non-continuous movement (Figure 31), the transport velocity decreased exponentially in dependence on the head-to-tubulin ratio (Figure 32). For both, KIF5A$_{fl}$ and KIF5A$_{560}$, a comparable exponential dependence of the velocity plotted against the head-to-tubulin ratio was observed, which is documented by similar decay constants (0.14 *vs*. 0.18), respectively.

Figure 32: *Effect of KIF5A_{fl} and KIF5A_{560} on the velocity.*
a) Dependence of the mean transport velocity on the head-to-tubulin ratio in the case of blocking by KIF5A_{fl} and KIF5A_{560}, respectively.
b) Velocity frequency histogram in the absence of blocking proteins.
c,d) Velocity frequency histograms in the presence of KIF5A_{fl} and KIF5A_{560} block proteins, respectively. The x-values indicate velocity intervals ± 50 nm s^{-1}.
n - number of beads measured.

Parallel to the decrease of the mean transport velocity, there was a decrease of the mean distances the beads moved along the microtubules (Figure 33a). The final level the beads moved was found at ~2 µm. Increasing the head-to-tubulin ratio up to 0.4 did not cause a stronger decrease. However, there was a lowered frequency of bead binding at high head-to-tubulin ratios.

Moreover, with increasing density of block proteins on the microtubule surface, the mean dwell time of the beads moving along the microtubule showed a tendency to higher values (Figure 33b). But as a rule, once bound to the microtubule, moving beads were usually observed to be able to continue movement after resting phases without diffusion from the microtubule rail.

Figure 33: *Effect of KIF5A$_{fl}$ and KIF5A$_{560}$ on the transport distance and dwell time.*
a) Dependence of the mean transport distance (length of the trajectory single beads were moved from the moment of association with a microtubule upon its final stopping or detachment) on the head-to-tubulin ratio.
b) Dependence of the mean dwell time (time period single beads were moved from the moment of association with a microtubule upon their final stopping or detachment) on the head-to-tubulin ratio.
For statistical analysis ≥40 single beads per head-to-tubulin ratio were analyzed.

Both KIF5A constructs represent dimeric proteins. Due to the flexibility of the coiled-coil region, KIF5A$_{fl}$ and KIF5A$_{560}$ are partially compacted bound to the microtubule surface rather than fully extended (Kerssemakers et al. 2006). Correspondingly, both constructs exerted a comparable inhibition of motility of the transporter kinesin. It can be assumed that not only the kinesin binding sites along the microtubule are blocked. But, the stalk and the tail region might additionally act as a steric hindrance constraining the binding and movement of the transporter kinesin particularly at high head-to-tubulin ratios (Figure 34).
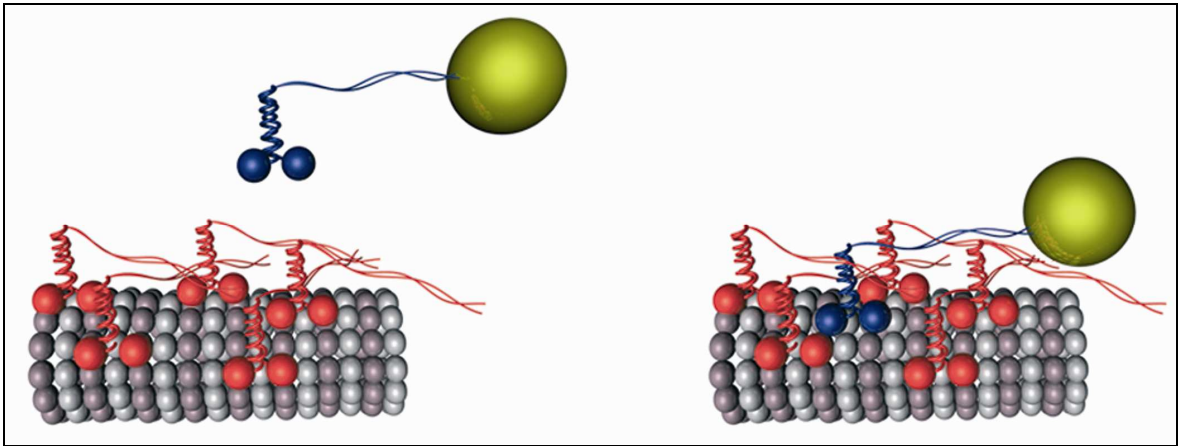
Figure 34: *Illustration of steric hindrance of kinesin binding and movement along the microtubule by KIF5A_fl.*

KIF5A_fl contains a pair of motor domains at the one end, followed by a long, highly flexible stalk and tail. The protein binds in a compact configuration with a height of 17 nm on the microtubule surface (Kerssemakers et al. 2006).

In the case of blocking by KIF5A_fl (red) two subsequent β-tubulins along the protofilament track are occupied. Beside the direct competition for binding sites along the microtubule, the stalk-tail part is considered to cause additionally a steric inhibition of binding and movement of the transporter kinesin (blue). The gold beads transported are depicted by yellow spheres.

4.3.3.2   Comparison of KIF5A$_{fl}$ and KIF5A$_{330}$ as block proteins

It was shown that KIF5A$_{fl}$ and KIF5A$_{560}$ exert a comparable effect on kinesin motility. To prove whether steric hindrance is caused by the long flexible stalk and tail region, the KIF5A was C-terminally truncated to obtain the motor domain, only. The kinesin-mediated transport was impeded in the presence of both, the long KIF5A$_{fl}$ and the short KIF5A$_{330}$ (Figure 35). But, in the presence of KIF5A$_{330}$ the resting phases were shorter than observed for KIF5A$_{fl}$ ones.
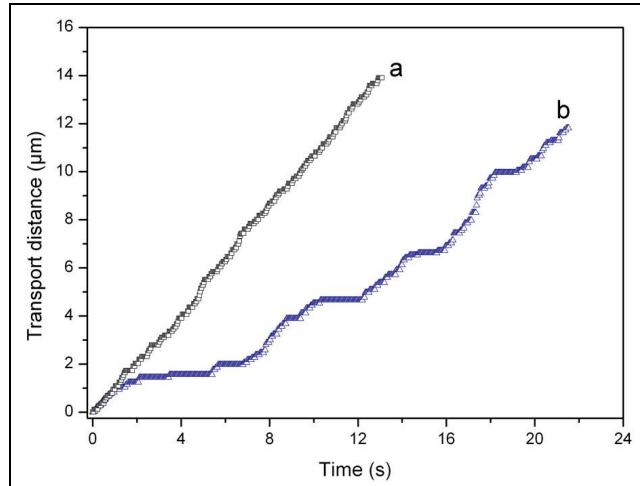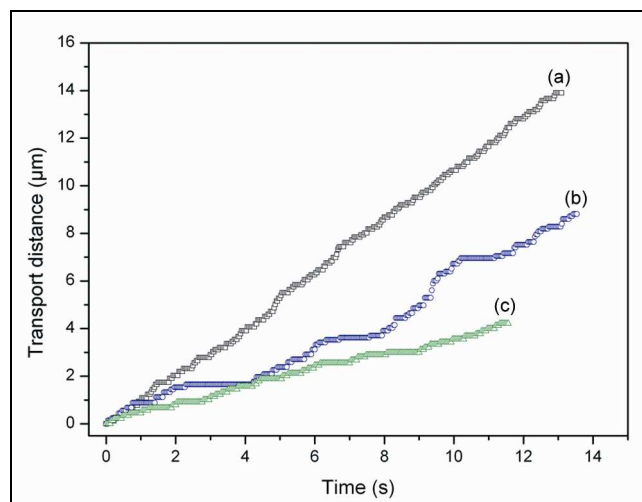

Figure 35: *Distance-time diagram in the presence KIF5A$_{fl}$ and KIF5A$_{330}$.*
a) Continuous transport in the absence of block proteins. Within the time interval of this sequence the mean transport velocity was 1061 nm s^{-1}.
b,c) Discontinuous transport with alternating phases of movement and resting observed in the presence of KIF5A$_{fl}$ and KIF5A$_{330}$ blockages, respectively. The mean velocities including the resting phases were 651 nm s^{-1} and 365 nm s^{-1}, respectively. The head-to-tubulin ratio was 0.1. This value, which determines the density of block proteins bound along the microtubule, was calculated on the basis of the number of motor domains (heads) the blockages comprises. The data were obtained by measuring the X-Y-shift of single beads on digitized video sequences (30 frames per second).

Both block proteins (KIF5A$_{fl}$ or KIF5A$_{330}$) caused the transport velocity to decrease exponentially in dependence on the kinesin head-to-tubulin ratio. But, at low head-to-tubulin ratios, the decrease was more pronounced in the case of the short KIF5A$_{330}$ compared to KIF5A$_{fl}$ (Figure 36), which is manifested by a significantly lower decay constant (0.01 *vs.* 0.18) determined by exponential fitting of the velocity data.
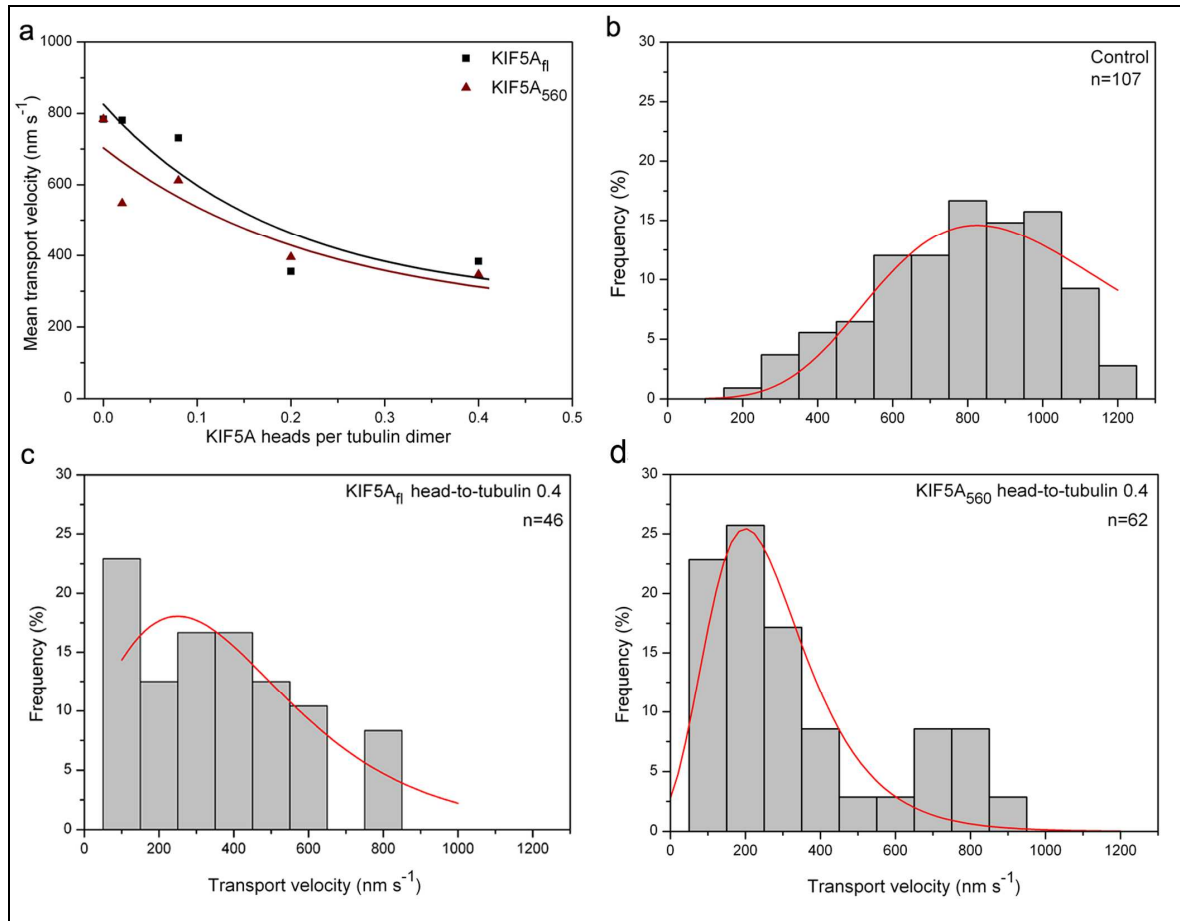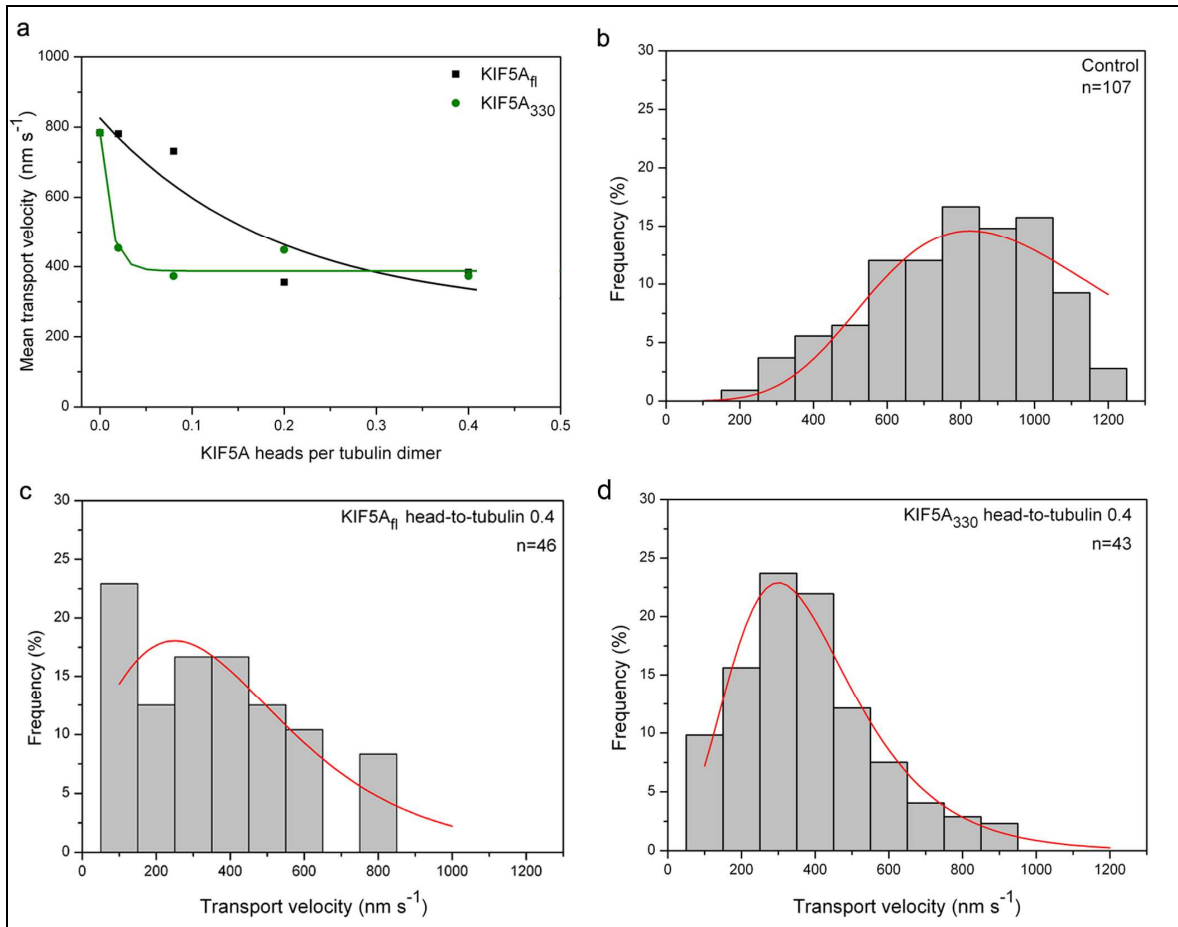
Figure 36: *Effect of KIF5A$_{fl}$ and KIF5A$_{330}$ on the velocity.*
a) Dependence of the mean transport velocity on the head-to-tubulin ratio in the case of blocking by KIF5A$_{fl}$ and KIF5A$_{330}$, respectively.
b) Velocity frequency histogram in the absence of blocking proteins.
c,d) Velocity frequency histograms in the presence of KIF5A$_{fl}$ and KIF5A$_{330}$ block proteins, respectively. The x-values indicate velocity intervals $\pm$ 50 nm s^{-1}.
n - number of beads measured.

Remarkably, in the case of KIF5A$_{330}$, increasing the head-to-tubulin ratio up to values >0.1 did not result in stronger velocity decrease. The microtubule surface seems rather to be saturated by block proteins. Increasing the head-to-tubulin ratio only caused the binding frequency of kinesin-complexed beads to the microtubule to be lowered, obviously due to the reduced number of free binding sites. But, even in this situation, more than 80% of the moving beads were able to overcome blockages after pausing without being released from its microtubule rail. In the other cases, the beads either detached from the microtubule or finally stalled.

Regardless of KIF5A$_{fl}$ or KIF5A$_{330}$ used as block proteins, movement was still observed over relatively long distances. Even at the highest blockage density the beads

were moved on average over 3.4 μm (for KIF5A$_{330}$ blockages; Figure 37a) and 2.0 μm (for KIF5A$_{fl}$ blockages; Figure 37a) without bead diffusion.
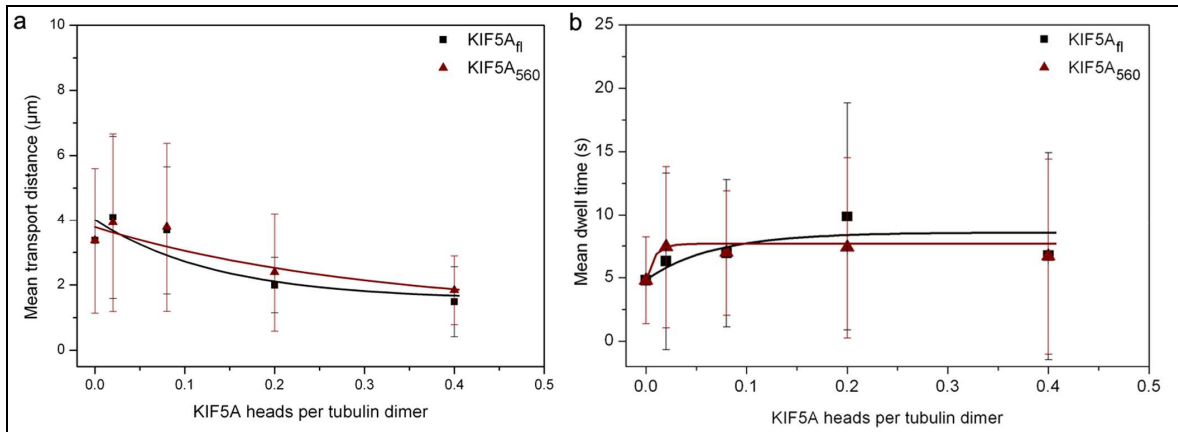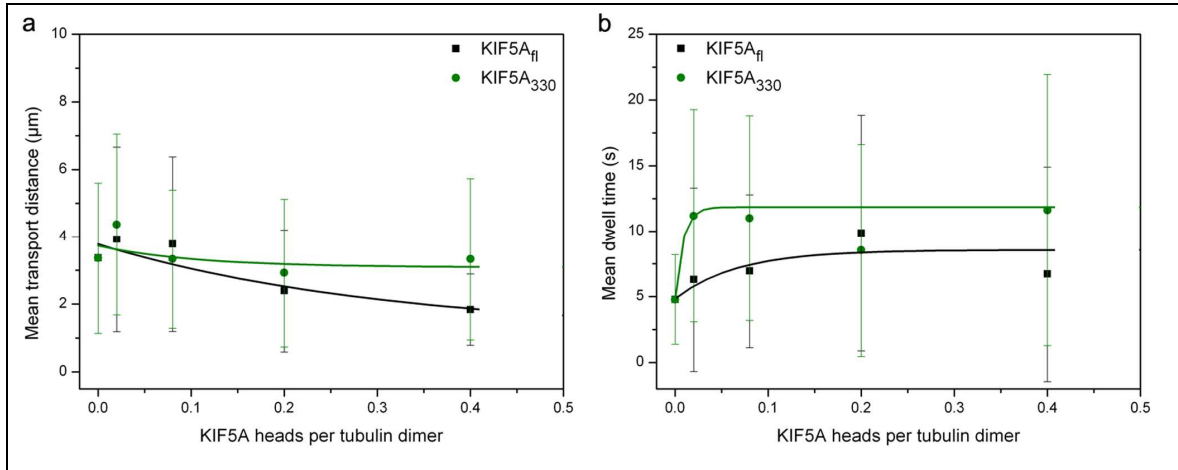

Figure 37: *Effect of KIF5A$_{fl}$ and KIF5A$_{330}$ on the transport distance and dwell time.*
a) Dependence of the mean transport distance (length of the trajectory single beads were moved from the moment of association with a microtubule upon its final stopping or detachment) on the head-to-tubulin ratio.
b) Dependence of the mean dwell time (time period single beads were moved from the moment of association with a microtubule upon their final stopping or detachment) on the head-to-tubulin ratio.
For statistical analysis ≥40 single beads per head-to-tubulin ratio were analyzed.

It has to be mentioned that lowering the mean bead transport velocity caused by the KIF5A motor domain was more pronounced. The result can be explained as follows: in the case of the dimeric full-length KIF5A two subsequent β-tubulins are blocked along the protofilament track. But, when KIF5A$_{330}$ is bound, the same number of kinesin heads is randomly distributed and not pairwise bound along the protofilament track. When the transporter kinesin encounters the blocked site, it seems to be unimportant whether the next but one kinesin binding site is free or not.

Moreover, the globular monomeric KIF5A$_{330}$ with dimensions around 7 nm -8 nm seems to bind more efficiently (Figure 38) to microtubules than the KIF5A$_{fl}$ with the complete neck, the long stalk and tail (Figure 34). Especially at higher head-to-tubulin ratios, the KIF5A$_{fl}$ blocks need more space which causes additionally a steric hindrance preventing binding and movement of the transporter kinesin along the microtubule surface. The observation that in the case of blocking by KIF5A$_{fl}$ the decrease of the mean transport distance (Figure 37a) was stronger and the resting phases were longer than with KIF5A$_{330}$ strengthen this suggestion.
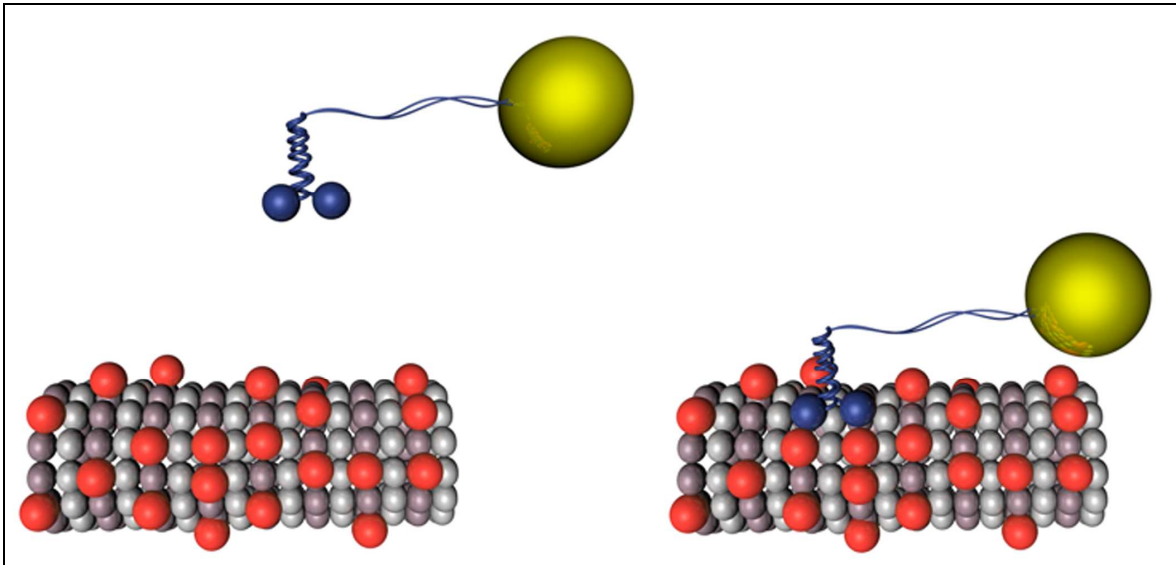
Figure 38: *Illustration of hindrance of kinesin binding and movement along the microtubule by KIF5A$_{330}$.*

The monomeric KIF5A$_{330}$ used as block protein (red) is a globular molecule with dimensions not exceeding those of tubulin dimers. Therefore, it does not additionally cause steric effects. As a consequence, all free kinesin binding sites around the blockage are practically accessible for the transporter kinesin (blue) without any steric interference. The gold beads transported are depicted by yellow spheres.

4.3.4 Visualization of block proteins on the microtubule surface

The final velocity level achieved with $KIF5A_{330}$ as block protein was reached at the relatively low head-to-tubulin ratio of about 0.1. An increase of this ratio to 0.4 did not cause stronger effects on the bead transport. The question arises how many molecules of the block proteins did really bind per microtubule length under the conditions realized in this study.

To get information on the density of block proteins bound along microtubules, a modified KIF5A motor domain construct, containing additionally a streptavidin binding motif ($KIF5A_{330}S$) was expressed. This construct was allowed to bind to microtubules in the presence of a non-hydrolyzable ATP analogue at conditions comparable to those applied for preparation of $KIF5A_{330}$-blocked microtubules. The ATPase activity and ability to bind to microtubules of the $KIF5A_{330}S$ construct could not be distinguished from the $KIF5A_{330}$ used for blocking.

$KIF5A_{330}S$ bound to the microtubules was visualized by electron microscopy after labelling with 10-nm streptavidin-coated gold beads. In dependence on the head-to-tubulin ratio, the mean distance between the blocking $KIF5A_{330}S$ molecules decreased (Figure 39). At a ratio of one kinesin head per 10 tubulin dimers, theoretically corresponding to one blocking molecule per 80-nm protofilament lengths, the mean distance between single $KIF5A_{330}S$ blockages was 266 nm $\pm$ 214 nm. This value corresponds well with the data obtained from the motility assay, where at the same head-to-tubulin ratio, the mean distance the beads were moved along $KIF5A_{330}$-decorated microtubules between resting phases was 226 nm $\pm$ 139 nm. Remarkably, increasing the head-to-tubulin ratio did not result in a more dense binding of $KIF5A_{330}S$.
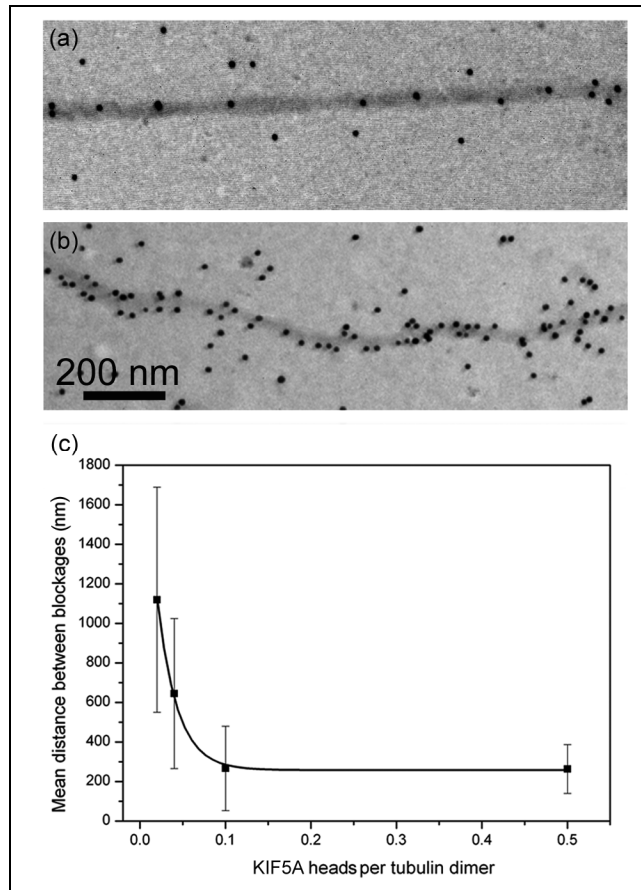
Figure 39: *Distribution of KIF5A$_{330}$S along microtubules.*
a,b) Images of microtubules showing the distribution of KIF5A$_{330}$S blockages proteins along microtubules at a head-to-tubulin ratio of 0.02 and 0.1, respectively.
c) Mean distances between single KIF5A$_{330}$S molecules as a function of the KIF5A$_{330}$S-to-tubulin ratio. The mean distances were calculated on the basis of the total length of 12 protofilaments constituting the microtubule wall. The higher standard deviations at low ratios might reflect a more random binding.

4.3.5 Transport of individual beads along a microtubule

Following the transport along a selected microtubule for a period significantly exceeding the dwell time of a single bead, the transport of further beads along the same microtubule rail was analyzed. The distance-time diagram in Figure 40, within the interval from 5 s to 25 s suggests that the beads No. 1 and 2 follow one and the same protofilament. Thereafter, resting phases were observed for these two beads at different positions suggesting that after passing sites of blocking they moved on along different protofilaments (corresponding to transport distance of ~3 µm). The distance-time diagram of bead No. 3 suggests the usage of another protofilament track immediately from the start point. Remarkably, the three beads rest at one and the same position (corresponding to transport distance of ~2.4 µm), obviously due to blocking of more than one kinesin-binding site on the microtubule surface. But nevertheless, all three beads were able to overcome the blockages on the microtubule surface after different resting times.
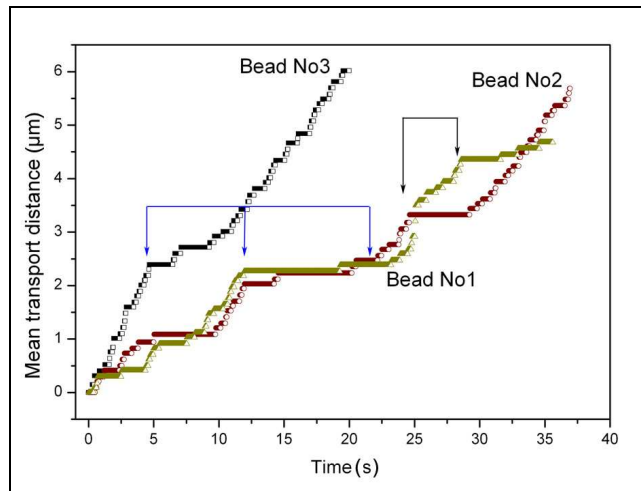
Figure 40: *Distance-time diagram of individual beads.*
Three individual beads were transported along one and the same microtubule. The mean transport velocities including the resting phases were 142 nm s^{-1}, 146 nm s^{-1}, and 350 nm s^{-1} for bead No. 1, 2, and 3, respectively. The KIF5A$_{fl}$ head-to-tubulin ratio was 0.2. This value, which determines the density of block proteins bound along the microtubule, was calculated on the basis of the number of motor domains (heads) the blockages comprises. The data were obtained by measuring the X-Y-shift of single beads on digitized video sequences (30 frames per second).

4.3.6 Bypassing mechanism

The mechanism of overcoming blocked kinesin binding sites proposed by Seitz and Surrey (2006) explains how the transporter kinesin can overcome sites along the protofilament which are occupied by reversibly attached proteins (see also 4.3.1). However, realization of the cargo transport over long distances seems to require a more efficient mechanism by which an obstacle blocking the kinesin binding site along the microtubules can be passed.

In the absence of blockages, kinesin is suggested to follow a linear trajectory by moving along a single protofilament (Kamimura and Mandelkow, 1992; Ray et al., 1993) even under sideways load (Block et al., 2003). In contrast, Yildiz et al. (2008) recently reported that, even in the absence of a lateral force, 13% of the kinesin molecules were able to perform ~6 nm sideways steps with equal preference to the left or right side. Such sideways steps might reflect that a single kinesin moving along the microtubule is able to change to a neighbouring protofilament. The frequency of sideways steps and the corresponding step size were found to depend on the length of the neck linkers (Yildiz et al., 2008). The ability of wild-type kinesin to perform sideways steps can be regarded as exceptional cases possibly due to irregularities in the microtubule lattice that have to be overcome.

In the present study, kinesin was shown to be able to move along microtubules decorated with irreversibly bound blockages competing for binding sites. Unlike observed for control preparations lacking blockages, movement was a non-continuous one, *i.e.* phases of transport alternated with resting phases. As a result, the mean velocities were lowered (Figure 32, Figure 36).

Kinesin moves in a hand-over-hand like fashion, whereby the leading head remains bound until the trailing head attaches to the next tubulin dimer. In the case of an irreversibly bound blockage the trailing head is not able to bind to the next tubulin dimer and the leading head cannot detach what in general should cause cargo stalling. But as a rule, bead movement was observed to continue after resting at sites of blockages, strongly suggesting a bypassing mechanism which is based on the high molecular flexibilty of the kinesin dimer, allowing different relative positions of both heads to each other. Bypassing is predicted on the assumption that the leading head remains bound to the original protofilament whereas the trailing one turns sidewards and contacts a tubulin binding site at a neighbouring protofilament. Finally, the leading head leaves the blocked protofilament and follows the trailing one along its new track. The kinesin step size is defined by

geometrical and mechanical limitations, *e.g.*, 8-nm centre-of-mass migration (Mandelkow and Johnson, 1998) or the torsional strain in the leading head to throw the trailing head forward, restricting possible paths to bypass (Figure 41).

The conclusion that a single kinesin molecule walking along an individual microtubule is able to change the protofilament track without being released can be strengthened by the following consideration: Control experiments with microtubules free of block proteins clearly demonstrated that, depending on actual length of microtubules, the gold beads moved over distances up to 10 μm. Under the conditions realized in this study, the taxol-stabilized microtubules reassembled from pure tubulin had mostly 12 protofilaments (Böhm et al., 1984). It is known that the protofilaments of such microtubules are tilted with respect to their long axis resulting in a right-handed helix with a super twist pitch of 3.4 μm (Ray et al., 1993). When a single kinesin molecule uses only one protofilament as track, the helical arrangement of the protofilaments enables transport distances of maximal about 3 μm. Otherwise the kinesin, including its 20-nm cargo, had to pass the space between the microtubule and the substratum to which the microtubules were immobilized.

It is concluded that bypassing is an evolutionary mechanism enabling the maintenance of the long-distance transport in the viscous matrix of the cell.
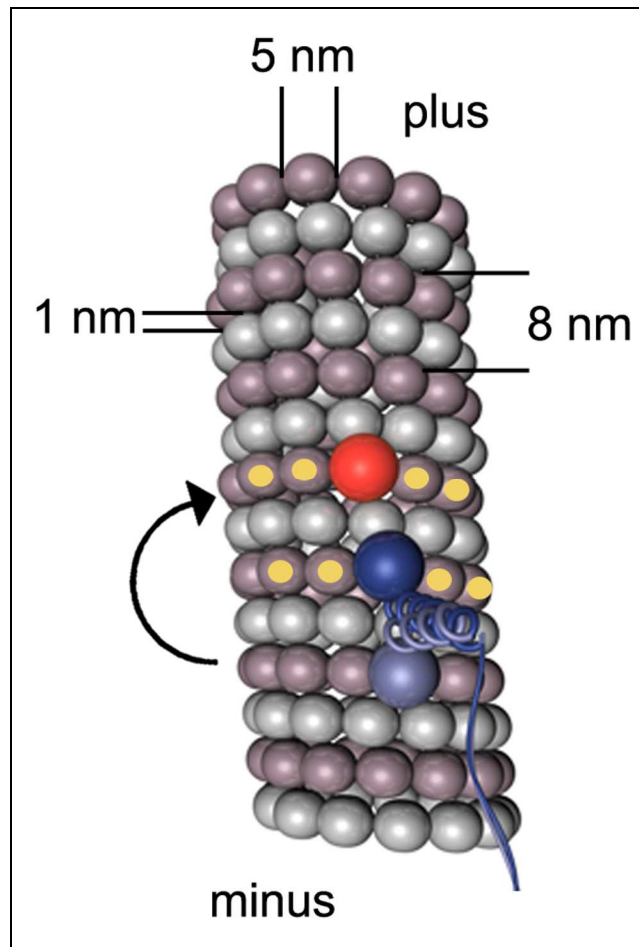
Figure 41: *Variations of overcoming blockages.*
The transporter kinesin is a dimer with two heads (light and dark blue) moving along a microtubule and encountering a blockage (red). Excluding backward steps, to overcome the block protein the trailing head can theoretically access four β-tubulin binding sites (yellow dots) both at the right and the left related to the moving direction.

It is assumed that two free neighbouring protofilaments on the right and on the left, corresponding to movement direction, are accessible to realize bypassing (Figure 41). For the single modes of bypassing described (see 4.3.6.1-4.3.6.4) step sizes were calculated between 8.6 and 20.6 nm for the first step (Table 2). These values are considered to be rather realistic as single kinesin heads take steps of 17.3 nm ± 3.3 nm (Yildiz et al., 2004). In the proposed models, backward steps of the leading head are excluded, as in this case the regular ATPase cycle and the resulting coordinated alternating movement of both heads would be disturbed. However, the bypassing modes are not mutually exclusive and it is likely that kinesin employs more than one strategy.

	Bypassing to the neighbouring protofilament		Bypassing to the next but one protofilaments	
	Step width (nm)			
	Mode I	Mode II	Mode III	Mode IV
Bypassing right in moving direction	8.6	15.8	11.7	17.2
Bypassing left in moving direction	10.2	17.7	14.1	20.6

Table 2: *Theoretical step widths of the trailing head to a free β-tubulin upon encountering the blockages.*
Calculations were performed using the following data: lateral spacing between the protofilaments – 5 nm; axial shift between adjacent protofilaments – 1 nm; tubulin dimer length – 8 nm.

4.3.6.1   Mode I

To perform an energetically efficient step the transporter tends to bind the nearest available free binding site on the microtubule (Figure 42). Therefore, the leading head remains bound to the original protofilament whereas the trailing one turns sideward and contacts a tubulin binding site located side by side at about 5-nm distance to the leading head (Figure 42b) on the adjacent protofilament. It is assumed that kinesin can overcome the blocked site to the left (10.2 nm step width) or right (8.6 nm step width, see also Table 2) corresponding to the movement direction. During the next ATPase cycle the former leading head is pulled through the gap between the blockage and the trailing head and becomes the leading head again (Figure 42c). The kinesin molecule continues now its movement along the new protofilament track.

This mode includes steps in which kinesin heads are located side by side. According to Hoenger et al. (1998) kinesin heads are able to bind in equimolar ratio to tubulin. That means, that at least under conditions of suppressed ATP activity a side by side location of both heads of the dimeric transporter kinesin or of one of its heads and a blocking molecule (see also Mode II) seems to be theoretically possible. However, the probability that the free head of the moving dimeric kinesin, looking for an alternative binding site by diffusional search, binds directly side by side to another head or blocking protein is considered to be lower than the binding at greater distance (see also Mode III, IV).
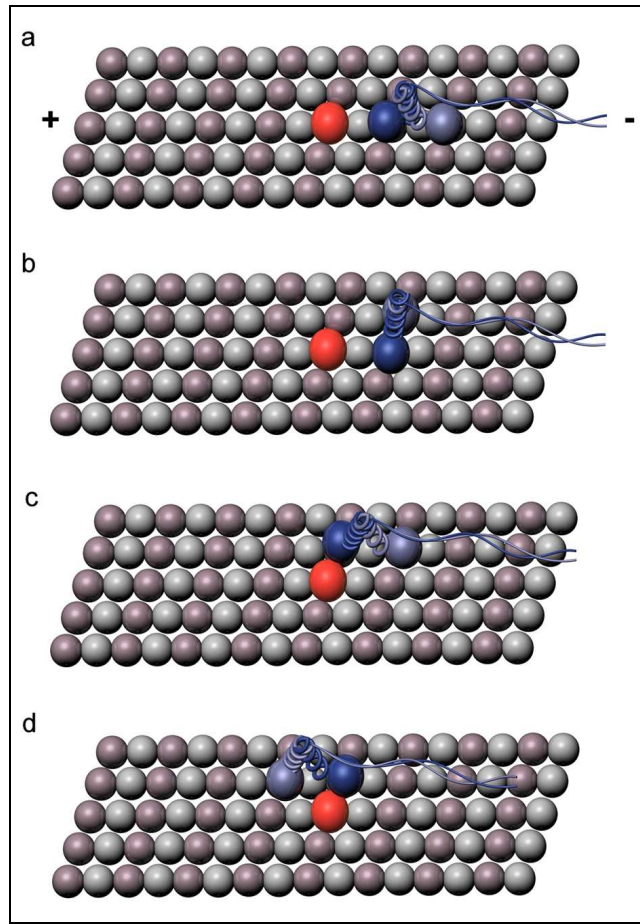
Figure 42: *Concept of kinesin bypassing: Mode I.*
The trailing head (light blue) binds to the β-tubulin of the adjacent protofilament and becomes located side by side with the leading head (dark blue). In the 2nd step, the former leading head is pushed forward and binds to the next free β-tubulin of the adjacent protofilament and becomes located side by side with the blockage (red).

4.3.6.2   Mode II

Like in Mode I, the trailing head is pulled forward and bypasses the blocked site by binding to an adjacent protofilament. Thereby, it binds side by side to the blockage on the adjacent protofilament (Figure 43b). The step is performed either to the adjacent protofilament on the left or the right, corresponding to step widths of 17.7 nm and 15.8 nm (Table 2), respectively, with respect to the moving direction. During the 2nd step, the former leading head is either pulled clockwise or counterclockwise in moving direction over the blocked site (Figure 43b/c) realized by a ~162° turn. A counterclockwise turn in moving direction is considered to be energetically not favoured.

It is suggested that transitions to the adjacent protofilament (Mode I, II), with a side by side location of one head with the other one or with a disturbance might occur in cases

when the kinesin binding site to the next dimer along the original protofilament track is hindered by structural discontinuities, *e.g.*, by defects of the microtubule lattice. In the case of disturbed kinesin binding sites by, *e.g.*, obstacle with dimensions in the range of a kinesin head, it is rather possible that the trailing head being pulled forward collides with the blockage which leads to transporter stalling and subsequent detachment.
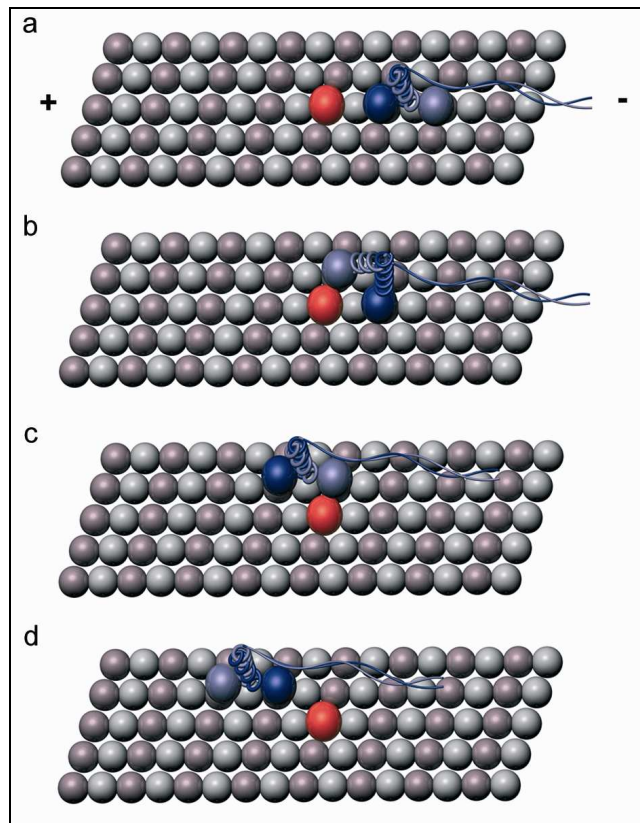
Figure 43: *Concept of kinesin bypassing: Mode II.*
The trailing head (light blue) binds side by side with the blockage (red). In the 2nd step, the former leading head (dark blue) is pushed forward and binds to the next free β-tubulin along the new protofilament track.

4.3.6.3   Mode III

It has been discussed that in the case of large obstacles a side by side arrangement of both heads or of one head and the blockage (see Mode I, II) seems to be less probable. It is more likely, that the free head of the moving kinesin transits to the next but one protofilament.

The leading head remains bound to the original protofilament whereas the trailing one contacts a tubulin binding site on the next but one protofilament located approximately perpendicular to the leading head (Figure 44b). Kinesin might take this step in both, left (14.1 nm step width) and right (11.7 nm step width; see also Table 2) direction, corresponding to the moving direction. Finally, the former leading head is pushed through the free space between the blocked site and follows the trailing one on the new track (Figure 44b/c).
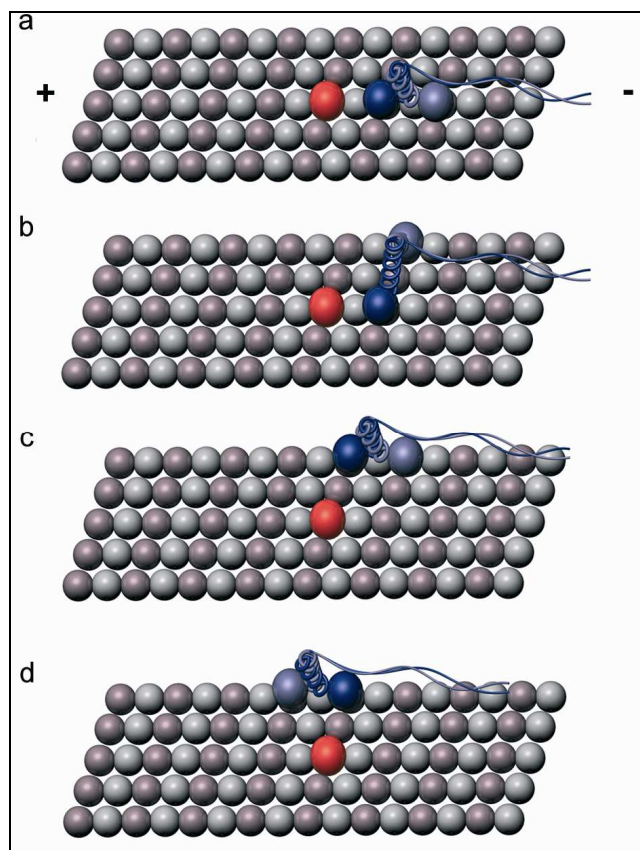
Figure 44: *Concept of kinesin bypassing: Mode III.*
The trailing head (light blue) turns sideward and binds approximately perpendicular to the β-tubulin of the next but one protofilament. In the 2nd step, the former leading head (dark blue) is pushed forward and also binds to this protofilament. The blockage is depicted in red.

4.3.6.4   Mode IV

Additionally, it is possible when encountering the blocked site, the trailing head makes a sideways step and changes to the next but one protofilament. Kinesin overcomes the blocked site by binding to the β-tubulin located approximately perpendicular to the blockage (Figure 45b). The performed step is accompanied by step widths of the trailing head of either 20.6 nm (bypassing left in moving direction) or 17.2 nm (bypassing right in moving direction; see also Table 2). During the 2nd step, the leading head is pulled clockwise in moving direction through the gap between the blockage and the former trailing head and binds also on the new protofilament track.

Though, in single cases kinesin heads were demonstrated to be able to perform steps of 17.3 nm ± 3.3 nm width (Yildiz et al., 2004). Bypassing left in moving direction is considered to be exceptional case as the large step width should be accompanied by raised intramolecular tension within the neck region.
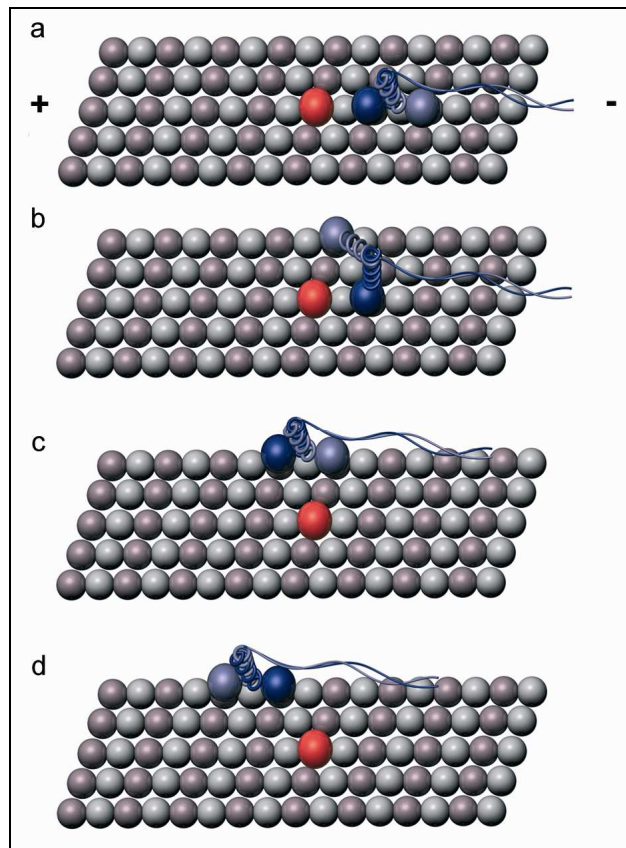
Figure 45: *Concept of kinesin bypassing: Mode IV.*
The trailing head (light blue) is pushed forward and binds to the β-tubulin of the next but one protofilament approximately perpendicular to the blockage (red). In the 2nd step, the former leading head (dark blue) binds to the next free β-tubulin along the new protofilament track.

4.3.7 Evaluation of the number of KIF5A molecules bound to the gold bead

Throughout the present study, 20-nm gold beads were complexed with $KIF5A_{fl}$ to follow kinesin movement along microtubules by AVEC-DIC microscopy. The question arises how many kinesin molecules were involved in the transport of a single gold bead. To answer this question, the KIF5A-complexed beads were transferred to Formvar/carbon-coated grids and either negatively stained by uranyl acetate or platinum-shadowed and examined by transmission electron microscopy. Independently of the preparation procedure, about 76% of the beads were observed to have bound only one KIF5A molecule (Figure 46).
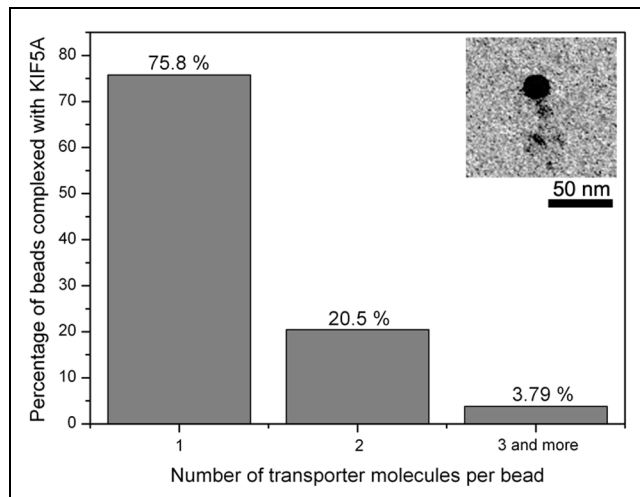
Figure 46: *Classification of the gold beads based on the number of KIF5A molecules bound.*
Altogether, 361 beads to which KIF5A was observed to be bound were evaluated for statistical analysis.
Insert: Transmission electron microscopy image (platinum-shadowed sample) depicts a 20-nm gold bead loaded with one $KIF5A_{fl}$ molecule.

4.3.7.1 Bypassing in the case of transport by multiple motors

Electron microscopic studies revealed that there was a fraction of beads (~25%) to which three and more motor molecules were bound. In this case, bypassing can be realized by the cooperative work of multiple motors. When the kinesin-bead complex encounters a blockage, the kinesin molecule which is actively involved in the bead transport detaches from the protofilament track and another kinesin molecule binds at a position sideward or in front of the blockage (Figure 47).

However, also in the case of binding of multiple motors to one and the same bead, bypassing might be realized by one active kinesin molecule whereas the other kinesin molecule remains passive.
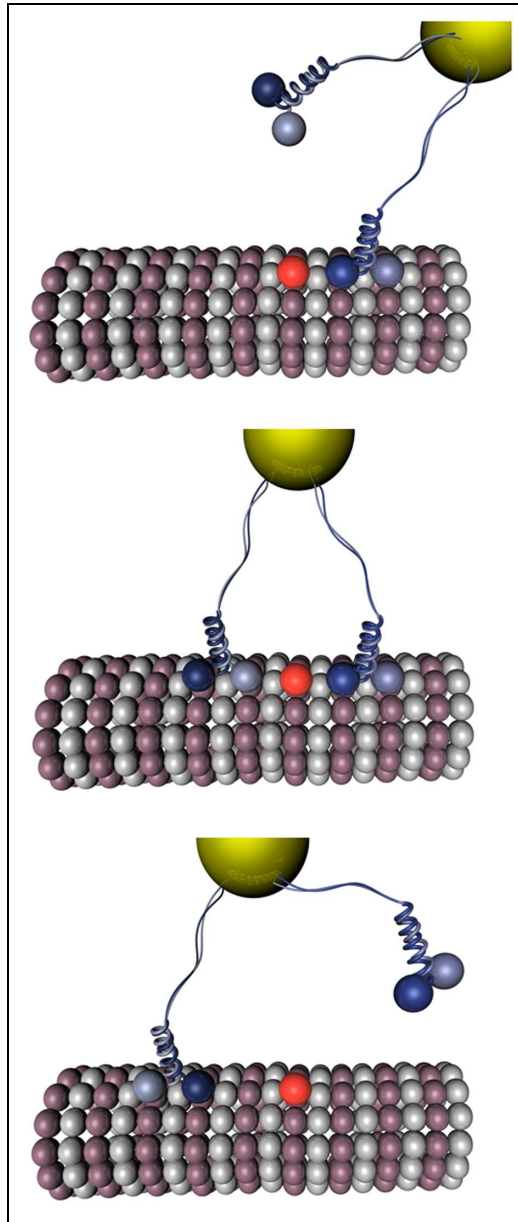
Figure 47: *Mechanism of bypassing blockages by multiple motors.*
Encountering the site of blockage, the bead oscillates and turns until a second kinesin contacts the microtubule wall leaving the blockage behind. After detaching of the first kinesin from the microtubule the bead moves on.

4.4   Kinesin-mediated cargo transport in the presence of Eg5

4.4.1   Strategy

It was found that Eg5 plays not only a major role in mitosis but is also suggested to be essential in developmental processes of the nervous system. For example, tubulin is reported to be delivered by the Eg5 motor to maintain the axonal growth (Myers and Baas, 2007).

Therefore, it seems to be likely, that in neuronal cells, Eg5 and KIF5A motors might encounter. In the previous chapter it was shown that kinesin overcomes irreversibly blocked kinesin binding sites. This result contradicts with the clonclusion of Seitz and Surrey (2006) whose experiments with motility-inhibited kinesin mutants might appropriately explain how kinesin overcomes reversibly blocked binding sites (see also 4.3.1). The question arises if nature has evolved a more effective mechanism still enabling the proper transport of organelles in the presence of other transporter proteins, *e.g.*, by performing bypassing.

To study effects of competing motors performing their normal physiological function Eg5 seems well suiteable. In comparison to KIF5 family members it represents a motor protein with about 20-fold lower transport velocity. This raises the question, whether the presence of a slowly moving motor thwarts a fast transporter.

To gain further insights into the interplay of competing motors with normal motility activity, the transport of the gold beads by KIF5A was investigated in the presence of Eg5.

4.4.2 Construct design

To study KIF5A-mediated motility in the presence of a motile competitor for binding sites along the microtubule a truncated Eg5 construct was expressed in *E. coli* without having any artificial tag or sequence.

The construct $Eg5_{513}$ (57.6 kD) is a dimeric protein (DeBonis et al., 2003) lacking parts of the stalk and tail region (Figure 48). It moves processively along the microtubule with a mean velocity of 58 nm s^{-1} ± 27 nm s^{-1}.
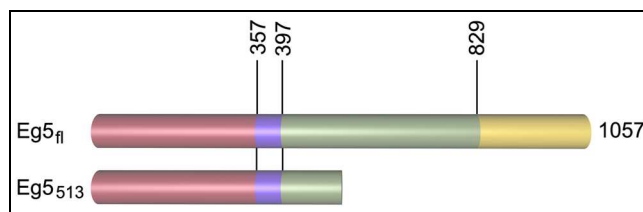
Figure 48: *Bar diagram depicting the domain structures of Eg5 constructs.*
The truncated construct $Eg5_{513}$ was used as a motile competitor for KIF5A binding sites along the microtubule. The motor domain is displayed in pink, neck linker/neck region in mauve, stalk in green and the tail region in yellow.

4.4.3 Exchangeable $Eg5_{513}$ as a motile competitor for KIF5A

$Eg5_{513}$ was allowed to bind to microtubules, under conditions preserving its ability to move. The Eg5-decorated microtubules were immobilized to PDDA-coated glass slides, without glutaraldehyde treatment. Thereafter, KIF5A-complexed gold beads were added and the movement was observed via AVEC-DIC microscopy.

The motility-efficient $Eg5_{513}$ was found to slow down the bead transport whereby, phases of movement alternated with resting ones. But, after pausing, the bead transport was usually continued (Figure 49).

Figure 49: *Distance-time diagram in the presence of exchangeable Eg5$_{513}$.*
a) Continuous transport in the absence of Eg5$_{513}$. Within the time interval of this sequence the mean transport velocity was 952 nm s^{-1}.
b) Discontinuous transport with alternating phases of movement and resting observed in the presence of exchangeable Eg5$_{513}$. The mean velocity including resting phases was 354 nm s^{-1}. The head-to-tubulin ratio was 0.5. This value, which determines the density of block proteins bound along the microtubule, was calculated on the basis of the number of motor domains (heads) the blockages comprises. The data were obtained by measuring the X-Y-shift of single beads on digitized video sequences (30 frames per second).

Depending on the Eg5$_{513}$ head-to-tubulin ratio the mean transport velocity decreased exponentially (Figure 50a, Figure 51) up to a final velocity level of 463 nm s^{-1} ± 56 nm s^{-1} at a head-to-tubulin ratio of 0.5. Correlating to this, the transport distance a bead was moved along the microtubule decreased (Figure 50b). Even at the highest head-to-tubulin ratio (one Eg5$_{513}$ head per two tubulin dimers), the beads were transported up to 2.8 µm.

Figure 50: *Effect of exchangeable Eg5$_{513}$ on the velocity and transport distance.*
a) Dependence of the mean transport velocity on the head-to-tubulin ratio.
b) Dependence of the transport distance (length of the trajectory single beads were moved from the moment of association with a microtubule upon their final stopping or detachment) on the head-to-tubulin ratio. For statistical analysis ≥50 single beads per head-to-tubulin ratio were analyzed.
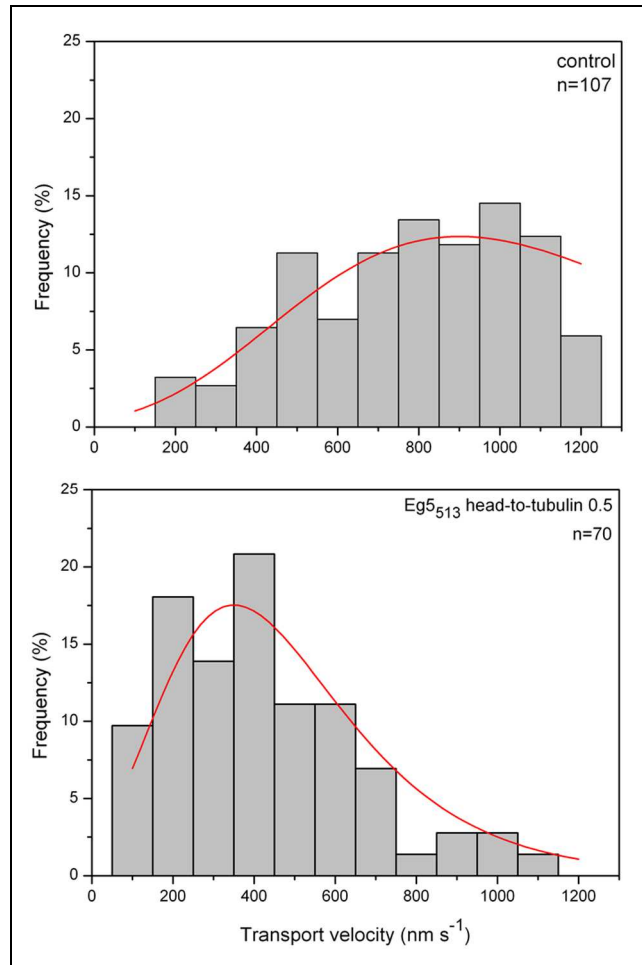
Figure 51: *Frequency diagram of velocity distribution in the presence of exchangeable Eg5$_{513}$.*
Velocity frequency histograms in the absence of Eg5$_{513}$ and in the presence of exchangeable Eg5$_{513}$. The x-values indicate velocity intervals $\pm$ 50 nm s^{-1}.
n - number of beads measured.

4.4.4 Irreversibly bound Eg5$_{513}$

It was shown that exchangeable, motile-competitive Eg5$_{513}$ competing with the KIF5A for binding sites along the microtubule, decelerates the bead transport. The extent of the decrease is comparable to KIF5A blockages described earlier (see 4.3). It is not clear if exchangeable Eg5$_{513}$ frees the binding site for kinesin or if kinesin is able to bypass blocked sites. Therefore, additional experiments were performed where Eg5$_{513}$ was artificially inactivated by chemical fixation. Due to this, Eg5$_{513}$ molecules were neither able to move nor to detach from the microtubule surface and act as rigid blockages.

As expected, the irreversibly bound Eg5$_{513}$ also decreased the transport velocity (Figure 52a, Figure 53) significantly. Surprisingly, the final velocity level at a head-to-

tubulin ratio of 0.5 ratio was 496 nm s^{-1} $\pm$ 75 nm s^{-1}, *i.e.* not significantly lower than in the case of exchangeable $Eg5_{513}$. Also the mean transport distance was found to be comparable to the values measured for the exchangeable $Eg5_{513}$ (Figure 52b).
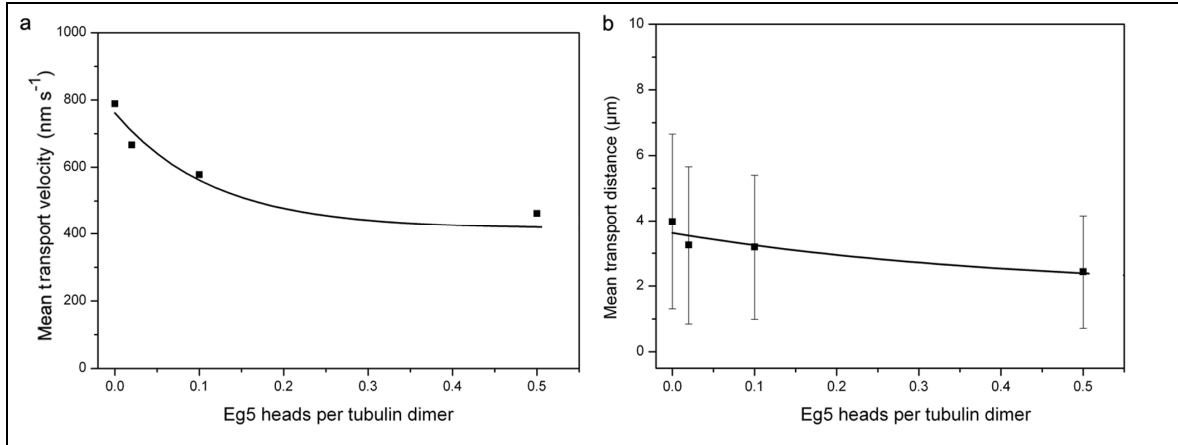
Figure 52: *Effect of irreversibly bound Eg5$_{513}$ on the velocity and transport distance.*
a) Dependence of the the mean transport velocity on the head-to-tubulin ratio.
b) Dependence of the the mean transport distance (length of the trajectory single beads were moved from the moment of association with a microtubule upon their final stopping or detachment) on the head-to-tubulin ratio.
For statistical analysis $\geq$50 single beads per head-to-tubulin ratio were analyzed.
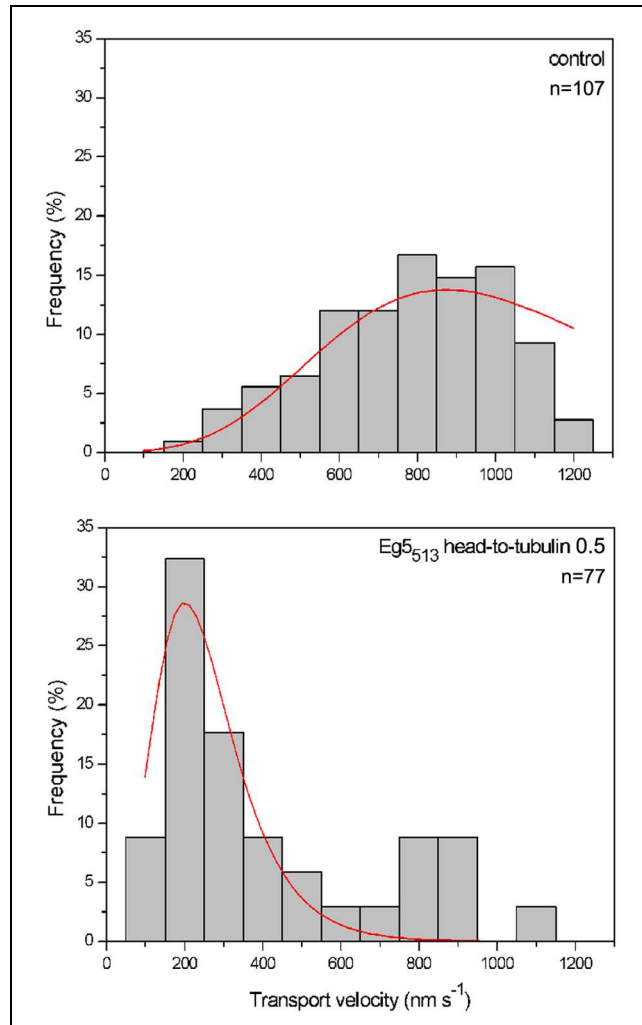
Figure 53: *Frequency diagram of velocity distribution in the presence of irreversibly bound Eg5$_{513}$.*
Velocity frequency histograms in the absence of Eg5$_{513}$ and in the presence of irreversibly bound Eg5$_{513}$. The x-values indicate velocity intervals $\pm$ 50 nm s^{-1}.
n - number of beads measured.

Noticeably, when irreversibly bound, Eg5$_{513}$ exerted longer resting phases on the kinesin-mediated transport (Figure 54) than in its native, exchangeable state (Figure 49). When exchangeably bound the competitive slowly moving Eg5$_{513}$ is in equilibrium between its binding and detachment which enables the transporting kinesin relatively easily to pass the blocked site. But, when irreversibly bound Eg5$_{513}$ represents a rigid blockage unable to detach from the microtubule which might be the reason for longer resting phases.
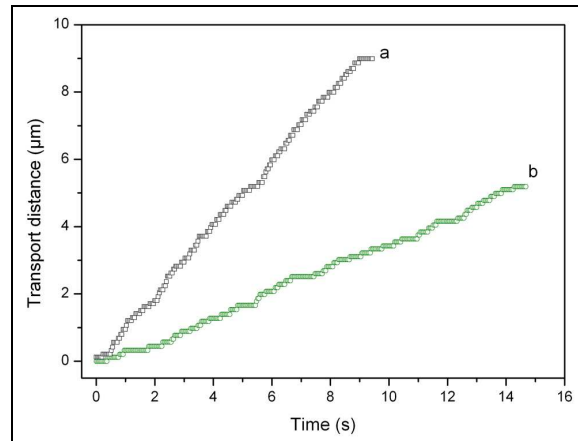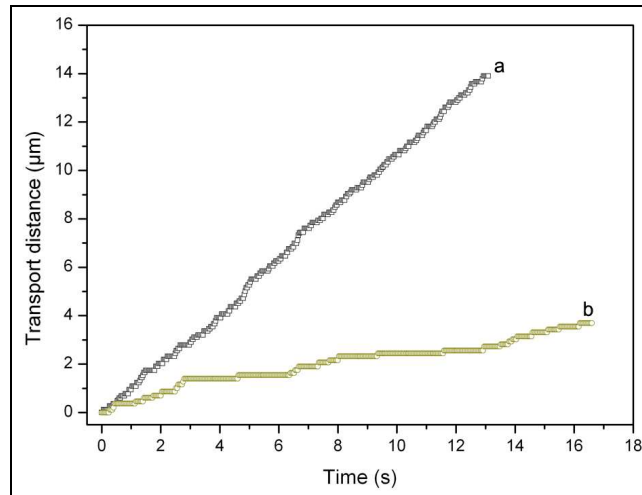
Figure 54: *Distance-time diagram in the presence of irreversibly bound Eg5$_{513}$.*
a) Continuous transport in the absence of Eg5$_{513}$. Within the time interval of this sequence the mean transport velocity was 1061 nm s^{-1}.
b) Discontinuous transport with alternating phases of movement and resting observed in the presence of irreversibly bound Eg5$_{513}$. The mean velocity including resting phases was 223 nm s^{-1}. The head-to-tubulin ratio was 0.5. This value, which determines the density of blockage proteins bound along the microtubule, was calculated on the basis of the number of motor domains (heads) the blockages comprises. The data were obtained by measuring the X-Y-shift of single beads on digitized video sequences (30 frames per second).

4.4.5   Comparison of the effect of exchangeable Eg5$_{513}$ and of irreversibly bound Eg5$_{513}$ on the kinesin-mediated transport

Independently of whether Eg5$_{513}$ was exchangeable or irreversibly bound on the microtubule surface, it exerted a decrease on the transport velocity. The decrease depend on the Eg5$_{513}$ head-to-tubulin ratio and could be fitted by an exponential curve (Figure 55a). Interestingly, chemical fixation did not lead to a stronger effect on the transport velocity. In both cases, the mean transport distance of the beads was slightly diminished (Figure 55b).
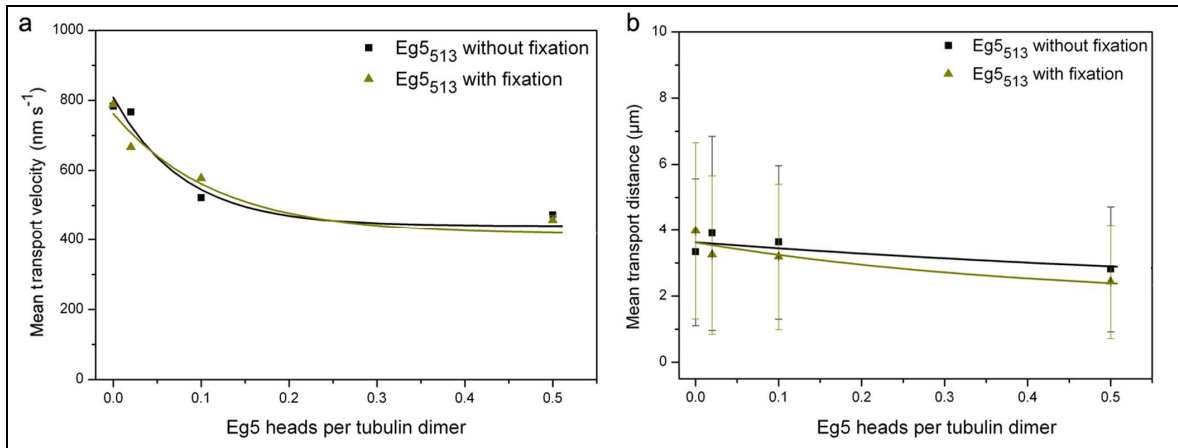
Figure 55: *Effect of exchangeable Eg5$_{513}$ and irreversibly bound Eg5$_{513}$ on the velocity and transport distance.*
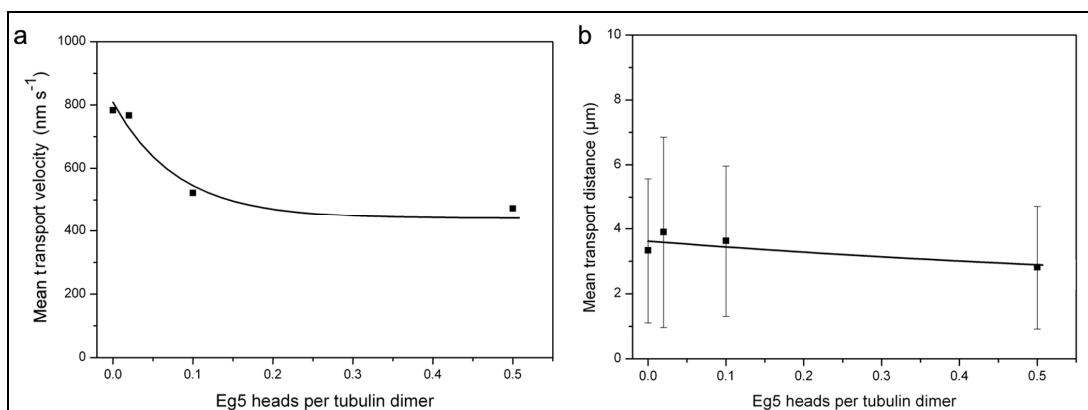a) Dependence of the mean transport velocity on the head-to-tubulin ratio.
b) Dependence of the mean transport distance (length of the trajectory single beads were moved from the moment of association with a microtubule upon their final stopping or detachment) on the head-to-tubulin ratio.
The data refer to Figure 50 for exchangeable Eg5$_{513}$ and Figure 52 for irreversibly bound Eg5$_{513}$, respectively. For statistical analysis ≥50 single beads per head-to-tubulin ratio were analyzed.

In solution, both kinesin heads have ADP bound which is released upon one head binds to the microtubule. The ATP-stimulated release of nucleotides varies between kinesin family members. Eg5$_{513}$ is characterized by a relatively slow nucleotide release (K$_D$: 5 s^{-1} - 10 s^{-1}) whereas kinesin-1 releases it nucleotides rapidly (K$_D$: 100 s^{-1}) (Valentine et al., 2007). The slow release, in the case of Eg5$_{513}$, causes a stronger binding of the motor protein during passing its ATPase cycle. *Vice versa*, the transporting kinesin should unbind faster when encountering the slowly moving blockage. But, diffusion of kinesin from the microtubule surface which should become evident by "jumps" in the corresponding distance-time diagram was not observed (Figure 49). Even at high Eg5$_{513}$ head-to-tubulin ratios the beads were transported over mean distances of about 2.4 µm - 2.8 µm (Figure 55b). But, with increasing head-to-tubulin ratio the binding efficiency of transporter molecules was reduced.

Remarkably, transport velocities which are typically measured for Eg5 (40 nm s^{-1}, Kalchishkova and Böhm, 2008) were not observed suggesting that transporting kinesin uses alternative mechanisms to overcome blocked sites rather than running behind the slowly motor.

These results contradict with the observations made by Seitz and Surrey (2006) who concluded that kinesin waits until an immotile motor releases the track. In general, it

seems to be possible that also the exchangeable Eg5 unbinds and frees the binding site for kinesin. However, the coincidence of the results obtained with the exchangeable and irreversible bound Eg5 strongly supports the postulated bypassing mechanism (4.3.6) where also sites occupied by a slowly moving motor bound to the protofilament track can be overcome. To maintain an efficient long-distance transport, waiting for the release of blockages seems to be disadvantageous from a cell physiological point of view.

4.5 Kinesin-mediated cargo transport in the presence of MAPs

4.5.1 Strategy

It has been shown that the kinesin-mediated transport is efficiently sustained even in the presence of irreversibly bound blockages (see chapter 4.3 and 4.4). In the corresponding experiments microtubules reconstituted from pure tubulin have been used. These microtubules have a smooth surface free of accessory proteins. This situation however, does not reflect the physiological reality within a living cell where the motor proteins frequently encounter non-motile microtubule-associated proteins (MAP) along their path.

In the last decade various *in vitro* studies were performed dealing with the molecular mechanisms of motor protein interaction with MAPs. Nevertheless, the results are controversially discussed. It is thought that MAPs affect the attachment frequency of transporting kinesin but not its motion (Seitz et al., 2002; Trinczek et al., 1999). On the other hand, Lopez et al. (1993) showed that kinesin motility is inhibited by MAP2 but not by tau. In contrast, it was recently reported that tau completely inhibits kinesin-mediated transport at a tau-to-tubulin ratio of 0.2 (Vershinin et al., 2008). The inconsistence of the results is most probably due to the different experimental procedures, including the actual type of applied associated protein, the concentration, ionic strength or buffer constituents.

To gain further insights into the mechanisms of kinesin motility generation in the presence of MAPs, the kinesin-mediated transport has been systematically studied using a long stretched MAP (MAP2) and a short one (tau), both in exchangeable state and after irreversible cross-linking to the microtubule.

4.5.2 Kinesin-mediated transport in the presence of the complete set of neuronal of MAPs

To maintain the great number of specialized cell functions, the motor protein-based transport along microtubules plays a fundamental role. Different cellular cargoes are moved by diverse motors from the cell center to the cell periphery and *vice versa*. The cargo transport into different directions must be highly regulated and coordinated. It is suggested to be controlled by filament-based regulation mechanisms, whereby microtubule-associated proteins seem to be involved in tuning the amount of allowed transport in a favoured direction (Reed et al., 2006; Vershinin et al., 2007; Vershinin et al., 2008).

Within the mammalian brain, typically three classes of associated proteins are expressed: MAP1, MAP2, and tau. These MAPs bind to the microtubule surface and form projections.

To prove the interaction of kinesin with the naturally occurring set of MAPs, microtubules were reconstituted from tubulin, obtained from porcine brain tissue by temperature-dependent microtubule disassembly/reassembly cycles (Shelanski et al., 1973). These microtubules, which contained circa 15% associated proteins (MAP1, MAP2, tau) by mass, were used to study the kinesin-mediated transport after immobilization. It was found that the complete set of MAPs inhibits the transport (Figure 56), which is expressed by the lowered mean transport velocity (266 nm s^{-1} ± 155 nm s^{-1} *vs.* 730 nm s^{-1} ± 194 nm s^{-1}), determined for the control with purified microtubules lacking associated proteins.
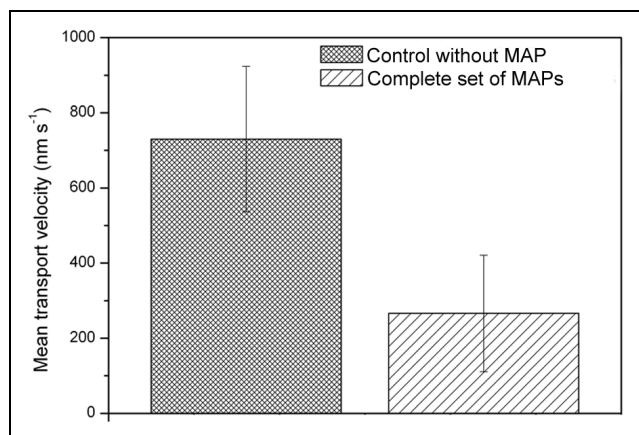
Figure 56: *Effect of the complete set of brain-specific MAPs on the mean velocity.*
Mean transport velocities measured for microtubules purified from associated proteins
(n=45) and in the presence of the full set of MAPs (n=32), respectively.
n - number of beads measured.

MAPs are more or less regularly distributed along the microtubules. Electron microscopic analysis of thin sections revealed that MAP2 appears in form of long side projections along the microtubule surface with a regular spacing.

The distribution of MAPs on the microtubule surface was studied by immunogold labelling and electron microscopy. Therefore, microtubules, containing MAPs, were labelled by MAP2 or tau antibody, respectively, and visualized by a gold-conjugated secondary antibody (Figure 57). Both, MAP2 and tau exhibited mean spacings of 17 nm ± 5 nm and 16 nm ± 6 nm, respectively, along the microtubule which is in the range of a MAP-to-tubulin ratio of 0.04, calculated on the basis of a 12 protofilament microtubule. The value is in agreement with the data given by Kim et al. (1979).
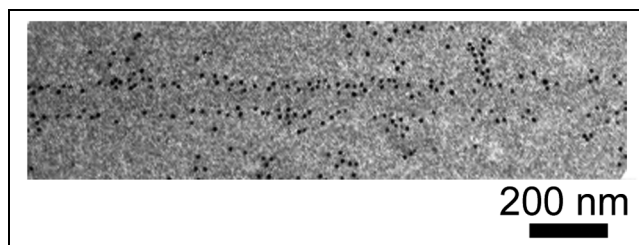
Figure 57: *Distribution of MAPs on the microtubule surface.*
Image of a microtubule showing the distribution of MAP2 at a MAP2-to-tubulin ratio of 0.1.

The question arises if the long MAP2 affects the transporting kinesin in more pronounced fashion than the relatively small tau. To answer this question the influence of either purified MAP2 or tau on the kinesin-mediated gold transport was studied.

4.5.3   Kinesin-mediated transport in the presence of MAP2

4.5.3.1   Exchangeable MAP2

Purified MAP2 was added to the microtubules and hold in its native state. Under such conditions, MAP2 remains exchangeable, whereby it is in equilibrium between phases of attachment and detachment. After microtubule immobilization to the substrate, kinesin-complexed gold beads were added and induced to move. Bead movement was observed to rest frequently, but usually could be continued (Figure 58).
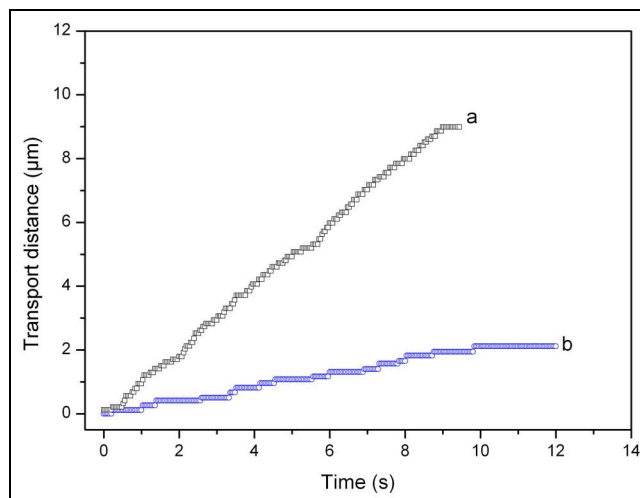
Figure 58: *Distance-time diagram in the presence of exchangeable MAP2.*
a) Continuous transport in the absence of MAP2. Within the time interval of this sequence the mean transport velocity was 952 nm s^{-1}.
b) Discontinuous transport with alternating phases of movement and resting observed in the presence of exchangeable MAP2. The mean velocity including resting phases was 176 nm s^{-1}. The MAP2-to-tubulin ratio was 0.5. The data were obtained by measuring the X-Y-shift of single beads on digitized video sequences (30 frames per second).

Correspondingly, the mean velocity decreased in dependence on the MAP2-to-tubulin ratio (Figure 59), determining the density of MAP2 bound along the microtubules. The final velocity level, found at 452 nm s^{-1} ± 37 nm s^{-1}, was reached at a MAP2-to-tubulin ratio of 0.5, significantly exceeding the physiologically relevant ratio (Vershinin et

al., 2008). At higher MAP2-to-tubulin ratios, binding of kinesin-complexed beads was completely abolished.
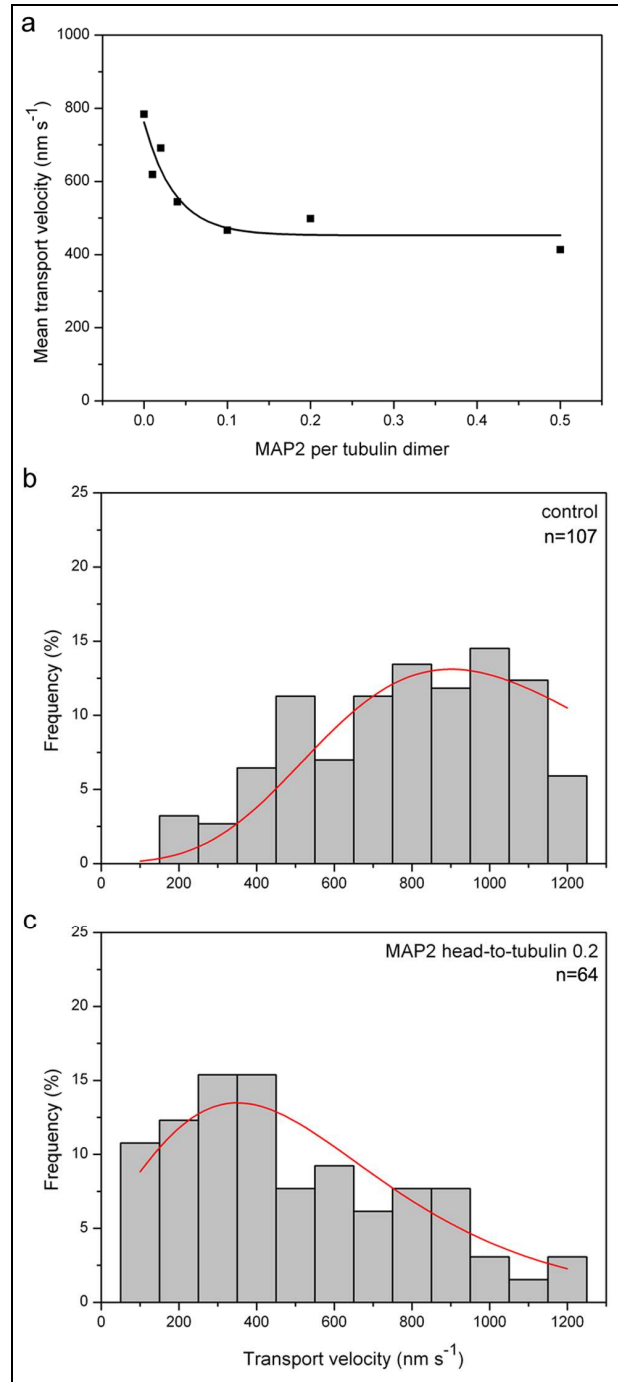
Figure 59: *Effect of exchangeable MAP2 on the velocity.*
a) Dependence of the mean transport velocity on the head-to-tubulin ratio in the case of blocking by exchangeable MAP2.
b,c) Velocity frequency histograms in the absence of MAP2 and in the presence of exchangeable MAP2, respectively. The x-values indicate velocity intervals ± 50 nm s^{-1}.
n - number of beads measured.

Parallel to the motility experiments, the effect of MAP2 on the catalytic activity of the kinesin was determined by measuring the ATP turnover rates. The k_{cat} values (ATP molecules hydrolyzed per head and second, measured at 37°C) were found to be lowered with increasing MAP2-to-tubulin ratio (Figure 60). The plot of the k_{cat} values against the MAP2-to-tubulin ratio correlates with the motility measurements (Figure 59a). The decrease of the ATPase activity is ascribed to steric inhibition of kinesin binding to the microtubules during the ATPase cycle at sites along the surface of the microtubule occupied by MAP2 molecules.
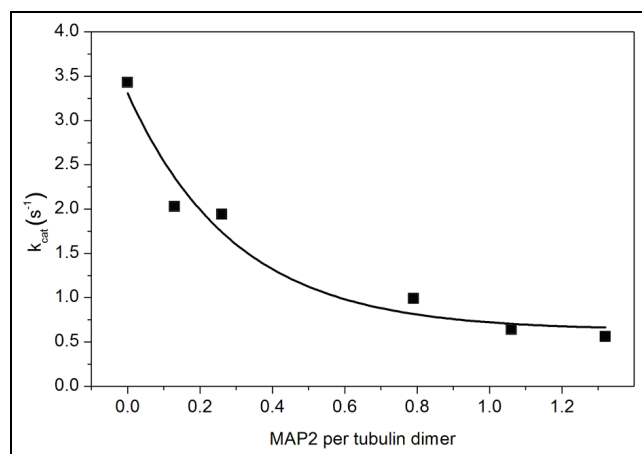
Figure 60: *Effect of exchangeable MAP2 on the catalytic activity of kinesin.* Determination of the ATPase activity of KIF5A in dependence on the MAP2-to-tubulin ratio.

4.5.3.2   Irreversibly bound MAP2

Reversibly bound MAP2 has been demonstrated to exert a significant decrease on the velocity. As MAP2 changes between binding and unbinding the question arises if irreversibly bound MAP2 exerts a stronger effect on the transport velocity. Therefore, MAP2 was cross-linked by glutaraldehyde to the microtubule surface. In this case, MAP2 became unable to detach from the microtubule surface.

Also in the case of irreversible MAP2 binding the transport velocity significantly decreased (Figure 61). The lowest mean velocity was 367 nm s^{-1} ± 41 nm s^{-1} measured at a MAP2-to-tubulin ratio of 0.2, which theoretically corresponds to one MAP2 molecule per 40-nm protofilament length, assuming a complete MAP2 binding. Increasing the MAP2-

to-tubulin ratio resulted in a practically complete inhibition of kinesin-complexed bead binding to the microtubules.
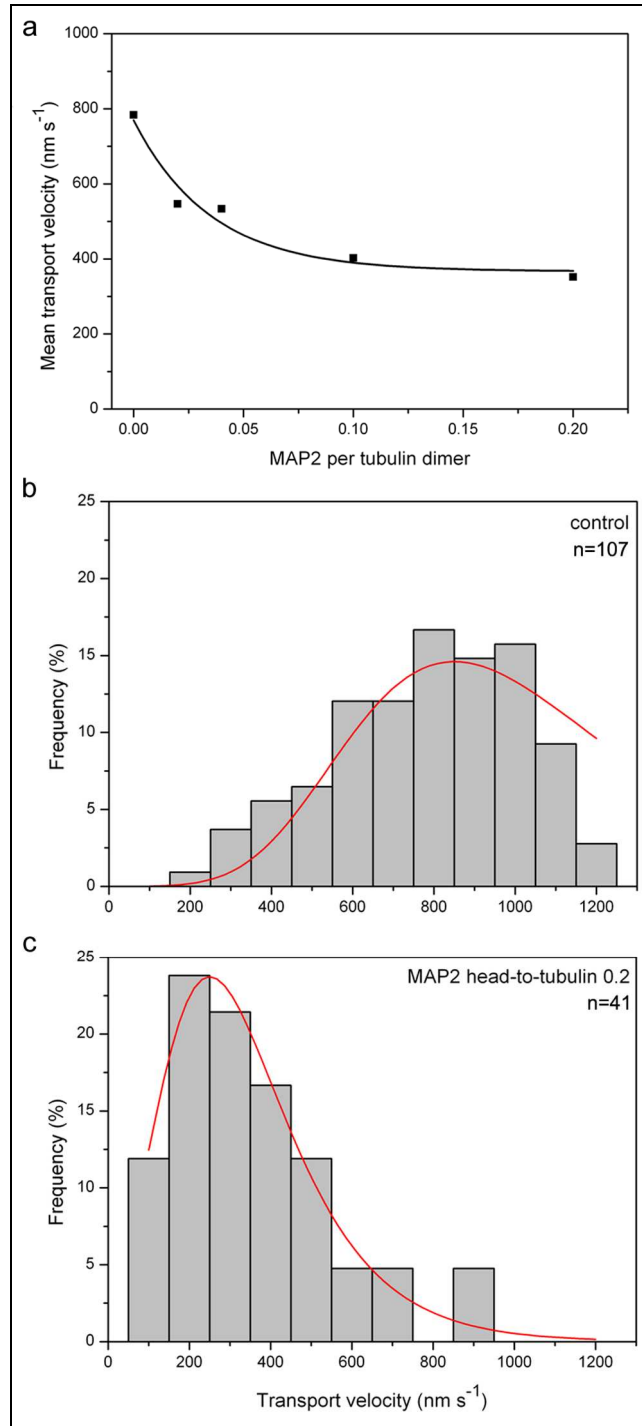
Figure 61: *Effect of irreversibly bound MAP2 on the velocity.*
a) Dependence of the mean transport velocity on the head-to-tubulin ratio in the case of blocking by irreversibly bound MAP2.
b,c) Velocity frequency histograms in the absence of MAP2 and in the presence of irreversibly bound MAP2, respectively. The x-values indicate velocity intervals ± 50 nm s^{-1}. n - number of beads measured.

4.5.3.3   Visualization of MAP2 by immunogold-labelling

Independently of whether MAP2 was exchangeable or irreversibly bound, the transport velocity showed an exponentially decreasing progression with a certain kind of saturation reached at MAP2-to-tubulin ratios of 0.2 to 0.5. A further increase of MAP2 did not lead to stronger effects.

As MAP2 is usually in a dynamic state between binding and unbinding, the actual number of MAP2 molecules bound to the microtubule surface is unknown. To gain insights into the real density of MAP2 bound, immunogold-labelling experiments were performed in which MAP2 was bound to the microtubules and chemically cross-linked. MAP2 was detected by an anti-MAP2 antibody and visualized by a 10-nm gold conjugated secondary antibody.

Depending on the MAP2-to-tubulin ratio, the mean distance between single MAP2 molecules decreased (Figure 62a). At a ratio of one MAP2 molecule per 2 tubulin dimers, a mean distance between the MAP2 molecules along the microtubule surface of 133 nm ± 35 nm per protofilament length (corresponding to ~11 nm along a 12-protofilament microtubule) was measured. This value corresponds well with the mean distances, the beads moved between resting phases which were 132 nm ± 31 nm at the same MAP2-to-tubulin ratio.

Along microtubules, purified from brain tissue by temperature-dependent cycles of disassembly/reassembly, containing the complete set of MAPs (MAP1, MAP2 and tau), MAP2 was found to be spaced at 195 nm ± 66 nm. When MAP2 was bound to taxol-stabilized microtubules reassembled from pure tubulin at a MAP2-to-tubulin ratio of 0.1, theoretically corresponding to one MAP2 bound per 10 tubulin dimers, the mean distance between MAP2 molecules was 163 nm ± 55 nm (Figure 62b). This lower value can be explained by the absence of MAP1 and tau which enables MAP2 to bind denser on the microtubule surface.

At a KIF5A head-to-tubulin ratio of 0.5, the mean distance between $KIF5A_{330}S$ molecules was found to be 263 nm ± 124 nm (see Figure 39) which is significantly different from MAP2 (133 nm ± 35 nm). The result indicates a more dense binding of MAP2 on the microtubule surface which is reflected in a stronger inhibition of kinesin binding. In contrast to KIF5A, MAP2 forms a loose coat on the microtubule surface by binding longitudinally (Al Bassam et al., 2002) along several αβ-tubulin dimers (McEwen et al., 1983) which might cause a more dense occupation.
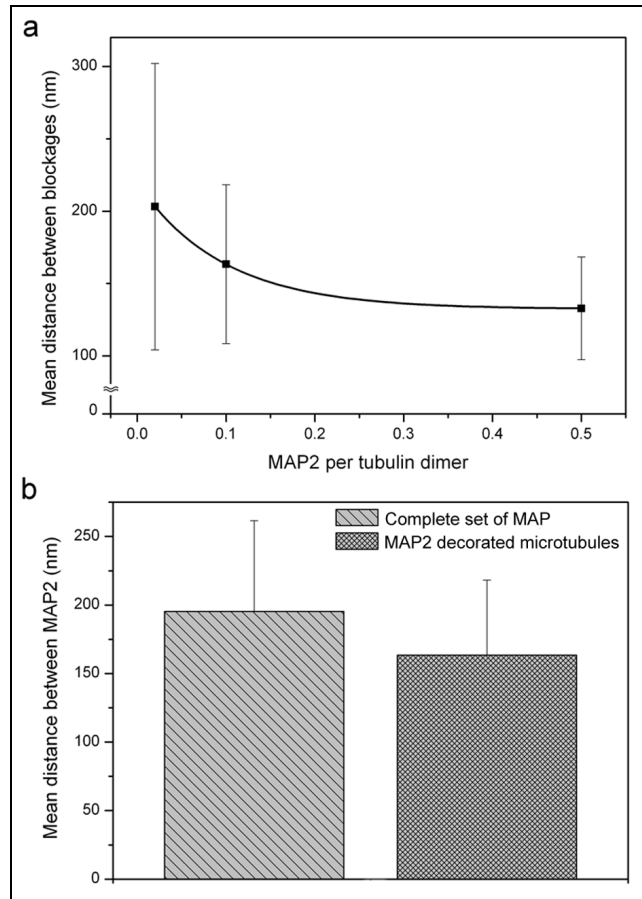
Figure 62: *Distances between MAP2 molecules along the microtubule.*
a) Mean distances between single, irreversibly bound MAP2 molecules as a function of the MAP2-to-tubulin ratio. The higher standard deviations at low ratios might reflect a more random binding.
b) Mean distance between MAP2 molecules on the surface of microtubules equipped with the complete set of MAPs naturally occurring in brain tissue and MAP2 irreversibly bound on the microtubule surface at a MAP2-to-tubulin ratio of 0.1. The mean distances were calculated on the basis of the total length of 12 protofilaments constituting the microtubule wall.

4.5.3.4   Comparison of the effect of exchangeable MAP2 and of irreversibly bound MAP2
on the kinesin-mediated transport

Independently of whether MAP2 was exchangeable or irreversibly bound to the microtubule surface, a significant decrease on the kinesin transport velocity was exerted (Figure 63).

When MAP2 molecules were irreversibly bound, the final level of kinesin binding was reached at a MAP2-to-tubulin ratio of 0.2, theoretically corresponding to one MAP2 molecule per 40-nm protofilament length. In this case, MAP2 is considered to act as a block protein, whose action is quite similar to that of the KIF5A blockages. Interestingly, the MAP2 which binds to microtubules at a site different from the KIF5A binding site (Song and Mandelkow, 1993) exerted a more significant inhibition on kinesin binding than KIF5A blockages (see also chapter 4.3). But nevertheless, the velocity levels of KIF5A blockages and MAP2 at a block protein-to-tubulin dimer ratio of 0.2 are in the same range ($\sim$350 nm s^{-1} - 400 nm s^{-1}). The high molecular weight MAP2 forms projections more than twice as long as KIF5A which seems to explain the stronger steric inhibition of kinesin binding to the microtubule surface.

In addition, MAPs are basic proteins which electrostatically interact with tubulin. When kinesin binds to the microtubules surface, its positive charged neck-coiled coil interacts with the negatively charged COOH-terminus of tubulin enabling a proper binding (Thorn et al., 2000). In the presence of MAP2, the negatively charged microtubule surface becomes neutralized which might cause an inhibition of kinesin binding.
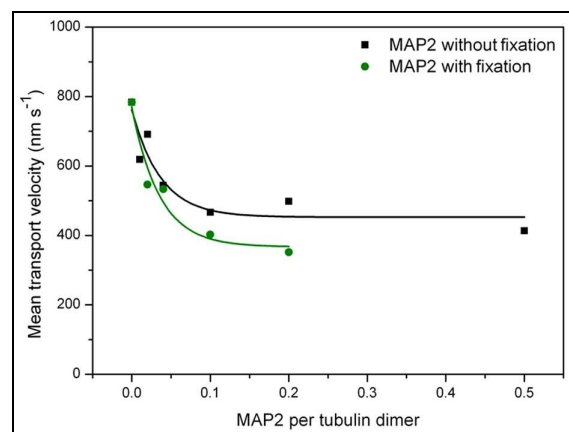
Figure 63: *Effect of exchangeable MAP2 and irreversibly bound MAP2 on the velocity.*
Dependence of the mean transport velocity on the MAP2-to-tubulin ratio. The data refer to Figure 59 for exchangeable MAP2 and Figure 61 for irreversibly bound MAP2, respectively.

Recent studies indicate that in solution MAP2 is unstructured, where extended it has dimensions up to 11 nm. Upon microtubule binding MAPs are suggested to change into an elongated configuration, binding along the protofilament ridges on the outer surface of microtubules (longitudinal binding) (Al-Bassam et al., 2002; Kawachi et al., 2003). It is likely that MAP2 binds in the groove between protofilaments accompanied by binding to several subsequent αβ-tubulin dimers (McEwen et al., 1983). It is assumed that this coating and the fact that MAP2 forms long sidearms (Voter and Erickson, 1982) represent severe obstacles that sterically hinder kinesin to move (Lopez and Sheetz, 1993). The inhibitory effect of MAP2 on kinesin motility was more pronounced in the case of irreversibly bound block proteins (Figure 63). Irreversibly bound MAP2 cannot be released and its long sidearms might cover the microtubule surface counteracting the binding of kinesin by masking its binding sites.

Especially at high MAP2-to-tubulin ratios, it is conceivable that kinesin binding to microtubules with irreversibly bound MAP2 is strongly inhibited by tangled MAP2 molecules (Figure 64) which are rigidly attached on the microtubule surface. Additionally, chemical fixation by glutaraldehyde might result in intermolecular cross-links leading to tangle formation.
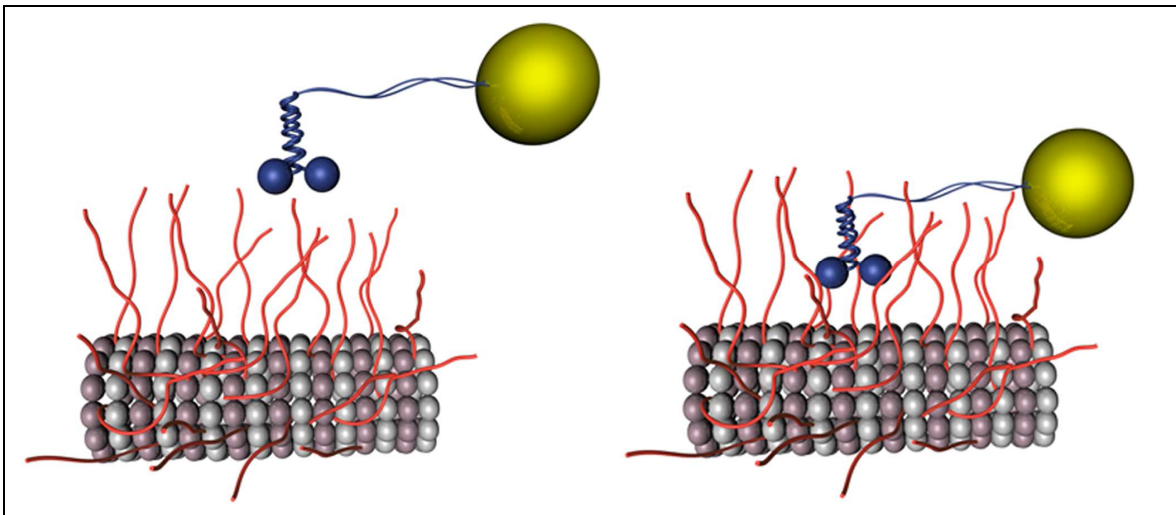
Figure 64: *Illustration of inhibited kinesin attachment to the microtubule by MAP2 at high MAP2-to-tubulin ratios.*
At high MAP2 densities kinesin cannot penetrate the tangled filaments and does not bind to the microtubule surface.

At low MAP2-to-tubulin ratios kinesin binding is less affected, independently of whether the MAP2 is exchangeable or irreversibly bound. Although, MAP2 is bound along the protofilament ridges and across dimers, the transporter will find options to overcome blockages by bypassing (Figure 65).

Seitz et al. (2002) reported that due to their high detachment/attachment rate MAPs do not represent serious obstacles since they can be pushed aside by a firmly bound motor. This contradicts with observations made by Wille et al. (1992b) who characterized MAP2 subspecies (MAP2c) as a protein tightly binding to the microtubule. The results presented in this study strongly suggest that MAP2 molecules cannot be easily pushed away and free the binding site for kinesin which should result in cargo stalling. As the beads were transported even in the presence of irreversibly bound MAP2, it is more likely that the transporter protein binds to an adjacent protofilament and bypasses the obstacle.
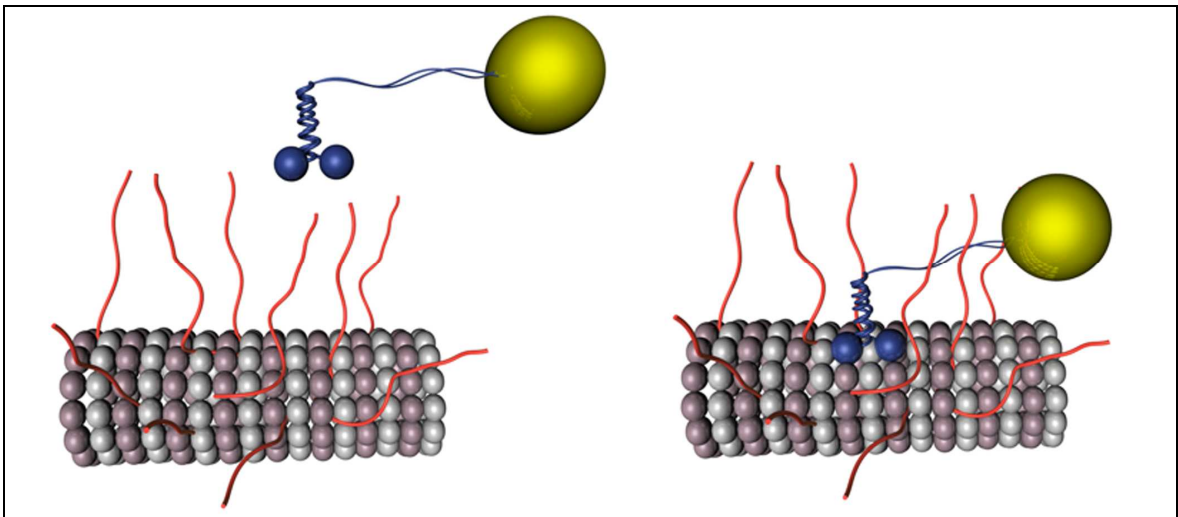
Figure 65: *Illustration of kinesin attachment to the microtubule in the case of low MAP2-to-tubulin ratios.*
At low MAP2 density kinesin is considered to be able to access its binding sites to move along the track and to bypass the filamentous sidearms. MAP2 only partially inhibits kinesin binding and consequently leads to a reduced transport velocity.

4.5.4 Kinesin-mediated cargo transport in the presence of tau

4.5.4.1 Exchangeable tau

Purified tau was added to taxol-stabilized MAP-free microtubules. Under these conditions, tau was exchangeably bound and was in equilibrium between detachment and attachment. The transport of individual beads was characterized by alternating phases of moving and resting (Figure 66). The beads followed, were usually able to overcome resting phases without being detached from the microtubule surface.
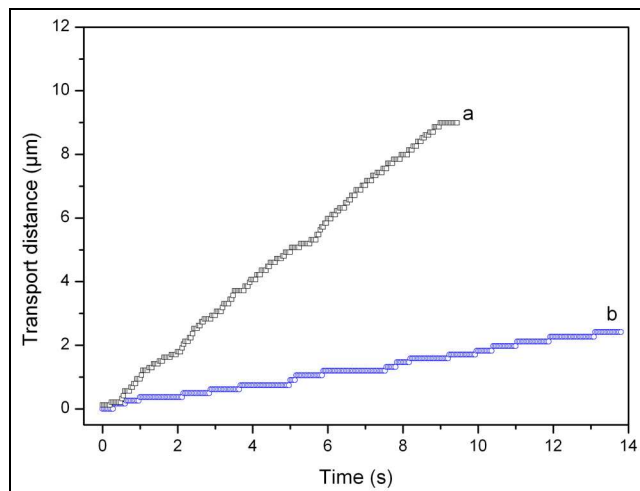
Figure 66: *Distance-time diagram in the presence of exchangeable tau.*
a) Continuous transport in the absence of tau. Within the time interval of this sequence the mean transport velocity was 952 nm s^{-1}.
b) Discontinuous transport with alternating phases of movement and resting observed in the presence of exchangeable tau. The mean velocity including resting phases was 202 nm s^{-1}. The tau-to-tubulin ratio was 1. The data were obtained by measuring the X-Y-shift of single beads on digitized video sequences (30 frames per second).

Depending on the tau-to-tubulin ratio the transport velocity decreased (Figure 67). At equimolar tau-to-tubulin ratio the final velocity level was found at 252 nm s^{-1} ± 55 nm s^{-1}.
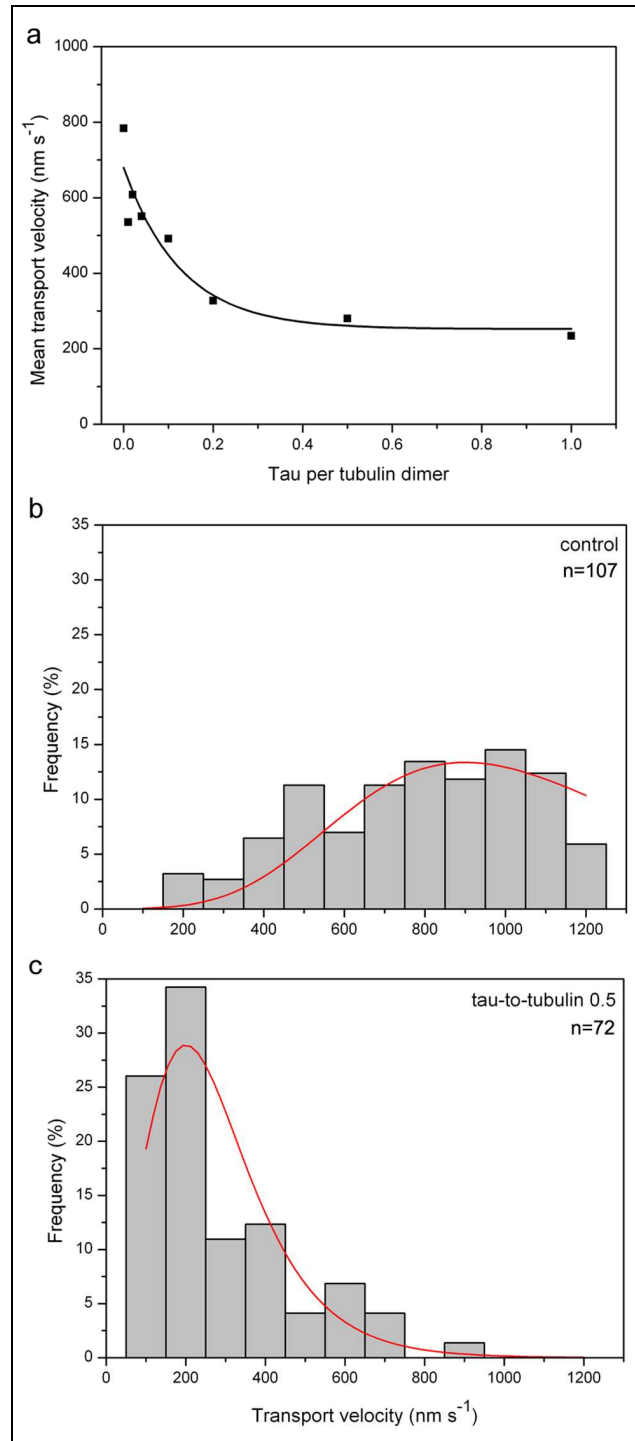
Figure 67: *Effect of exchangeable tau on the velocity.*
a) Dependence of the mean transport velocity on the head-to-tubulin ratio in the case of blocking by exchangeable tau.
b,c) Velocity frequency histograms in the absence of tau and in the presence of exchangeable tau, respectively. The x-values indicate velocity intervals ± 50 nm s^{-1}.
n - number of beads measured.

Additionally, the effect of tau on the catalytic activity of kinesin was determined by measuring the ATP-turnover rates. The k_{cat} values were found to be lowered with increasing tau-to-tubulin ratios (Figure 68), which is consistent with the reduced mean transport velocity. The diminished ATPase activity might reflect a steric inhibition of kinesin binding to the microtubule. Noticeably, the decrease of the microtubule-stimulated ATP-release was more pronounced for MAP2 (Figure 60) most probably due to a stronger steric effect on kinesin binding evoked by larger projection domains on the microtubule surface.
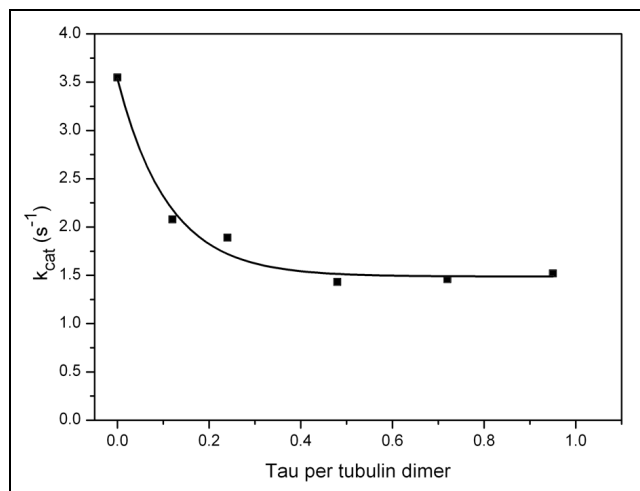
Figure 68: *Effect of exchangeable tau on the catalytic activity of kinesin.*
Determination of the ATPase activity of KIF5A in dependence on the tau-to-tubulin ratio.

4.5.4.2 Irreversibly bound tau

Even exchangeably bound tau exerted a significant decrease on the transport velocity. To prove if irreversible binding causes stronger effects, tau was chemically cross-linked on the microtubule surface. In this case the detachment of tau was avoided, so that tau should act as a rigid blockage.

In the case of irreversibly bound tau, the transport velocity decreased significantly (Figure 69). The lowest velocity (427 nm s^{-1}± 114 nm s^{-1}) was measured at a tau-to-tubulin ratio of 0.1 which theoretically corresponds to one tau per 80-nm protofilament length assuming that all applied tau was bound. However, unlike the exchangeable tau, the irreversibly bound protein caused a complete inhibition of kinesin binding to the microtubules at tau-to-tubulin ratios above 0.1.
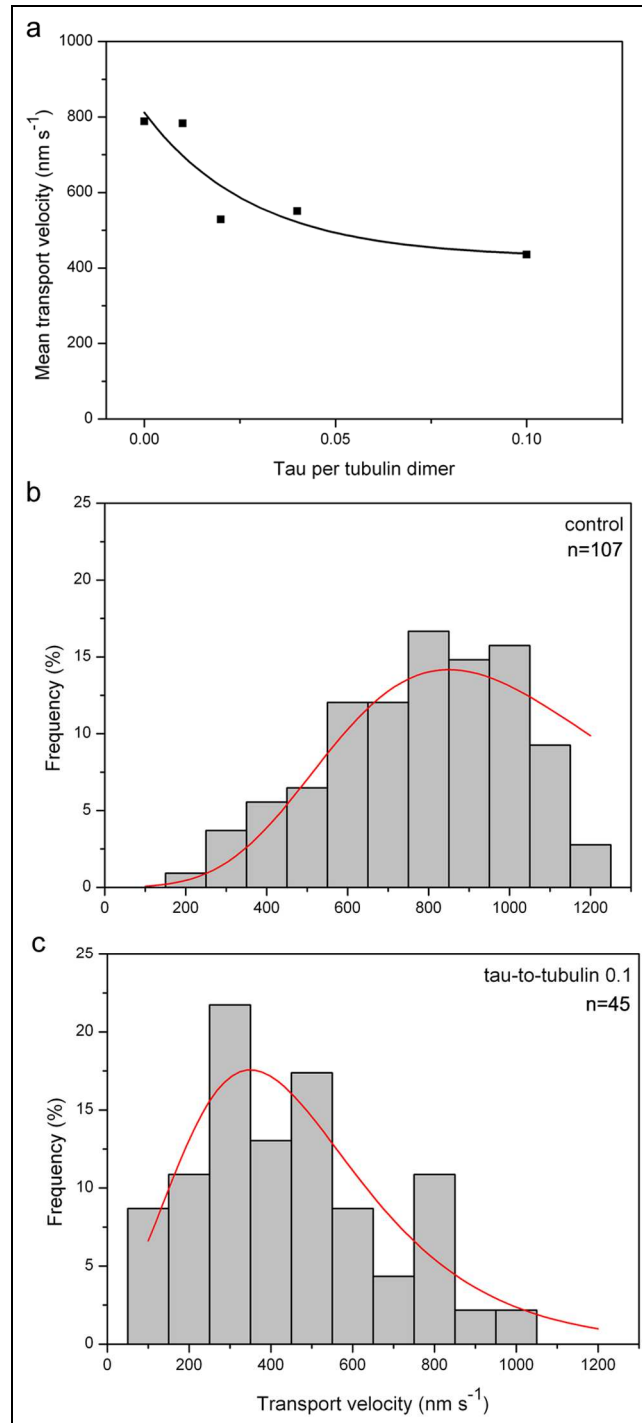
Figure 69: *Effect of irreversibly bound tau on the velocity.*
a) Dependence of the mean transport velocity on the head-to-tubulin ratio in the case of blocking by irreversibly bound tau.
b,c) Velocity frequency histograms in the absence of tau and in the presence of irreversibly bound tau, respectively. The x-values indicate velocity intervals $\pm$ 50 nm s^{-1}.
n - number of beads measured.

4.5.4.3   Comparison of the effect of exchangeable tau and of irreversibly bound tau on the kinesin-mediated transport

Both, exchangeable and irreversibly bound tau was found to decrease the velocity of kinesin-complexed beads (Figure 70). But, unlike exchangeable tau, irreversibly bound tau prevented the binding of kinesin at a tau-to-tubulin ratio >0.1, completely.
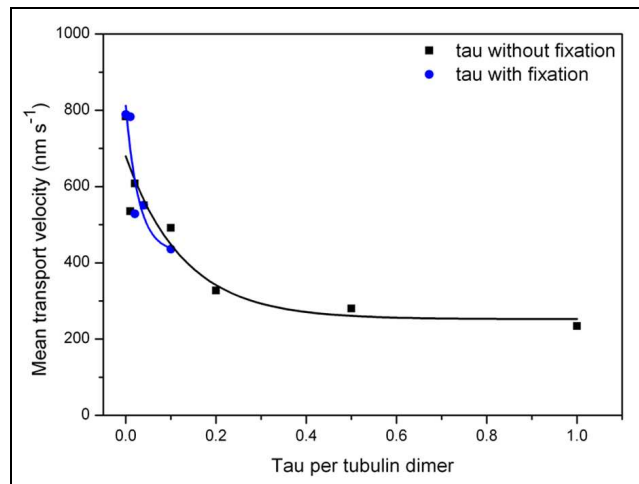
Figure 70: *Effect of exchangeable tau and irreversibly bound tau on the velocity.*
Dependence of the mean transport velocity on the tau-to-tubulin ratio. The data refer to Figure 67 for exchangeable tau and Figure 69 for irreversibly bound tau, respectively.

In the case of exchangeable binding, tau is considered to be in equilibrium between attachment and detachment enabling kinesin binding and movement even at equimolar tau-to-tubulin ratios. The relative weak interaction of tau with the microtubule seems to be an additional argument for its easy displacement (Butner and Kirschner, 1991).

When tau was chemically fixed it forms rigid obstacles that have to be overcome. In solution, tau has no defined structure and remains flexible (Schweers et al., 1994). Upon microtubule binding, tau transits into ordered conformation accompanied by a reduced flexibility (Kotani et al., 1990). In this state, tau molecules have a rod-like shape of about 35-nm length (Wille et al., 1992a), forming extensions along the microtubule surface, which might cause a severe steric inhibition like observed in the case of irreversibly bound tau.

The inhibition of kinesin attachment exerted by tau was less pronounced than for MAP2. This might be due to the much longer projections (185 nm) causing a more distinct

steric inhibition. Consequently, transporting kinesin was still able to move at high tau-to-tubulin ratios.

It was found that tau binds to distinct sites on the microtubule surface. When tau was added to preassembled microtubules, it was reversibly bound and remained exchangeable. But, tau was irreversibly bound into the microtubule wall when tau was present already at the beginning of microtubule assembly (Makrides et al., 2004). In the presented work tau was added to preassembled microtubules. It is suggested that only a small fraction of tau follows the protofilament ridges while the majority remains flexible bound and fills up the gaps between protofilaments and also binds across protofilaments (Santarella et al., 2004). Under the conditions used in this study, it is assumed that tau forms a loose coat on the microtubule masking kinesin binding sites.

Evidence concerning the binding on α- or β-tubulin is contradictory. Santarella et al. (2004) reported that the major tau binding site is located on α-tubulin at the opposite site of the outer protofilament rim where kinesin binds. Taken the distinct binding sites into consideration (kinesin binds on β-tubulin), one could expect that kinesin and tau do not compete for microtubule binding and tau should not affect kinesin motility. On the other hand, it was reported that tau binds longitudinally along the outer ridges of microtubule protofilaments (Al-Bassam et al., 2002). The inhibitory effects of tau on kinesin motility might argue for a steric inhibition by the filamentous structures of tau (see also Vershinin et al., 2008). But nevertheless, kinesin was able to bind to and move even in the case when the microtubule rail was decorated with irreversibly bound tau, presumably by changing to a neighbouring protofilament (see also bypassing 4.3.6).

It has to be mentioned that the bypassing model seems to contradict conclusions drawn by Dixit et al. (2008) who studied the behaviour of kinesin motility in the presence of tau. The authors reported that exchangeable tau inhibit kinesin-mediated motility by causing the detachment of the motor from the microtubule rails at patches of bound tau. Tau patches were reported to be formed by tau association into clusters along the microtubule surface. Under the conditions used in this study, cluster formation can be excluded as the tau proteins passed a 100-kD ultra-filter during purification, whereby in the residual fraction no tau was found (Figure 16).

It was reported that the microtubule stabilizing drug taxol reduced the amount of tau incorporated into the microtubule wall (Kar et al., 2003). Taxol and tau are thought to share an overlapping binding site on the microtubule surface located at β-tubulin which weakens the binding efficiency of tau. In the present study, microtubules co-assembled

with taxol have been used. As previously mentioned, under these conditions tau is preferentially located on the microtubule surface. To get more insights into the effect of tau on kinesin, motility experiments were additionally performed with microtubules, reconstituted from pure tubulin plus tau in the absence of taxol. Under these experimental conditions, tau is allowed to bind both, in exchangeable fashion on the microtubule surface and incorporated within the microtubule wall. In this case, kinesin motility was not affected by tau (Figure 71), suggesting that the majority of tau is integrated inside the microtubule structure. There was obviously a minor residual fraction of tau, exchangeable on the microtubule surface that could be easily bypassed by kinesin (Figure 72).
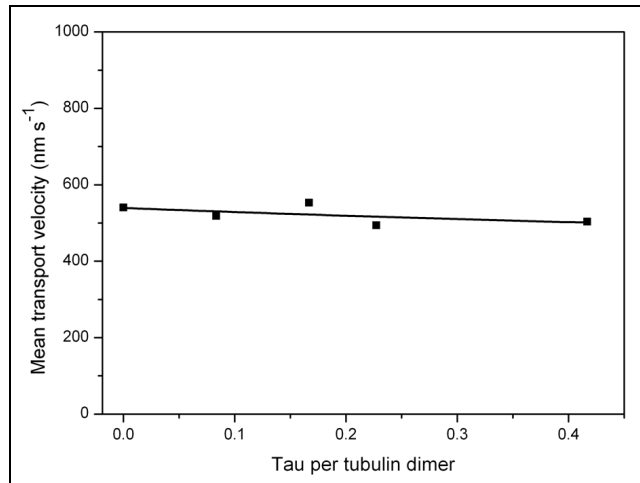
Figure 71: *Effect of tau present during microtubule formation in the absence of taxol on the velocity.*
Dependence of the mean transport velocity on the tau-to-tubulin ratio added to tubulin during assembly. For statistical analysis ≥ 50 single beads were analyzed.
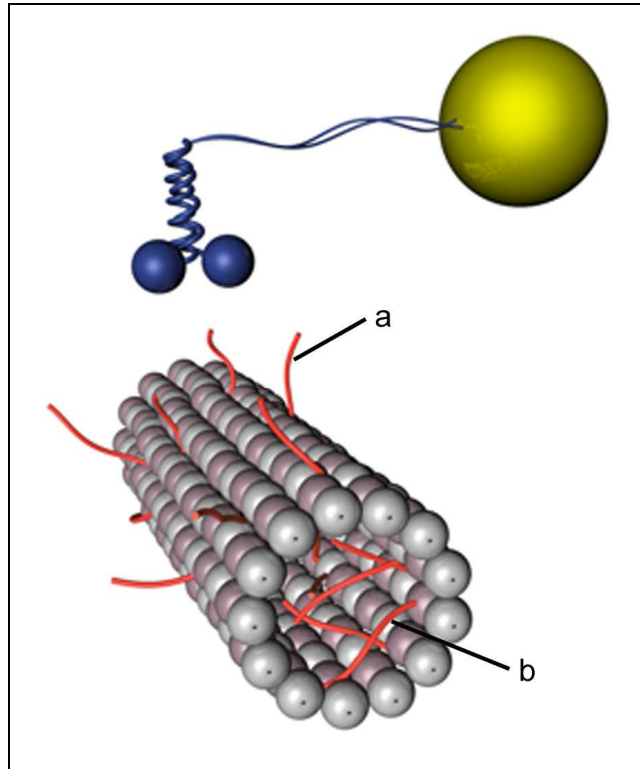
Figure 72: *Illustration of tau bound both, inside the microtubule wall and on the microtubule surface.*
a) Tau binds on the microtubule surface in exchangeable form or
b) is incorporated into the microtubule structure.
The surface-bound tau is able to interfere with the transport of kinesin complexed beads.

4.6 Concluding discussion

In general, kinesin is commonly believed to move along a single protofilament (Kamimura and Mandelkow, 1992; Ray et al., 1993) which seems to be thermodynamically favoured.

A single-motor-molecule approach was presented in which kinesin binding sites along the microtubules were artificially occupied by block proteins, which were inactivated and chemically cross-linked after binding to the tubulin to avoid an exchange. Thereafter, native kinesin was coupled to 20-nm gold beads and allowed to move along such microtubules.

First, KIF5A constructs were used for blocking the microtubule track. Independent of the construct used as block protein, the transporter kinesin was able to continue movement after resting at blocked sites. The results obtained strongly suggest that single kinesin molecules are able to overcome irreversibly bound blockages on the microtubule surface without diffusing from the microtubule rail, even in the case when exactly the kinesin-binding sites were firmly occupied. However, the size of the block protein seems to play an important role in the efficiency of hindering the kinesin transport. In contrast to the bigger constructs $KIF5A_{fl}$ and $KIF5A_{560}$, the globular monomeric motor domain $KIF5A_{330}$ appears to bind more efficiently on the microtubule surface which was reflected in a more steep velocity decrease (Figure 36). On the other hand, the long stalk and tail of $KIF5A_{fl}$ additionally exert a steric effect on kinesin-binding.

But nevertheless, moving beads were able to overcome blocked sites, most presumably by a bypassing mechanism. It is hypothesized that the leading head remains bound to the original protofilament whereas the trailing one turns sidewards and contacts a binding site on a neighbouring protofilament. Subsequently, the leading head leaves the blocked site and follows the trailing head along its new track.

The results contradict with the findings of Seitz and Surrey (2006) who reported that a kinesin mutant, which was able to bind to microtubules but not to move, would free the binding site for the transporter. To corroborate the bypassing model additional experiments were performed using the slowly moving Eg5 also occupying kinesin binding sites on the microtubule. Both, Eg5 in the exchangeable and in the irreversibly bound state were observed to inhibit the movement of the transporter kinesin, whereby the effects were comparable. Surprisingly, transport velocities which are typically measured for Eg5 were not observed suggesting that transporting kinesin bypasses the occupied binding site rather

than running behind the slowly motor. These results support the postulated bypassing mechanism and indicate that under the conditions realized in this study, the block protein cannot be simply pushed away.

Moreover, structural microtubule-associated proteins also exerted a significant effect on kinesin motility. In contrast to KIF5A and Eg5 block proteins, MAPs do not bind to the kinesin binding site, but rather form extensions on the microtubule surface masking kinesin binding sites along several protofilaments which leads to inhibition of kinesin binding. It was shown that MAPs slow down the kinesin-mediated transport which might argue for complex regulatory functions controlling the intracellular transport (Reed et al., 2006; Vershinin et al., 2007; Vershinin et al., 2008). But, under the conditions applied in this study, the transporter kinesin was able to overcome also the MAPs without diffusing from the microtubule, independently of the type of binding, *i.e.* exchangeable or irreversible. This mechanism is considered to be of great relevance as in living organisms structural MAPs and motor proteins coexist and each of them has to fulfill their special tasks.

The present study describes for the first time the movement of kinesin-complexed gold beads, along immobilized microtubules to which block proteins were irreversibly attached. A so far unknown mechanism was proposed which ensures the long-distance movement of kinesin. The ability to bypass blockages is regarded as a basic mechanism by which the track fidelity of a molecular motor, carrying not only cell organelles but also nanoscaled cargoes, along filamentous rails can be improved. The results obtained seem to provide a good basis for future nanotechnological applications of kinesins and its integration in the development of novel nanoscaled actuators. Future medical applications can benefit from the fact that kinesin bypasses blockages. Drugs can be encapsulated into artificial particles and be transported by such protein shuttles to a predetermined destination even in the case of blocked or defective microtubules (plaques or amyloid fibrilles in Alzheimer`s disease; Pissuwan et al., 2006; Waltham, 2006). It is conceivable to use molecular motors transporting antibody-labelled cargoes to pick-up virus particles or proteins from solutions, which can be useful in sensing applications. The ability to perform bypassing can be also advantageous for lab-on-chip designs with desireable applications in sorting, separation and purification requiring controlled motion along a specific route. Moreover, using molecular motors, target molecules can be captured and concentrated to increase detection sensitivity (van den Heuvel and Dekker, 2007).

But, to reach the ambitious aim of nanotechnological application of kinesin motors further studies have to be performed to fully understand the transport mechanisms and motor-cargo or cargo-cargo interaction, respectively.

5 SUMMARY

Within cells, kinesin molecules moving along a single protofilament track encounter other proteins which hinder kinesin to bind to the microtubule surface and consequently inhibit its movement. This might finally cause cargo stalling, comparable with a traffic jam. The present thesis describes the movement of kinesin-complexed gold beads along immobilized microtubules to which block proteins that compete with the transporter protein for microtubule binding sites were irreversibly attached.

It was clearly demonstrated that block proteins (KIF5A constructs) exerted a significant decrease on the transport velocity of kinesin. The transport was interrupted at sites of blockages, but continued after a certain resting time without bead detaching from the microtubule surface. The results strongly suggest that single kinesin molecules are able to bypass sites of blockages by changing to a neighbouring protofilament if the next tubulin dimer along the protofilament track is occupied. This bypassing mechanism is supported by the observation of Yildiz et al. (2008) that in single cases kinesin molecules perform 6-nm sideways steps, which correspond to the lateral distance between the protofilaments of the microtubule wall.

To prove whether a moving motor can be overtaken by the fast moving transporter kinesin by bypassing, the bead transport was studied in the presence of the slowly moving motor Eg5. It was found that, exchangeable bound Eg5 exerted a decrease on the velocity of the transporter kinesin. But, the low velocities typically measured for Eg5 were not reached. This result provides evidence that upon encountering a blockage, transporting kinesin performs bypassing rather than waiting till the obstacle detaches and frees the binding site.

In living cells diverse microtubule-associated proteins (MAP) are expressed and found to bind to microtubules. The study revealed that the presence of two typical neuronal MAPs (MAP2 and tau) led to a significantly decreased transport velocity and, parallel, to a lowered ATPase activity. This inhibition seems to be due to a steric hindrance caused by filamentous side-projections leading to cargo stalling especially at high MAP-to-tubulin ratios. Vershinin et al. (2008) suggest that the cargo transport is highly regulated and coordinated, presumably by a filament-based regulation mechanism, whereby microtubule-associated proteins seem to be involved in tuning the amount of allowed transport in a favoured direction. The observation that MAPs inhibit the kinesin-mediated transport supports this idea.

Bypassing can be regarded as a so far unknown mechanism which ensures the long-distance movement of kinesin.

6 ZUSAMMENFASSUNG

Kinesine sind maßgeblich an intrazellulären Transportvorgängen beteiligt. Es wird allgemein akzeptiert, dass die Kinesinbewegung entlang eines einzelnen Protofilaments der thermodynamisch bevorzugte Transportmechanismus ist. Dabei können Kinesinmoleküle auf andere Proteine treffen, die deren Bindung auf der Mikrotubulusoberfläche behindern. Letztendlich kann dies zum Erliegen der Transportprozesse, unter bestimmten Bedingungen zu Effekten vergleichbar mit einem Verkehrsstau, führen. Die vorliegende Arbeit beschreibt den Transport von Kinesin-komplexierten Goldkugeln entlang immobilisierter Mikrotubuli, an deren Oberfläche Blockproteine, die mit dem Transporterprotein um Bindungsplätze konkurrieren, irreversibel gebunden wurden.

Es konnte gezeigt werden, dass in Gegenwart von Proteinblockaden (KIF5A-Konstrukte) die Transportgeschwindigkeit signifikant erniedrigt wurde. Dabei war der Transport unterbrochen, konnte aber nach einer Verweilzeit fortgesetzt werden, ohne dass das Kinesins vom Mikrotubulus abgelöst wurde. Die Ergebnisse der Studie deuten darauf hin, dass Kinesin in der Lage ist blockierte Bindungsstellen zu überwinden, indem es auf ein anderes Protofilament wechselt und dort den Transport fortsetzt. Der vorgeschlagene *Bypassing-Mechanismus* wird durch Beobachtungen von Yildiz et al. (2008), dass in Einzelfällen Kinesin 6-nm Schritte zur Seite machen kann, unterstützt. Diese Schrittweite entspricht der lateralen Entfernung zwischen Protofilamenten.

Zur Bestätigung des postulierten Mechanismus wurden zusätzlich Experimente durchgeführt, bei denen getestet wurde, ob der langsame Motor Eg5 von dem schnelleren Kinesin überholt werden kann. Mit reversibel gebundem Eg5 wurde zwar eine diskontinuierliche Bewegung von Kinesin beobachtet, aber für Eg5 typische Geschwindigkeiten wurden nicht gemessen. Im Fall der irreversiblen Bindung wurde ein vergleichbarer Effekt der Geschwindigkeitsabnahme beobachtet. Die Untersuchungen mit Eg5 stützen die These, dass Kinesine blockierte Bindungstellen mit Hilfe eines *Bypassing-*Mechanismus überwinden.

In Zellen werden diverse Mikrotubulus-assoziierte Proteine (MAP) exprimiert, die an Mikrotubuli binden. Es wurde gezeigt, dass die Gegenwart von zwei typischen neuronalen MAP (MAP2 und Tau) sowohl zu einer verringerten Transportgeschwindigkeit als auch zu einer verringerten ATPase-Aktivität von Kinesin führte. Aufgrund der filamentösen Strukturen der MAP werden sterische Behinderungen erzeugt, die zur Inhibition des Transports, besonders bei hoher MAP2-Dichte auf der Mikrotubulusoberfläche führen. Untersuchungen von Vershinin et al. (2008) deuten darauf hin, dass die Koordination des Zellorganell-Transports vermutlich durch komplexe Regulationsmechanismen, bei denen MAP involviert sind, erfolgt. Die Beobachtung, dass MAP den Kinesin-vermittelten Transport inhibieren, unterstützt die Annahme.

Der in dieser Arbeit präsentierte *Bypassing-Mechanismus* beschreibt einen bislang unbekannten Mechanismus, der den Kinesin-vermittelten Frachtentransport über lange Strecken ermöglicht.

7 REFERENCES

Aizawa H., Sekine Y., Takemura R., Zhang Z., Hirokawa N., Kinesin family in murine central nervous system. *J. Cell Biol.* **1992**, *119*, 1287-1296.

Al-Bassam J., Ozer R. S., Safer D., Halpain S., Milligan R. A., MAP2 and tau bind longitudinally along the outer ridges of microtubule protofilaments. *J. Cell Biol.* **2002**, *157*, 1187-1196.

Alberts B., Bray D., Lewis J., Raff M., Roberts K., Watson J. D., Molecular Biology of the Cell, Garland Publishing, Inc., New York, **2002** (4th ed.).

Allen R. D., Allen N. S., Travis J. L., Video-enhanced constrast, differential interference constrast (AVEC-DIC) microscopy - A new method cabable of analyzing microtubule-related motility in the reticulopodial network of Allogromia Latiocollaris. *Cell Motil. Cytoskel.* **1981**, *1*, 291-302.

Amos L. A., Microtubule structure and its stabilisation. *Org. Biomol. Chem.* **2004**, *2*, 2153-2160.

Asbury C. L., Fehr A. N., Block S. M., Kinesin moves by an asymmetric hand-over-hand mechanism. *Science* **2003**, *302*, 2130-2134.

Baas P. W., Deitch J. S., Black M. M., Banker G. A., Polarity orientation of microtubules in hippocampal neurons: uniformity in the axon and nonuniformity in the dendrite. *Proc. Natl. Acad. Sci. U. S. A.* **1988**, *85*, 8335–8339.

Bachand G. D., Rivera S. B., Carroll-Portillo A., Hess H., Bachand M., Active capture and transport of virus particles using a biomolecular motor-driven, nanoscale antibody sandwich assay. *Small* **2006**, *2*, 381-385.

Beeg J., Klumpp S., Dimova R., Gracià R. S., Unger E., Lipowsky R., Transport of beads by several kinesin motors. *Biophys. J.* **2008**, *94*, 532-541.

Berg H. C., Constraints on models for the flagellar rotary motor. *Philos. Trans. R. Soc. London* **2000**, *Ser. B 355*, 491-501

Berg H. C., Torque generation by the flagellar rotary motor. *Biophys. J.* 1995, *68*, S163-S167.

Berg J. M., Tymoczo J. L., Stryer L., Clarke N. D., Biochemistry, Spektrum Akademischer Verlag GmbH Heidelberg **2003** (4th ed.).

Block S. M., Goldstein L. S. B., Schnapp B. J., Bead movement by single kinesin molecules studied with optical tweezers. *Nature* **1990**, *348*, 348-352.

Block S. M., Asbury C. L., Shaevitz J. W., Lang M. J., Probing the kinesin reaction cycle with a 2D optical force clamp. *Proc. Natl. Acad. Sci. U. S. A.* **2003**, *100*, 2351-2356.

Bloom G. S., Wagner M. C., Pfister K. K., Brady S. T., Native structure and physical properties of bovine brain kinesin and identification of the ATP-binding subunit polypeptide. *Biochemistry* **1988**, *27*, 3409-3416.

Boal A. K., Tellez H., Rivera S. B., Miller N. E., Bachand G. D., Bunker B. C., The stability and functionality of chemically crosslinked microtubules. *Small* **2006**, *2*, 793-803.

Böhm K. J., Vater W., Fenske H., Unger E., Effect of microtubule-associated proteins on the protofilament number of microtubules assembled in vitro. *Biochim. Biophys. Acta* **1984,** *800,* 119-126.

Böhm K. J., Stracke R., Unger E., Speeding up kinesin-driven microtubule gliding in vitro by variation of cofactor composition and physicochemical parameters. *Cell Biol. Int.* **2000**, *24*, 335-341.

Böhm K. J., Stracke R., Mühlig P., Unger E., Motor protein-driven unidirectional transport of micrometer-sized cargoes across isopolar microtubule arrays. *Nanotechnology* **2001**, *12*, 238-244.

Brady S. T., A novel brain ATPase with properties expected for the fast axonal transport motor. *Nature* **1985**, *317*, 73-75.

Burton P. R., Dendrites of mitral cell neurons contain microtubules of opposite polarity. *Brain Res.* **1988**, *473*, 107-115.

Butner K. A., Kirschner M. W., Tau protein binds to microtubules through a flexible array of distributed weak sites. *J. Cell Biol.* **1991**, *115*, 717–730.

Chen J., Kanai Y., Cowan N. J., Hirokawa N., Projection domains of MAP2 and tau determine spacings between microtubules in dendrites and axons. *Nature* **1992**, *360*, 674-677.

Chrétien D., Metoz F., Verde F., Karsenti E., Wade R. H., Lattice defects in microtubules: protofilament numbers vary within individual microtubules. *J. Cell Biol.* **1992**, *117*, 1031-1040.

Chrétien D., Fuller S. D., Microtubules switch occasionally into unfavorable configurations during elongation. *J. Mol. Biol.* **2000**, *298*, 663-676.

Cleveland D. W., Hwo S. Y., Kirschner M. W., Physical and chemical properties of purified tau factor and the role of tau in microtubule assembly. *J. Mol. Biol.* **1977**, *116*, 227-247.

Cleveland D. W., Hwo S. Y., Kirschner M. W., Purification of tau, a microtubule-associated protein that induces assembly of microtubules from purified tubulin. *J. Mol. Biol.* **1977**, *116*, 207-225.

Cochran J. C., Sontag C. A., Maliga Z., Kapoor T. M., Correia J. J., Gilbert S. P., Mechanistic analysis of the mitotic kinesin Eg5. *J. Biol. Chem.* **2004,** *279*, 38861-38870.

Cross R. A., On the hand-over-hand footsteps of kinesin heads. *J. Muscle Res. Cell Motil.* **1995**, *16*, 91-94.

Cross R. L., The rotary binding change mechanism of ATP synthases. *Biochim. Biophys. Acta-Bioenerg.* **2000**, 1458, 270-275.

DeBonis S., Simorre J. P., Crevel I., Lebeau L., Skoufias D. A., Blangy A., Ebel C., Gans P., Cross R., Hackney D. D., Wade R. H., Kozielski F., Interaction of the mitotic inhibitor monastrol with human kinesin Eg5. *Biochemistry* **2003**, *42*, 338-349.

Dehmelt L., Halpain S., The MAP2/Tau family of microtubule-associated proteins. *Genome Biol.* **2004**, *6*, 204.

Dinu C. Z., Opitz J., Pompe W., Howard J., Mertig M., Diez S., Parallel manipulation of bifunctional DNA molecules on structured surfaces using kinesin-driven microtubules. *Small* **2006**, *2,* 1090-1098.

Dixit R., Ross J. L.,Goldman Y. E., Holzbaur E. L, Differential regulation of dynein and kinesin motor proteins by tau. *Science* **2008,** *319*, 1086-1089.

Doot R. K., Hess H., Vogel V., Engineered networks of oriented microtubule filaments for directed cargo transport. *Soft Matter* **2007**, *3*, 349-356.

Dreblow K., Kalchishkova N., Böhm K. J., Kinesin bypassing blockages on microtubule rails. *Biophys. Rev. Lett.* **2009**, *4*, 141–153.

Drubin D., Kirschner M., Purification of tau protein from brain. *Methods Enzymol.* **1986**, *134*,156-160.

Duncan J. E., Goldstein L. S. B., The Genetics of Axonal Transport and Axonal Transport Disorders. *PLoS Genet.* **2006**, *2*, e124.

Endow S. A., Barker D. S., Processive and nonprocessive models of kinesin movement. *Annu. Rev. Physiol.* **2003**, *65*, 161-75.

Engelbrecht S., Junge W., ATP synthase: a tentative structural model. *FEBS Lett.* **1997**, *414*, 485-491.

Friedhoff P., Mandelkow E.: in Guidebook to the cytoskeletal and motor proteins (eds. Th. Kreis and R. Vale) Oxford University press **1999**, 230-236.

Gelles J., Landick R., RNA polymerase as a molecular motor. *Cell* **1998**, *93*, 13-16.

Gindhart J. G. Jr., Desai C. J., Beushausen S., Zinn K., Goldstein L. S. B., Kinesin light chains are essential for axonal transport in Drosophila. *J. Cell Biol.* **1998**, *141*, 443-454.

Gottlieb R. A., Murphy D. B., Analysis of the microtubule-binding domain of MAP-2. *J. Cell Biol.* **1985**, *101*, 1782-1789.

Hackney D. D., Highly processive microtubule-stimulated ATP hydrolysis by dimeric kinesin head domains. *Nature* **1995**, *377*, 448-450.

Hagiwara H., Yorifuji H., Sato-Yoshitake R., Hirokawa N., Competition between motor molecules (kinesin and cytoplasmic dynein) and fibrous microtubule-associated proteins in binding to microtubules. *J. Biol. Chem.* **1994**, *269*, 3581-3589.

Hancock W. O., Howard J., Processivity of the motor protein kinesin requires two heads. *J. Cell Biol.* **1998**, *140*, 1395-1405.

Hiratsuka Y., Tada T., Oiwa K., Kanayama T., Uyeda T. Q., Controlling the direction of kinesin-driven microtubule movements along microlithographic tracks. *Biophys. J.* **2001**, *81*, 1555-1561.

Hirokawa N., Pfister K. K., Yorifuji H., Wagner M. C., Brady S. T., Bloom G. S., J., Submolecular domains of bovine brain kinesin identified by electron microscopy and monoclonal antibody decoration. *Cell* **1989**, *56*, 867-878.

Hirokawa N., Takemura R.: in Molecular Motors (ed. M. Schliwa) Wiley-VCH **2003**, 79-109.

Hirokawa N., Noda Y., Intracellular transport and kinesin superfamily proteins, KIFs: Structure, function, and dynamics. *Physiolog. Rev.* **2008**, *88*, 1089-1118.

Hoenger A., Sack S., Thormahlen M., Marx A., Muller J., Gross H., Mandelkow E., Image reconstructions of microtubules decorated with monomeric and dimeric kinesins: Comparison with x-ray structure and implications for motility. *J. Cell Biol.* **1998**, *141*, 419-430.

Hoenger A., Thormählen M., Diaz-Avalos R., Doerhoefer M., Goldie K. N., Müller J., Mandelkow E., A new look at the microtubule binding patterns of dimeric kinesins. *J. Mol. Biol.* **2000**, *297*, 1087-103.

Howard J., Mechanics of Motor Proteins and the Cytoskeleton, Sinauer Associates, Inc. **2001**, 245-262.

Hua W., Young E. C., Fleming M. L., Gelles J., Coupling of kinesin steps to ATP hydrolysis. *Nature* **1997**, *388*, 390-393.

Hua W., Chung J., Gelles J., Distinguishing inchworm and hand-over-hand processive kinesin movement by neck rotation measurements. *Science* **2002**, *295*, 780-781.

Hurd D. D., Stern M., Saxton W. M., Mutation of the axonal transport motor kinesin enhances paralytic and suppresses Shaker in Drosophila. *Genetics* **1996**, *142*, 195-204.

Kalchishkova N., Böhm, K. J., The role of Kinesin neck linker and neck in velocity regulation. *J. Mol. Biol.* **2008**, *382*, 127-135.

Kalchishkova N., Dissertation **2009**, FSU Jena.

Kamimura S., Mandelkow E., Tubulin protofilaments and kinesin-dependent motility. *J. Cell Biol.* **1992**, *118,* 865-875.

Kanai Y., Okada Y., Tanaka Y., Harada A., Terada S., Hirokawa N., KIF5C, a novel neuronal kinesin enriched in motor neurons. *J. Neurosci.* **2000**, *20*, 6374-6384.

Kapitein L. C., Peterman E. J. G., Kwok B. H., Kim J. H., Kapoor T. M., Schmidt C. F., The bipolar mitotic kinesin Eg5 moves on both microtubules that it crosslinks. *Nature* **2005**, *435*, 114-118.

Kar S., Fan J., Smith M. J., Goedert M., Amos L. A., Repeat motifs of tau bind to the insides of microtubules in the absence of taxol. *EMBO J.* **2003**, *22*, 70-77.

Kaseda K., Higuchi H., Hirose K., Alternate fast and slow stepping of a heterodimeric kinesin molecule. *Nat. Cell Biol.* **2003**, *5*, 1079-1082.

Kasprzak A. A., Hajdo L., Directionality of kinesin motors. *Acta Biochim. Pol.* **2002**, *49*, 813-821.

Kawachi A., Ichihara K., Hisanaga S., Iida J., Toyota H., Hotani H., Itoh T. J., Different protofilament-dependence of the microtubule binding between MAP2 and MAP4. *Biochem. Biophys. Res. Commun.* **2003**, *305*, 72-78.

Kerssemakers J., Howard J., Hess H., Diez S., The distance that kinesin-1 holds its cargo from the microtubule surface measured by fluorescence interference contrast microscopy. *Proc. Natl. Acad. Sci. U. S. A.* **2006**, *103*, 15812-15817.

Kikkawa M., Sablin E. P., Okada Y., Yajima H., Fletterick R. J., Hirokawa N., Switch-based mechanism of kinesin motors. *Nature* **2001**, *411*, 439-445.

Kim H., Binder L. I., Rosenbaum J. L., The periodic association of MAP2 with brain microtubules in vitro. *J. Cell Biol.* **1979**, *80,* 266-276.

Kim A. J., Endow S. A., A kinesin family tree. *J. Cell Sci.* **2000**, *113*, 3681-3682.

Korten T., Diez S., Setting up roadblocks for kinesin-1: mechanism for the selective speed control of cargo carrying microtubules. *Lab Chip* **2008**, *8*, 1441-1447.

Kotani S., Kawai G., Yokoyama S., Murofushi H., Interaction mechanism between microtubule-associated proteins and microtubules. A proton nuclear magnetic resonance analysis on the binding of synthetic peptide to tubulin. *Biochemistry* **1990,** *29,* 10049–10054.

Kristofferson D., Purich D. L., Time scale of microtubule length redistribution. *Arch. Biochem. Biophys.* **1981**, *211*, 222-226.

Kristofferson D., Mitchison T., Kirschner M., Direct observation of steady-state microtubule dynamics. *J. Cell. Biol.* **1986**, *102*, 1007-1019.

Kull F. J., Sablin E. P., Lau R., Fletterick R. J., Vale R. D., Crystal structure of the kinesin motor domain reveals a structural similarity to myosin. *Nature* **1996**, *380*, 550-555.

Krzysiak T. C., Wendt T., Sproul L. R., Tittmann P., Gross H., Gilbert S. P., Hoenger A., A structural model for monastrol inhibition of dimeric kinesin Eg5. *EMBO J.* **2006**, *25*, 2263-2273.

Laemmli U. K., Cleavage of structural proteins during the assembly of the head of bacteriophage T4. *Nature* **1970**, *227,* 680-685.

Lawrence C. J., Dawe R. K., Christie K. R., Cleveland D. W., Dawson S. C., Endow S. A., Goldstein L. S. B., Goodson H. V., Hirokawa N., Howard J., Malmberg R. L., McIntosh J. R., Miki H., Mitchison T. J., Okada Y., Reddy A. S. N., Saxton W. M., Schliwa M., Scholey J. M., Vale R. D., Walczak C. E., Wordeman L., A standardized kinesin nomenclature. *J. Cell Biol.* **2004**, *167*, 19-22.

Limberis L., Stewart R. J., Toward kinesin-powered microdevices. *Nanotechnology* **2000**, *11*, 47-51.

Lindwall G., Cole R. D., Phosphorylation affects the ability of tau protein to promote microtubule assembly. *J. Biol. Chem.* **1984**, *259*, 5301-5305.

Lopez L. A., Sheetz M. P., Steric inhibition of cytoplasmic dynein and kinesin motility by MAP2. *Cell Motil. Cytoskeleton.* **1993**, *24*, 1-16.

Lowry O. H., Rosebrough N. J., Farr A. L., Randall R. J., Protein measurement with the Folin phenol reagent. *J. Biol. Chem.* **1951**, *193*, 265-275.

Makrides V., Massie M. R., Feinstein S. C., Lew J., Evidence for two distinct binding sites for tau on microtubules. *Proc. Natl. Acad. Sci. U. S. A.* **2004**, *101*, 6746-6751.

Mandelkow E. M., Mandelkow E., Tau in Alzheimer's disease. *Tr. Cell Biol.* **1998**, *8*, 425-427.

Mandelkow E., Johnson K. A., The structural and mechanochemical cycle of kinesin. *Trends Biochem. Sci.* **1998**, *23*, 429-433.

Martin B., Pallen C. J., Wang J. H., Graves D. J., Use of fluorinated tyrosine phosphates to probe the substrate specificity of the low molecular weight phosphatase activity of calcineurin. *J. Biol. Chem.* **1985**, *260*, 14932-14937.

Martin M., Iyadurai S. J., Gassman A., Gindhart J. G., Hays T. S. Saxton W. M., Cytoplasmic dynein, the dynactin complex, and kinesin are interdependent and essential for fast axonal transport. *Mol. Biol. Cell* **1999**, *10*, 3717-3728.

Mazumdar M., Cross R. A., Engineering a lever into the kinesin neck. *J. Biol. Chem.* **1998**, *273*, 29352-29359.

McEwen B. F., Ceska T. A, Crepeau R. H., Edelstein S. J., Structural changes in tubulin sheets upon removal of microtubule-associated proteins. *J. Mol. Biol.* **1983**, *166*, 119-140.

Miki H., Setou M., Kaneshiro K., Hirokawa N., All kinesin superfamily protein, KIF, genes in mouse and human. *Proc. Natl. Acad. Sci. U. S. A.* **2001**, *98*, 7004-7011.

Montemagno C., Bachand G., Constructing nanomechanical devices powered by biomolecular motors. *Nanotechnology* **1999**, *10*, 225-231.

Myers K. A., Baas P. W., Kinesin-5 regulates the growth of the axon by acting as a brake on its microtubule array. *J. Cell Biol.* **2007**, *178*, 1081-91.

Neek-Amal M., Hamedani Radja N., Ejtehadi M. R., Effective potential of longitudinal interactions between microtubule protofilaments. *Phys. Rev. E Stat. Nonlin. Soft Matter Phys.* **2008**, 78, 011912.

Olmsted J.B., Microtubule-associated proteins. *Ann. Rev. Cell Biol.* **1986**, *2*, 421-457.

Pissuwan D., Valenzuela S. M., Cortie M. B., Therapeutic possibilities of plasmonically heated gold nanoparticles. *Trends Biotechnol.* **2006**, *24*, 62-67.

Ramachandran S., Ernst K. H., Bachand G. D., Vogel V., Hess H., Selective loading of kinesin-powered molecular shuttles with protein cargo and its application to biosensing. *Small* **2006**, *2*, 330-334.

Ray S., Meyhöfer E., Milligan R. A., Howard J., Kinesin follows the microtubule's protofilament axis. *J. Cell Biol.* **1993**, *121*, 1083-1093.

Reed N. A., Cai D. W., Blasius T. L., Jih G. T., Meyhöfer E., Gaertig J., Verhey K. J., Microtubule acetylation promotes kinesin-1 binding and transport. *Curr. Biol.* **2006**, *16*, 2166-2172.

Rice S., Lin A. W., Safer D., Hart C. L., Naber N., Carragher B. O., Cain S. M., Pechatnikova E., Wilson-Kubalek E. M., Whittaker M., Pate E., Cooke R., Taylor E. W., Milligan R. A., Vale R. D., A structural change in the kinesin motor protein that drives motility. *Nature* **1999**, *402*, 778-784.

Sack S., Müller J., Marx A., Thormählen M., Mandelkow E. M., Brady S. T., Mandelkow E., X-ray structure of motor and neck domains from rat brain kinesin. *Biochemistry* **1997**, *36*, 16155-16165.

Santarella R. A., Skiniotis G., Goldie K. N., Gross H., Mandelkow E. M., Mandelkow E., Hoenger A., Surface-decoration of microtubules by human tau. *J. Mol. Biol.* **2004**, *339*, 539-553.

Saxton W. M., Porter M. E., Cohn S. A., Scholey J. M., Raff E. C., McIntosh J. R., Drosophila kinesin: characterization of microtubule motility and ATPase. *Proc. Natl. Acad. Sci. U. S. A.* **1988**, *85*, 1109-1113.

Saxton W. M., Hicks J., Goldstein L. S. B., Raff E. C., Kinesin heavy chain is essential for viability and neuromuscular functions in Drosophila, but mutants show no defects in mitosis. *Cell* **1991**, *64*, 1093-1102.

Schief W. R., Howard J., Conformational changes during kinesin motility. *Curr. Opin. Cell Biol.* **2001**, *13*, 19-28.

Schliwa M., Woehlke G., Molecular motors. *Nature* **2003**, *422*, 759-765.

Schnitzer M. J., Block S. M., Kinesin hydrolyses one ATP per 8-nm step. *Nature* **1997**, *388*, 386-390.

Schweers O., Schonbrunn-Hanebeck E., Marx A., Mandelkow E., Structural studies of tau protein and Alzheimer paired helical filaments show no evidence for beta-structure. *J. Biol. Chem.* **1994**, *269*, 24290-24297.

Seitz A., Kojima H., Oiwa K., Mandelkow E. M., Song Y. H., Mandelkow E., Single-molecule investigation of the interference between kinesin, tau and MAP2c. *EMBO J.* **2002**, *21*, 4896-4905.

Seitz A., Surrey T., Processive movement of single kinesins on crowded microtubules visualized using quantum dots. *EMBO J.* **2006**, *25*, 267-277.

Shao Q., Gao Y. Q., On the hand-over-hand mechanism of kinesin. *Proc. Natl. Acad. Sci. U. S. A.* **2006**, *103*, 8072-8077.

Shelanski M. L., Gaskin F., Cantor C. R., Microtubule assembly in the absence of added nucleotides. *Proc. Natl. Acad. Sci. U. S. A.* **1973,** *70***,** 765-768.

Sindelar C. V., Budny M. J., Rice S., Naber N., Fletterick R., Cooke R., Two conformations in the human kinesin power stroke defined by X-ray crystallography and EPR spectroscopy. *Nat. Struct. Biol.* **2002**, *9*, 844-848.

Skowronek K. J., Kocik E., Kasprzak A. A., Subunits interactions in kinesin motors. *Eur. J. Cell Biol.* **2007**, *86*, 559-568.

Song Y. H., Mandelkow E., Recombinant kinesin motor domain binds to beta-tubulin and decorates microtubules with a B surface lattice. *Proc. Natl. Acad. Sci. U. S. A.* **1993,** *90*, 1671-1675.

Stenoien D. L., Brady S. T., Immunochemical analysis of kinesin light chain function. *Mol. Biol. Cell* **1997**, *8*, 675-689.

Svoboda K., Schmidt C. F., Schnapp B. J., Block S. M., Direct observation of kinesin stepping by optical trapping interferometry. *Nature* **1993**, *365*, 721-727.

Thorn K. S., Ubersax J. A., Vale R. D., Engineering the processive run length of the kinesin motor. *J. Cell Biol.* **2000**, *151*, 1093-1100.

Trinczek B., Ebneth A., Mandelkow E. M., Mandelkow E., Tau regulates the attachment/detachment but not the speed of motors in microtubule-dependent transport of single vesicles and organelles. *J. Cell Sci.* **1999**, *112*, 2355-2367.

Turner D., Chang C. Y., Fang K., Cuomo P., Murphy D., Kinesin movement on glutaraldehyde-fixed microtubules. *Anal. Biochem.* **1996**, *242*, 20-25.

Unger E., Böhm K. J., Vater W., Structural diversity and dynamics of microtubules and polymorphic tubulin assemblies. *Electron Microsc. Rev.* **1990**, *3*, 355-395.

Vale R. D., Reese T. S., Sheetz M. P., Identification of a novel force-generating protein, kinesin, involved in microtubule-based motility. *Cell* **1985**, *42*, 39-50.

Vale R. D., Fletterick R. J., The design plan of kinesin motors. *Annu. Rev.Cell Dev. Biol.* **1997**, *13*, 745-777.

Vale R. D., Milligan R. A., The way things move: looking under the hood of molecular motor proteins. *Science* **2000**, *288*, 88-95.

Vale R. D., The molecular motor toolbox for intracellular transport. *Cell* **2003**, *112*, 467-480.

Vallee R., Structure and phosphorylation of microtubule-associated protein 2 (MAP 2). *Proc. Natl. Acad. Sci. U. S. A.* **1980**, *77*, 3206-3210.

Valentine M. T., Fordyce P. M., Block S. M., Eg5 steps it up! *Cell Division* **2006**, *1*, 31.

Valentine M. T., Gilbert S. P., To step or not to step? How biochemistry and mechanics influence processivity in Kinesin and Eg5. *Curr. Opin. Cell Biol.* **2007**, *19*, 75-81.

van den Heuvel M. G. L., Dekker C., Motor proteins at work for nanotechnology. *Science* **2007**, *317*, 333-336.

Verhey K. J., Lizotte D. L., Abramson T., Barenboim L., Schnapp B. J., Rapoport T. A., Light chain-dependent regulation of kinesin's interaction with microtubules. *J. Cell Biol.* **1998**, *143*, 1053-1066.

Vershinin M., Carter B. C., Razafsky D. S., King S. J., Gross S. P., Multiple-motor based transport and its regulation by Tau. *Proc. Natl. Acad. Sci. U. S. A.* **2007**, *104*, 87-92.

Vershinin M., Xu J., Razafsky D. S., King S. J., Gross S. P., Tuning microtubule-based transport through filamentous MAPs: the problem of dynein. *Traffic* **2008**, *9*, 882-892.

von Massow A., Mandelkow E. M., Mandelkow E., Interaction between kinesin, microtubules, and microtubule-associated protein 2. *Cell Motil. Cytoskel.* **1989**, *14*, 562-571.

Voter W. A., Erickson H. P., Electron microscopy of MAP 2 (microtubule-associated protein 2). *J. Ultrastruct. Res.* **1982**, *80*, 374-382.

Walt D. R., Agayn V. I., The chemistry of enzyme and protein immobilization with glutaraldehyde. *Trend Anal. Chem* **1994**, *13*, 425-430.

Waltham M., Gold is newest weapon in battle against Alzheimer's. *Health News* **2006**, *12*, 10.

Wang M. D., Manipulation of single molecules in biology. *Curr. Opin. Biotechnol.* **1999**, *10*, 81-86.

Weingarten M. D., Lockwood A. H., Hwo S. Y., Kirschner M. W., A protein factor essential for microtubule assembly. *Proc. Natl. Acad. Sci. U. S. A.* **1975**, *72*, 1858-1862.

Wille H., Drewes G., Biernat J., Mandelkow E. M., Mandelkow E., Alzheimer-like paired helical filaments and antiparallel dimers formed from microtubule-associated protein tau in vitro. *J. Cell Biol.* **1992**, *118*, 573-584.(a)

Wille H., Mandelkow E. M., Mandelkow E., The juvenile microtubule-associated protein MAP2c is a rod-like molecule that forms antiparallel dimers. *J. Biol. Chem.* **1992**, *267*, 10737-10742.(b)

Woehlke G., Schliwa M., Walking on two heads: the many talents of kinesin. *Nat. Rev. Mol. Cell Biol.* **2000**, *1*, 50-58.

Yang J. T., Saxton W. M., Stewart R. J., Raff E. C., Goldstein L. S., Evidence that the head of kinesin is sufficient for force generation and motility in vitro. *Science* **1990**, *249*, 42-47.

Yildiz A., Tomishige M., Vale R. D., Selvin P. R., Kinesin walks hand-over-hand. *Science* **2004**, *303*, 676-678.

Yildiz A., Selvin P. R., Kinesin: walking, crawling or sliding along? *Trends Cell Biol.* **2005**, *15*, 112-120.

Yildiz A., Tomishige M., Gennerich A., Vale R. D., Intramolecular strain coordinates kinesin stepping behavior along microtubules. *Cell* **2008**, *134*, 1030-1041.

Yokokawa R., Takeuchi S., Kon T., Nishiura M., Sutoh K., Fujita H., Unidirectional transport of kinesin-coated beads on microtubules oriented in a microfluidic device. *Nano Lett.* **2004**, *4*, 2265-2270.

Yokokawa R., Tarhan M. C., Kon T., Fujita H., Simultaneous and bidirectional transport of kinesin-coated microspheres and dynein-coated microspheres on polarity-oriented microtubules. *Biotechnol. Bioeng.* **2008**, *101*, 1-8.

Curriculum Vitae

Personal Data ————————————————————————

Name: Kerstin Dreblow

Date of Birth: 08.08.1981

Place of Birth   Meiningen

Nationality: German

Education ————————————————————————

09/1988-07/1992	Elementary school at the former Otto-Buchwitz Oberschule Vachdorf
09/1992-06/2000	Secondary school at the Moritz-Seebeck Gymnasium Meiningen (later renamed as Henfling Gymnasium)
06/2000	Diploma from German secondary school qualifying for university admission or matriculation

Academic studies

WS 2000/2001- WS 2004/2005	Study of Chemistry at Friedrich-Schiller-University Jena
1.11.2004-31.7.2005	Diploma Thesis: "Modelluntersuchungen zur Immissionsbelastung von Gräsern mit Platingruppenelementen" Supervisor: Prof. Dr. J. W. Einax in Cooperation with Thüringer Landesanstalt für Landwirtschaft
10.10.2005	Acquisition of academic degree: diploma (MSc)

Graduation

01.06.2006-31.08.2009	PhD student at Leibniz Institute for Age Research – FLI Jena in the lab of Prof. Dr. K. O. Greulich Supervisor: Prof. Dr. W. Weigand

Jena, June 03rd 2009   Kerstin Dreblow

Lebenslauf

Persönliche Daten ———————————————————————

Name:	Kerstin Dreblow
Geburtsdatum:	08.08.1981
Geburtsort:	Meiningen
Nationalität:	Deutsch

Bildungsweg ———————————————————————

Schulbildung

09/1988-07/1992	ehemalige Otto-Buchwitz Oberschule Vachdorf
09/1992-06/2000	Moritz-Seebeck Gymnasium Meiningen (später umbenannt in Henfling Gymnasium)
06/2000	Allgemeine Hochschulreife

Studium

WS 2000/2001- WS 2004/2005	Chemiestudium an der Friedrich-Schiller-Universität Jena (Studienrichtung Umweltchemie)
1.11.2004-31.7.2005	Diplomarbeit: „Modelluntersuchungen zur Immissionsbelastung von Gräsern mit Platingruppenelementen" unter Anleitung von Prof. Dr. J. W. Einax in Kooperation mit der Thüringer Landesanstalt für Landwirtschaft
10.10.2005	Hochschulabschluss: Diplom-Chemikerin (Umweltchemie)

Promotion

01.06.2006-31.08.2009	Doktorandin am Leibniz Institut für Altersforschung – FLI Jena in der Arbeitsgruppe von Prof. Dr. K. O. Greulich Betreuer: Prof. Dr. W. Weigand

Jena, den 03.06.2009   Kerstin Dreblow

List of publications

Publication:

- Dreblow K., Kalchishkova N., Böhm K. J., Kinesin bypassing blockages on microtubule rails. *Biophysical Reviews and Letters* **2009**, *4*, 141–153.

- Dreblow K., Kalchishkova N., Böhm K. J., Kinesin movement along microtubules with irreversibly blocked kinesin binding sites. under review

- Dreblow K., Böhm K. J., Inhibition of kinesin-mediated motility by microtubule-associated proteins. *Eur. J. Cell Biol.* **2009**, 88 *(Suppl. 59)*, p. 13.

- Dreblow K., Böhm K. J., KIF5A-mediated transport in the presence of an additional, slowly moving, motor. *Eur. J. Cell Biol.* **2008**, *87 (Suppl. 58)*, p. 24.

Poster presentations:

- Dreblow K., Böhm K. J., Cargo transport by the neuron-specific KIF5A motor in the presence of microtubule-associated proteins. 3rd FLI Retreat on Molecular Mechanisms of Senescence and Ageing. Bad Blankenburg, May 24–26, 2009.

- Dreblow K., Böhm K. J., Inhibition of kinesin-mediated motility by microtubule-associated proteins. 1st Joint Congress of the Swiss and German Society of Cell Biology/ 32nd Annual Meeting of the German Society for Cell Biology, Konstanz, March 24-27, 2009.

- Dreblow K., Böhm K. J., KIF5A-mediated transport in the presence of an additional, slowly moving, motor. SFB523 Symposium Intracellular Transport and Trafficking, Göttingen, April 3-4, 2008, Abstract p. 40.

- Dreblow K., Böhm K. J., KIF5A-mediated transport in the presence of Eg5, 31st Annual Meeting of the German Society for Cell Biology, Marburg, March 12-15, 2008.

- Dreblow K., Kalchishkova N., Jayamani A., Böhm K. J., Molecular mechanisms of kinesin bypassing roadblocks. Minerva-Weizman Workshop Moving Cells - From Molecules to Animals, Rehovot (Israel), November 24-28, 2007. Abstract p.12.

- Dreblow K., Jayamani A., Kalchishkova N., Böhm K. J., Molecular mechanisms of kinesin movement along overcrowded microtubules. GBM Fall Meeting - Molecular Life Science, Hamburg, September 16-19, 2007. Abstract p.36.

- Dreblow K., Jayamani A., Stracke R., Böhm K. J., Molecular Mechanisms of kinesin-mediated motility - Kinesin movement affected by external forces. 2nd FLI Retreat on Molecular Mechanisms of Senescence and Ageing. Bad Blankenburg, June 03-05, 2007.

Oral presentations:

- Dreblow, K., Kinesin bypassing roadblocks irreversibly bound to microtubules. STREP Workshop, Potsdam, September 10-11, 2007.

- (invited) Dreblow K., Kalchishkova N., Jayamani A., Böhm K. J., Molecular mechanisms of kinesin bypassing roadblocks. Minerva-Weizmann Workshop Moving Cells - From Molecules to Animals, Rehovot (Israel), November 24-28, 2007.

Danksagung

An dieser Stelle möchte ich mich bei all jenen bedanken, die zum Gelingen der Arbeit beigetragen haben.

Zuallererst möchte ich Herrn Prof. Dr. W. Weigand für sein Vertrauen und seine Bereitschaft in die unbekannte Welt der Molekularen Motoren einzutauchen, danken. Er hat meiner Arbeit sehr viel Vertrauen entgegengebracht und war stetig an deren Entwicklung interessiert. Für die gewährten Freiheiten und die Anfertigung des Erstgutachtens möchte ich ihm meinen großen Dank aussprechen.

Ebenso bin ich Herrn Prof. Dr. K. O. Greulich zu großem Dank verpflichtet, für die Möglichkeit die Arbeit in seiner Arbeitsgruppe durchzuführen und für die Erstellung des Zweitgutachtens.

Ein besonderes Dankeschön gebührt Dr. K. J. Böhm, der mir stets mit Rat und Tat zur Seite stand und mir die Arbeit sowohl auf einem wissenschaftlich sehr interessanten Thema, als auch in einem familiären Umfeld ermöglichte. Ich bin ihm zu Dank verpflichtet für seine Geduld, Disskussionsbereitschaft, Motivation und die Beantwortung all meiner Fragen.

Nikolina Kalchishkova danke ich für die Klonierung der verwendeten Proteine. Ihre wertvollen Anregungen, das freundschaftliche Arbeitsklima und die unzähligen Diskussionen haben zum Entstehen der Arbeit beigetragen. Des Weiteren danke ich Marina Wollman für die Expremierung und Reinigung der Proteine und Roland Stracke für die Einführung in die AVEC-DIC und Elektronenmikroskopie.

Katrin Buder sowie den Mitarbeitern des Elektronenmikroskopischen Zentrums am Universitätsklinikum Jena, vor allem Dr. Martin Westermann, danke ich für die Hilfestellung bei der Präparation der Proben und bei der Arbeit mit dem Elektronenmikroskop.

Für die freundliche Überlassung des ImageJ Plug-In zur Datenauswertung danke ich Janina Beeg und Ruben Serral Graciá vom Max-Planck-Institut für Kolloid- und Grenzflächenforschung Potsdam-Golm.

Ich möchte den Mitarbeitern der Arbeitsgruppe von Prof. K. O. Greulich, insbesondere Paulius Grigaravičius, Shamci Monajembashi und Maria Radeva, für Ihre Unterstützung, freundschaftliche Arbeitsatmosphäre und den vielen unvergesslichen Momenten danken.

Theodor Alpermann und vor allem Tobias Niksch danke ich für ihre stetige Unterstützung sowie Hilfe während des Studiums und darüber hinaus.

Von ganzem Herzen danke ich meiner Familie und Tobias für ihre liebevolle Unterstützung, das unermüdliche Verständnis während all der Jahre und ihr Glaube an mich und meine Arbeit.

Leider lässt sich eine wahrhafte Dankbarkeit

mit Worten nicht ausdrücken.

Johann Wolfgang von Goethe

Selbstständigkeitserklärung

Ich erkläre, dass ich die vorliegende Arbeit selbstständig und nur unter Verwendung der angegebenen Hilfsmittel, persönlichen Mitteilungen und Quellen angefertigt habe.

Jena, den 03.06.2009   Kerstin Dreblow